การสร้างแบบจำลองและการควบคุมของนาโนฟิลเตรชัน
สำหรับสารประกอบอินทรีย์ในสารละลายเจือน้ำโดยใช้ตัวควบคุมแบบจีเอ็มซี

นายสัมพันธ์พงศ์ เพ็ญสิริกุล

วิทยานิพนธ์นี้เป็นส่วนหนึ่งของการศึกษาตามหลักสูตรปริญญาวิศวกรรมศาสตรมหาบัณฑิต
สาขาวิชาวิศวกรรมเคมี ภาควิชาวิศวกรรมเคมี
คณะวิศวกรรมศาสตร์ จุฬาลงกรณ์มหาวิทยาลัย
ปีการศึกษา 2546

ISBN 974-17-4436-6

MODELING AND CONTROL OF NANOFILTRATION FOR ORGANIC COMPONENT IN AQUEOUS SOLUTION USING GMC CONTROLLER

Mr. Sampanpong Bhensirikul

A Thesis Submitted in Partial Fulfillment of the Requirements
for the Degree of Master of Engineering in Chemical Engineering

Department of Chemical Engineering
Faculty of Engineering
Chulalongkorn University

Academic Year 2003
ISBN 974-17-4436-6

Thesis Title	MODELING AND CONTROL OF NANOFILTRATION FOR ORGANIC COMPONENT IN AQUEOUS SOLUTION USING GMC CONTROLLER
By	Mr. Sampanpong Bhensirikul
Field of Study	Chemical Engineering
Thesis Advisor	Associate Professor Paisan Kittisupakorn, Ph.D.

Accepted by the Faculty of Engineering, Chulalongkorn University in Partial Fulfillment of the Requirements for the Master 's Degree

…… Dean of the Faculty of Engineering
(Professor Direk Lawansiri, Ph. D.)

THESIS COMMITTEE

…….. Chairman
(Professor Piyasan Praserthdam, D. Eng.)

……..…… Thesis Advisor
(Associate Professor Paisan Kittisupakorn, Ph. D.)

…….. Member
(Montree WongSri, D. Sc.)

…….. Member
(Assistant Professor Wirat Vanichsriratana, Ph. D.)

สัมพันธ์พงศ์ เพ็ญสิริกุล : การสร้างแบบจำลองและการควบคุมของนาโนฟิลเตรชันสำหรับสารประกอบอินทรีย์ในสารละลายเจือน้ำโดยใช้ตัวควบคุมแบบจีเอ็มซี (MODELING AND CONTROL OF NANOFILTRATION FOR ORGANIC COMPONENT IN AQUEOUS SOLUTION USING GMC CONTROLLER) อ. ที่ปรึกษา : รศ.ดร. ไพศาล กิตติศุภกร, 118 หน้า. ISBN 974-17-4436-6

กระบวนการแยกสารด้วยเยื่อแผ่นได้เข้ามามีบทบาทในอุตสาหกรรมหลายประเภท แต่การควบคุมเชิงพลวัตรของกระบวนการแยกสารด้วยเยื่อแผ่นยังไม่มีการศึกษามากนัก เนื่องจากการศึกษาพฤติกรรมเชิงพลวัตรของกระบวนการยังไม่สามารถสร้างแบบจำลองเพื่ออธิบายกลไกการแยกสารของกระบวนการเยื่อแผ่นได้ดีเท่าที่ควร และการควบคุมกระบวนการแยกสารโดยใช้กระบวนการเยื่อแผ่นนั้นต้องอาศัยแบบจำลองทางคณิตศาสตร์ที่มีความน่าเชื่อถือมาใช้ในการอธิบายกลไกที่ซับซ้อนต่างๆ ที่เกิดขึ้น เช่น กลไกการถ่ายเทมวล, คอนเซนเตรชัน โพลาไรเซชัน และการเกิดการอุดตัน เป็นต้น ดังนั้นการพัฒนาแบบจำลองให้สอดคล้องกับกระบวนการจริงจึงเป็นขั้นตอนที่สำคัญขั้นตอนหนึ่ง ก่อนที่จะนำแบบจำลองนั้นมาใช้ในการทำนายและควบคุมพฤติกรรมของกระบวนการแยกสารด้วยเยื่อแผ่น

ระบบที่นำมาศึกษาในงานวิจัยนี้คือกระบวนการแยกน้ำออกจากสารละลายเจือน้ำของกรดแทนนิค โดยใช้เยื่อแผ่นชนิดนาโนฟิลเตรชัน แบบจำลองทางคณิตศาสตร์ของระบบนี้ถูกพัฒนาขึ้นเพื่อใช้อธิบายพฤติกรรมของระบบ และใช้ในการหาค่าเป้าหมายที่เหมาะสมของตัวแปรควบคุมในกระบวนการซึ่งก็คือค่าฟลักซ์ของน้ำ โดยใช้ความดันเป็นตัวแปรปรับ ตัวควบคุมแบบจีเอ็มซีถูกนำมาใช้ร่วมกับตัวกรองคาลมานเพื่อควบคุมค่าฟลักซ์ของน้ำให้อยู่ที่ค่าเป้าหมายที่ต้องการ จากผลที่ได้จะเห็นว่าตัวควบคุมแบบเจเนอริกโมเดลร่วมกับตัวกรองคาลมานให้ผลการควบคุมที่ดีและมีความทนทานในสภาวะที่มีความผิดพลาดของค่าพารามิเตอร์ของแบบจำลองกระบวนการ

ภาควิชาวิศวกรรมเคมี ลายมือชื่อนิสิต.....

สาขาวิชาวิศวกรรมเคมี ลายมือชื่ออาจารย์ที่ปรึกษา.....

ปีการศึกษา 2546

##4370644021 : MAJOR CHEMICAL ENGINEERING
KEY WORD : OPTIMIZATION / CONTROL / GENERIC MODEL CONTROL / MEMBRANE SEPARATION / NANOFILTRATION

SAMPANPONG BHENSIRIKUL : MODELING AND CONTROL OF NANOFILTRATION FOR ORGANIC COMPONENT IN AQUEOUS SOLUTION USING GMC CONTROLLER. THESIS ADVISOR : ASSOC. PROF. PAISAN KITTISUPAKORN, Ph.D., 118 pp.
ISBN 974-17-4436-6

Membrane separation process has become an important unit in many industrials. Dynamic control of membrane separation process has not been received much study because studying of dynamic membrane process behavior still does not develop a satisfied model to explain membrane separation mechanism. Controlling of membrane separation process needs a reliability mathematical model to explain the complicated mechanisms such as mass-transfer mechanism, concentration polarization, and fouling. It is important to develop the model to represent the real process before using the model to predict and handle the response of membrane separation process.

In this research, a nanofiltration membrane process for tannic acid component in aqueous solution has been studied. The mathematical model of this system is developed to explain behavior of the system and determine the optimal set point of controlled variable, water-permeate flux, using applied pressure as a manipulated variable. A GMC controller coupled with a Kalman filter is implemented to track optimal water flux set point. The GMC coupled with Kalman filter has been found to be effective and robust with respect to changes in process parameters.

Department Chemical Engineering Student's signature…….
Field of Chemical Engineering Advisor's signature……
Academic Year 2003

ACKNOWLEDGEMENTS

I would like to sincerely thank my adviser, Associate Professor Paisan Kittisupakorn, for his helpful suggestions, encouraging guidance, and generous supervision throughout my thesis work. Furthermore, I am grateful to Professor Piyasan Praserthdam, Dr. Montree Wongsri, and Assistant Professor Wirat Vanichsriratana for serving as chairman and member of thesis committees, respectively.

I especially want to thank my colleagues and all members in the process control laboratory for the pleasant collaboration and the way they contributed to my development.

Being able to finish my master program is also dependent on “home base”. I want to thank everyone in my family for the education and guidance they gave me in my way to adulthood; my father and mother for my concrete constitution and mentality and my sister for her confidence.

CONTENTS

CONTENTS (continued)

PAGE

CONTENTS (continued)

PAGE

LIST OF TABLES

PAGE

LIST OF FIGURES

LIST OF FIGURES (continued)

PAGE

LIST OF FIGURES (continued)

PAGE

NOMENCLATURES

Notation

A_m	=	membrane surface area, m^2
B_n	=	n th virial coefficient, $m^{3(n-1)}kg^{-n+1}$
C	=	solute concentration, kg/m^3
C_b	=	concentration in the bulk solution, kg/m^3
C_f	=	concentration in the feed solution, kg/m^3
C_g	=	concentration in the gel layer, kg/m^3
C_m	=	concentration at the membrane surface on the bulk solution side, kg/m^3
C_p	=	concentration in the permeate solution, kg/m^3
D	=	molecular diffusion coefficient, m^2/min
$e(t)$	=	error
$g(x)$	=	vector of inequalities of dimension m_2
$h(x)$	=	vector of equations of dimension m_1
J_v	=	permeate flux, $m^3/m^2 \bullet min$
K	=	Kalman gain matrix
K_1, K_2	=	tuning parameter of GMC
k	=	mass-transfer coefficient, m/min
L	=	length of membrane module, m
P	=	estimation error covariance matrix
$p(t)$	=	controller output
Q	=	process noise covariance matrix
R	=	measurement noise covariance matrix
R	=	gas-law constant = 8.3143 $J \bullet mol^{-1} \bullet K^{-1}$
Re	=	Reynolds number
R_{cp}	=	resistance of the concentration polarization, m^{-1}
R_g	=	resistance of the gel layer, m^{-1}
R_m	=	resistance of the membrane, m^{-1}
R_{total}	=	total resistance of the membrane, m^{-1}
r	=	product recovery
S_c	=	Schmidt number

NOMENCLATURES (continued)

S_h	=	Sherwood number
T	=	absolute temperature, K
t	=	time, min
u	=	manipulated variable
V	=	feed solution volume, m^2
V_0	=	initial feed volume, m^2
V_{out}	=	permeant volume, m^2
v	=	cross-flow velocity, m/min
x	=	state variable
y	=	output of the process model

Greek Letters

δ	=	thickness of the concentration polarization layer, m
ε	=	resistance per unit of the gel layer thickness, m^{-2}
λ	=	Lagrange multiplier
μ	=	dynamic viscosity, Pa·min
ρ_g	=	density of the gel layer, kg/m^3
ΔP	=	applied pressure, Pa
$\Delta\pi$	=	osmotic pressure between the bulk sol^{n}. and the permeate, Pa
Δt	=	sampling period
ξ	=	damping constant
τ	=	time constant
τ_D	=	derivative time constant
τ_I	=	integral time constant

Subscript

0	=	initial
b	=	bulk solution
cp	=	concentration polarization
f	=	feed solution

NOMENCLATURES (continued)

g	=	gel layer
m	=	membrane
p	=	permeate
sp	=	setpoint
total	=	total

Superscript

int	=	internal
ext	=	external

CHAPTER 1

INTRODUCTION

In recent years, membrane has become an important unit operation in chemical technology because many industries concern about colloidal particles, including the following: natural organic matter (NOM), heavy metals, and nonmetallic inorganic ions from contaminated waters and industrial effluents. A large variety of membranes are used in numerous processes devoted to molecular-scale separation in liquids or gases. The most classic operations are electrodialysis, reverse osmosis, ultrafiltration, and nanofiltration. Membranes applications in water and wastewater treatment have grown rapidly because they have many advantages than other separation processes such as it separates components as pure as other separation units and energy consumption is much lower than. The lower energy consumption can be explained in term of latent heat that membrane separation processes do not require latent heat in change of phase, unlike distillation and evaporation. Furthermore, membrane processes are appropriate to manufacture high purity, quality, and valuable products. Nowadays membranes are higher quality and lower price so the membrane processes have been applied to replace other separation processes in most plants. In the future membrane process probably play important role in environment because of high potential for recovery.

The economics of membrane filtration processes are dependent on the permeate flux (Chellam and Wiesner, 1997). Almost membrane separation processes are found operating condition that could be obtained maximizing permeate flux rate by using optimal condition experiments. But permeate flux in cross-flow filtration is controlled by dynamic process of gel-layer formation and growth. A serious limitation in such process is the progressive permeate flux deterioration due to two phenomena: membrane fouling and concentration polarization. The resistances that occur in membrane process could be cause by the membrane, concentration polarization, internal pore fouling, and gel-layer

formation. Membrane fouling can be reversible when flux recovery can be achieve by chemical cleaning or fluid dynamics, or irreversible when flux recovery is not possible.

The desire to maximize filtration rate using minimum energy is presents as the motivation for this research. The model-base control is required to control the process automatically so the reliable membrane transport model, developed for prediction and simulation of membrane filtration dynamics with reference to permeate flux, is necessary.

In this work, the nanofiltration of aqueous solutions containing organic compounds developed by Chieh Tu et al. (2001) is considered. Nanofiltration membranes are a new class of membrane, which have properties in between those of ultrafiltration membranes and reverse-osmosis membrane. In this process the nanofiltration membrane, which is a plate-and-frame system, is simulated to perform the filtration tests to remove tannic acid, a model compound representing natural organic matter, under different operating conditions including transmembrane pressure, reject flow rate, and acid concentration. The primary purpose of this research is to develop process model incorporating the concentration polarization and gel layer formation in the filtration process and control the permeation rate of a chemical species through the membrane. Applied pressure is used to control the operating flux at it desired trajectory. A generic model control (GMC) coupled with a Kalman filter is implemented to track an optimal operating flux.

1.1 Objectives of Research

The objectives of this research are:

1. To study and develop membrane transport model for nanofiltration process,
2. To study the parameters of process that affect to performance of the nanofiltration process,
3. To study algorithm of Generic Model Control (GMC) and design a control configuration for the process to track the obtained optimal operating flux,
4. To study and develop computer program for nonlinear control of the process,
5. To assess the performance and robustness of the GMC controller and compare result with PID controller.

1.2 Scope of Research

The scope of this research can be listed as follows:

1. A nanofiltration membrane for removal tannic acid is studied in this research.
2. An off-line optimal control problem is solved with fixed batch time to find the optimal flux. A nonlinear programming problem (NLP) is solved using a successive quadratic programming (SQP) based optimization technique.
3. A generic model control (GMC) coupled with Kalman filter is applied to handle the studied process. Applied pressure is selected as a manipulated variable.
4. The control response of GMC is compared with PID by using computer simulation.
5. The simulated program of the membrane separation process is developed by using MATLAB language.

1.3 Contributions of Research

The contributions of this research can be listed as follows:

1. The mechanisms of transport phenomena and flux decline that occur in nanofiltration have been studied.
2. The factors of flux decline during operation have been specified.
3. Mathematical model of a nanofiltration process has been developed.
4. The computer programs developed by MATLAB language have been simulated to study the behavior of a nanofiltration process.
5. A nanofiltration process has been controlled to achieve a desire objective.

1.4 Activity Plan

1. Relevant information regarding membrane separation process is reviewed.
2. Mathematical model of a nanofiltration membrane is developed to present behavior of the process.
3. Relevant information regarding optimization and control are reviewed.
4. Kalman filter is applied to estimate uncertain parameters.
5. An optimal operating flux of a nanofiltration process is determined to achieve the desired objective.
6. A suitable control law is designed to track the obtained optimal operating flux.
7. All simulation results are collected and summarized.
8. Edit and improve the report.

This thesis is divided into six chapters

Chapter 1 is an introduction to this research. This chapter consists of research objective, scope of research, contribution of research, and activity plan.

Chapter 2 reviews the literature for work related to modeling of nanofiltration system, Generic Model Control (GMC) strategy, optimization and Kalman filter.

Chapter 3 covers some background information of membrane separation process (nanofiltration), optimization, Generic model control (GMC), and Kalman filter.

Chapter 4 describes the membrane separation process, a modeling of nanofiltration for tannic acid in aqueous solution and control configuration. Simulation results obtained by simulating the optimization formulation and the formulation of a GMC controller are detailed in each section.

Chapter 5 presents the conclusions of this research and makes the recommendations for future work.

This is follow by:

References

Appendix A: Mathematical Model Development,
Appendix B: Mass Transfer Coefficient Determination,
Appendix C: System Checking,
Appendix D: Integral Error Criteria,
Appendix E: Successive Quadratic Programming (SQP).

CHAPTER 2

LITERATURE REVIEW

2.1 Nanofiltration and Membrane Filtration Process

Porter (1972) studied concentration polarization with membrane. Nanofiltration and ultrafiltration are pressure-driven processes, in which water is forced to permeate the small membrane pores by the application of pressure. The permeate flux rate is generally proportional to the applied pressure until the accumulation of solutes in the concentration polarization layer reaches a threshold concentration that limits further increases in flux. The amount or thickness of solute accumulation is also dependent on the flow hydrodynamics at the membrane surface. Increasing the Reynolds number of the flow produces greater shear at the membrane surface causing a reduction in the amount of foulant material.

Bhattacharyya and Madadi (1988) developed the mathematical model for separation of phenolic compounds by low pressure composite membranes. The set of differential equations based on solute diffusion through membranes. The solute adsorption phenomenon, which creates large flux drops for polymer membranes, was investigated, accounted for in the mathematical model, and used in the computer program. The validity of the model was tested for single and multiple component systems using experimental data. The systems studied in this work were chloro-and nitrophenols in water.

Li et al. (1996) presented numerical, finite difference methods to calculate water concentration profiles over the time course from initial water uptake to equilibrium in poly (vinyl chloride)-based ion selective membrane.

Hong et al. (1997) proposed kinetics of permeate flux decline in crossflow membrane filtration of colloidal suspensions. The membrane filtration experiments were performed to systematically investigate the dynamic behavior of permeate flux in cross flow membrane filtration of colloidal suspensions. The model was based on a simplified particle mass balance for the early stages of crossflow filtration. Experimental results and model predictions verify that permeate flux in crossflow membrane filtration of colloidal suspensions declines more rapidly with increasing transmembrane pressure, and when filtering suspensions with higher feed particle concentration and smaller particle size.

Cho (1998) developed a gel resistance model for a membrane filtration. The development required an understanding of the factors related to NOM fouling. Considerable research in this area had revealed that the NOM accumulation at the membrane surface is dependent on operating parameters (e.g., pressure, feedwater velocity) and properties of the NOM, feed water, and membrane.

Afonso et al. (1998) studied mass transfer of salt in the tangential turbulent flow inside a nanofiltration tubular membrane. This could be described by a modified eddy diffusive model, which accounts for the effect of high permeation fluxes on the mass transfer rates through permeation Reynolds number. For the mass transfer to be modeled, the following phenomena were then considered: concentration polarization in the feed solution; Donnan equilibrium in the interfaces feed-membrane active layer and permeate-membrane active layer; diffusion, convection, and electromigration in the membrane active layer, described by the extended Nernst-Planck equations. The prediction of the nanofiltration performance in terms of permeation fluxes and salt rejections is achieved through an integrated model, considering the mass transfer mechanisms both in the feed solution adjacent to the membrane and in the membrane phase.

Bowen and Mohammad (1998) developed a predictive model for the performance of a nanofiltration membrane in separating the components of a dye/salt solution. A diafiltration process involving a mixture of dye and NaCl has been modeled

using a Donnan-steric pore model which was based on the extended Nernst-Planck equation. Finally, the model was used to investigate optimization of the processing conditions and also the membrane parameters.

Bhattacharjee et al. (1998) described the mechanism of concentration polarization of interacting solute particles in cross-flow membrane filtration and permeate flux declination during cross-flow membrane filtration. In this work, the solution was assumed to be a pseudo-one-component system. The mathematical model was illustrated as the steady-state differential solute material balance in the polarized layer.

Williams et al. (1999) proposed the predictive reverse osmosis model for the application to dilute organic-water systems. This research established the permeate flux quality and flux drop characteristics of membrane involving the separation of dilute organic (nonionized and ionized) pollutants and to develop a transport theory based on fundamental diffusion-adsorption models. Two models are presented in this work: a modified steady-state solution diffusion model and an unsteady-state diffusion adsorption model which are able to predict flux and permeate concentrations from a single reverse osmosis experiment.

De Carlo and Meirina (2000) developed a simplified time domain process model of ultrafiltration in hemodialysis. Using a variable displacement pump to control the dialysate flow rate, a transmembrane pressure gradient is generated to force excess water in the blood to flow across the membrane into the dialysate. This work investigates the modeling and adaptive control the ultrafiltration process for a single pass delivery system. The controller design takes an adaptive PID approach to control the ultrafiltration process based on a physical model of the filtration process.

Jounela and Oja (2000) studied the modeling module for a pressure filter. Their work presents the intelligent control system designed for a variable-volume pressure filter. The system consists of the modeling, classification, economic, fault diagnosis and control modules. The modeling module of the intelligent system predicts

filtration using the two-stage hybrid model. The first stage model is based on a numerical model for compressive cake filteration and the second stage model is the identified grey-box model based on the classical filtration model.

Chieh Tu et al. (2001) studied a membrane transport model, developed for prediction and simulation of nanofiltration dynamics with refference to permeate flux. The important membrane transport phenomena that affect to flux decline contain concentration polarization and gel layer formation. Membrane filtration tests using tannic acid as a model organic compound were designed for investigating permeate flux, as well as solute concentration profiles for permeates and concentrates. The experiments were conducted under various operating conditions by varying several parameters including solute concentration, transmembrane pressures, and reject flow rates.

Van Der Bruggen and Vandecasteele (2001) studied different mechanisms of flux decline for the nanofiltration of aqueous solutions containing organic compounds. Experiments with different organic components in aqueous solution showed that adsorption resulted in a strong decrease of the water flux. The results of flux decline as a function of the concentration could well be fitted with the Freundlich equation for adsorption. This research focuses on pore blocking and adsorption inside the membrane pores. Blocking of the pores by adsorbed compounds was studied to explain mechanism of flux decline.

Alvarez et al. (2001) developed the model to predict flux and aroma compounds rejection in a reverse osmosis concentration of apple juice. The equations describing mass transport in the membrane were developed from flux equations of the system and the film theory. In this work, the permeability of the membrane and the solute transport parameters were determined from the experiments with water and with aqueous solutions of apple juice aroma compounds, respectively.

Timmer (2001) proposed the use of nanofiltration for concentration and demineralization in the dairy industry. Models were developed, based on the extended

Nernst-Planck equation, which describe the salt rejection as a function of the flux for binary and ternary salt solutions. Effects of concentration polarization, composition of feed and concentration are incorporated in the model. Furthermore, mass transfer in boundary layer and mass transfer inside the membrane were calculated separately and the distribution of the solute at the membrane/boundary layer interface was described.

Lee et al. (2002) proposed determination of mass transport characteristics for natural organic matter (NOM) in ultrafiltration and nanofiltration membranes. This study is mainly concerned with establishing a reliable method of the quantitative analysis of natural organic matter transport characteristics through ultrafiltration and nanofiltration membranes with molecular weight cutoffs of 8000 (GM) and 250 (ESNA), respectively.

Bowen et al. (2002) developed the linearized transport model for nanofiltration. Finite difference linearization of pore concentration gradient in nanofiltration membranes simplified the solution of a three-parameter model for electrolyte rejection by removing the requirement for numerical integration of the extended Nernst-Planck equation. The validity of the linearized model was first experimentally tested by comparing with a rigorous characterization of the Desal-DK nanofiltration membrane. Overall, the model was powerful tool for characterization of nanofiltration membranes and subsequent prediction of separation performance due to the removal of the need for complex nonlinear numerical methods through the reduction of the governing equations to algebraic expressions.

2.2 Generic Model Control (GMC)

Lee and Sullivan (1988) proposed a model-base control algorithm, GMC capable of using nonlinear process model directly. In GMC scheme, first-principles models derived from dynamic material and energy balances are mostly used. The direct implement of the nonlinear process model could be imbedded into the GMC controller without resorting to linearization. They generalized relatively easy GMC framework that relied upon the process model to approximate plant behavior. In 1989, Lee et al. extended the application of the model bases GMC controller to forced circulation single-stage evaporator. The control strategy employing a process model derived from fundamental mass and energy balances was shown to outperform single loop and predictive control strategies by a significant amount. The control structure was first presented in general form and then specifically applied to this process. Later, Lee et al. (1991) applied the use of GMC for controlling the level in a surge tank. This work focuses on the effect of certain user–selectable parameters on the controlled response to changes in the inlet flow rate and model inaccuracies. The overall algorithm was shown to be significantly lower in computational requirements than previously proposed algorithms for surge tank control. Implementation was straightforward and was suitable for even small-scale process control computing systems.

Cott and Macchietto (1989) presented a new model-based controller for the initial heat-up and subsequent temperature maintenance of exothermic batch reactors. The controller was developed by using the Generic Model Control framework of Lee and Sullivan, which provided a rigorous and effective way of incorporating a nonlinear energy balance model of the reactor and the heat-exchange apparatus into the controller. It also allowed the use of the same control algorithm for both heat-up and temperature maintenance, thereby eliminating the need to switch between two separate control algorithms as was the case with today's more commonly used strategies. A deterministic on-line estimator was used to determine the amount and rate of heat released by the reaction. This information was, in turn, utilized to determine the change in jacket temperature setpoint in order to keep the reaction temperature on its desired trajectory.

The performance of the new GMC-based controller was compared to that of the commonly used dual-mode controller. Simulation studies showed the new controller to be as good as the dual-mode controller for a nominal case for which both controllers were will tuned. However, the new controller was shown to be much more robust with respect to changes in process parameters and to model mismatch.

Kershenbaum and Kittisupakorn (1994) studied a temperature control of a batch reactor using GMC controller. In this study, the amount of heat released by the reactions had been estimated online using an extended Kalman filter, and incorporated into the GMC algorithm. Simulation results had shown that the Kalman filter gave an accurate estimate of the amount of heat released and together with the GMC controller, gave reliable robust control. An experimental extension of the work using the PARSEX (Partially simulated Exothermic) reactor showed that the extended Kalman filter was rather more sensitive to plant/model mismatch than would have been predicted from simulations alone.

Farrell and Tsai (1995) implemented a GMC algorithm for batch crystallization process. The resulting algorithm which was called batch GMC (BGMC) algorithm utilized a time variant reduced-order input-output model derived by correlating historical data of solubility vs. weight mean size. Control of the weight mean size trajectory in response to seed disturbances was demonstrated in this paper.

Khandalekar and Riggs (1995) applied the nonlinear process model based control (PMBC) to the Amoco/Lehigh University Model IV FCC industrial challenge problem. In particular, PMBC was applied for the control of reactor temperature, regenerator temperature and the flue gas oxygen concentration. The GMC law was used for the nonlinear PMBC controller. Both the nonlinear PMBC and conventional PE controllers were tested first for the unconstrained control. Finally, the nonlinear PMBC constraint controllers were used for optimization studies to analyze the operation at the economic optimum in the face of variations in feed characteristics and variations in operative constraints.

Vega et al. (1995) used a dynamic model of the evolution of the temperature of a batch cooling crystallizer for the development of a GMC system for the crystallizer. This servo-control system had been found experimentally to work adequately. The crystallizer had also been controlled with a conventional PI controller, and the process had been simulated with the model. Simulations were accurate enough to allow the model to be used for the design of control strategies for programmed cooling crystallizers. The methodology described could be adapted to the study of other systems or control algorithms.

Dunia and Edgar (1996) improved a generic model control algorithm for linear systems. This work evaluated the basic GMC algorithm when applied to SISO linear processes and provided insight regarding its limitation to ensure robust stability. The basic algorithm of GMC was presented as a special case of feed-back linearization. The effect of sampling time on the reference trajectory for discrete systems was analyzed in order to avoid unstable responses for perfect models. Finally, a predictive GMC was developed to handle models with dead time in a reliable way.

Nussara (1999) presented the application of GMC to control the temperature of a batch polyvinyl chloride polymerization reactor. In this work, heat released of reactions was needed in the GMC formulation but not available for measurement, on-line heat released estimator was used to estimate the heat released of the reactions. The GMC controller coupled with the estimator could give better control performance than the PID controller could. Furthermore, the GMC controller was more robust than the PID controller in the presence of plant/model mismathches.

Aziz et al. (2000) designed and implemented three different types of controllers namely PI,PID (both in DM strategy) and GMC controllers to track the optimal reactor temperature profiles using a complex reaction scheme in a batch reactor. Off-line optimal control problem had been formulated and solved to obtain the optimum temperature profiles (dynamic set point for controllers) to maximize the amount of the desired product while minimizing the waste by-product. Neural network technique was

used as the on-line estimator the amount of heat released by the reaction within the GMC algorithm. The GMC controller coupled with a neural network was found to be more effective and robust than the PI and PID controllers in tracking the optimal temperature profiles to obtain the desired products on target.

Xie et al. (2000) developed a quqadratic programming-based optimization algorithm, which had the ability to handle linear constraints of manipulated and controlled variables and their moving velocities. By combination of the proposed optimization algorithm with the generic model control scheme, a novel approach to constrained generic model control based on quadratic programming was proposed for nonlinear affine systems with relative order one. Computer simulation results show that the proposed approach had definite robustness against process/model parameter mismatches, it could be applied in real time, and it appeared to hold a considerable promise in process control.

Meethong (2002) studied the GMC for a concentration control of continuous stirred tank reactor with first-order exothermic reactor, which was the process of relative degree two. This research used an internal controlled variable, the key component that made the control variable to be effected directly like the relative degree one processes. The results showed that the GMC with internal controlled variable could use the techniques that improved the robustness like a conventional GMC.

Moolasartsatorn (2002) recently implemented GMC coupled with extended Kalman Filter (EKF) for a pervaporative membrane reactor thatestorification of acetic acid and butanol was considered. Both optimal temperature set point and optimal temperature profile obtained in the off-line optimization were tracked in this research.

2.3 Optimization

Tremblay and Luus (1989) proposed to present a computational procedure to enable one to examine benefits to be expected from non-steady-state operation of chemical reactors. Three examples showed that the proposed algorithm using dynamic programming can be used for a wide variety of problems, such as to maximize the yield, average rate of production or average concentration overtime. It was found that dynamic programming performed well even for a 6^{th} order system. The optimum period, split of period and amplitude of the input could be obtained in a reasonable computation time when the optimal input signal was in fact periodic in nature.

Chang and Hseih (1995) proposed an integrated method for optimization and control of semibatch reactors. Based on the desired control objective, dynamic programming was applied to obtain optimal operating trajectories. Yield optimization was assured for a real plant by tracking model-dependent optimal trajectories according to the proposed modified globally linearizing control (MGLC) structure. The behavior of the proposed MGLC structure was predictable and reliable, with tuning parameters based on the proposed tuning method if the manipulated variables were not constrained.

Garcia et al. (1995) converted the optimal control problem into a nonlinear programming problem solved by the generalized reduced gradient procedure coupled with the golden search method, for the search of the total batch time for fine chemical productions in batch reactors. The efficiency of the methodology was shown by its application to different formulations of the problem for different chemical reaction schemes and with stress laid on the influence of the constraints on the limitation of temperature variations and byproduct formation.

Chang et al. (1996) proposed an integrated method for optimization and control of batch reactors. Based on the desired performance index, the modified two-step method was applied to optimize an operating trajectory. Yield optimization was assured for a real plant by tracking the model-dependent optimized trajectory through the

proposed modified globally linearizing control (MGLC) structure. Experimental results revealed that the proposed MGLC structure could be applied in tracking an operating trajectory determined on-line or off-line.

Rojnuckarin and Floudas (1996) applied an optimal control strategy to the problem of finding the flux profiles for the conversion of methane to ethylene and acetylene in a plug flow reactor. The optimal control approach implemented in the paper belonged to the class known as gradient methods in function space. The optimal control designs were performed with respect to the final mass fractions of ethylene and acetylene in a plug flow reactor using heat, oxygen, and chlorine fluxes as controls.

Carrasco and Banga (1997) considered the dynamic optimization (optimal control) of chemical batch reactors. The solution of these types of problems was usually very difficult due to their highly nonlinear and multimodal nature. Two algorithms based on stochastic optimization were proposed as reliable alternatives. These stochastic algorithms were used to successfully solve four difficult case studies taken from the recent literature: the Denbign's system of reactions, the oil shale pyrolysis problem, the optimal fed-batch control of induced foreign protein production by recombinant bacteria, and the optimal drug scheduling of cancer chemotherapy. The advantages of these alternative techniques, including ease of implementation, global convergence properties, and good computational efficiency, were discussed.

Guntern et al. (1998) proposed a methodology for the optimization of semibatch reactors using dynamic programming. This included synthesis of a mathematical model, analysis of the performance of the process at its present state, definition of a set of decision variables, and optimization and simplification of this optimum toward feasibility, The methodology was applied to an industrial case study in the fine chemical industry using the lowest product cost as the objective function.

Luus and Okongwu (1999) determined the optimal flow rates of heating and cooling fluids instead of finding only the optimal temperature profile, so that the

yield of a desired product in a batch reactor was maximized. The purpose of this paper was to investigate such an approach in the control of typical chemical reactors by considering two examples. By using iterative dynamic programming (IDP) in multi-pass fashion, the optimal policy could be readily obtained. Optimization as carried out on two typical batch reactor problems showed that if the heat transfer coefficient was reasonably chosen, then the optimal yield could be significantly larger than what could be expected from the best isothermal operation.

2.4 Kalman Filter

Kalman (1960) published a famous paper describing a recursive solution to the discrete data linear filtering problem. This paper formulated and solved the Wiener problem from the state point of view. The Kalman filter has been the subject of extensive research and application, particularly in the area of autonomous or assisted navigation

Alag and Gilyard (1990) presented a Kalman algorithm for estimation of unmeasured output variables for an F100 turbofan engine. The approach was based on explicitly modeling the effects of off-nominal engine behavior as biases on the measured output variables. Results were presented for estimates of the output variables and were compared with values obtained from detailed nonlinear simulation of the engine. The evaluation was carried out for both a nominal engine and an engine in which intentional deterioration was introduced. The proposed estimation algorithm was able to accurately predict the values of the output variables for the simulation studies for both nominal and degraded engine conditions. The proposed algorithm had been validated by comparing its estimates with the values from the detailed nonlinear simulation, and it had performed well on flight data.

Myers and Luecke (1991) described and illustrated an efficient new algorithm on process examples for solution of the extended Kalman filter equations for a continuous dynamic system with discrete measurements. Implicit simultaneous methods,

which were powerful in terms of accuracy and efficiency, were utilized for numerical integration. At the internal integration step level, the new algorithm exploited the decoupled nature of the state estimate and error covariance equations along with the symmetry of the error covariance matrix. The error control strategy included both the state estimates and error covariance.

Avery (1992) presented an approach to track fitting that uses an iterative algorithm to correctly account for the effects of multiple scattering and energy loss along the track trajectory. This technique, known generally as a Kalman filter, was first applied to track fitting by Billoir (1984) and was used by several CERN experiments. In this work, The tracks was measured through a two step process. First, detector measurements were put through a pattern finding algorithm to select a subset that seems consistent with belonging to a single track This set of measurements was then fit statistically through a maximum likelihood method to determine the most probable set of track parameters consistent with the measurements. Errors in these parameters were estimated from the measurement uncertainties and other factors, as discussed below. Measurements may be further eliminated during the track fit if they were found to be of sufficiently poor quality or not consistent with belonging to the track. Because of its well understood properties, the least squares algorithm was most commonly used to fit the track parameters and estimate the parameter errors.

Russell et al. (2000) investigated a model-based inferential quality monitoring approach for a class of batch systems. First, an extended Kalman filter based fixed-point smoothing algorithm was presented and compared to a popular approach to estimating the initial conditions. Subsequently, a nonlinear optimization-based approach was introduced and analyzed. A sub-optimal on-line approximation to the optimization problem was developed and shown to be directly related to the extended Kalman filter based results. Finally, some practical implementation aspects were discussed, along with simulation results from and industrially relevant example application.

Lersbamrungsuk (2000) designed and developed two software programs based on Kalman filter. The first one, named kSTAPEN+, was a software component based on Kalman filter. In kSTAPEN+, users could define their own systems including states and parameters to be estimated. After running the program, estimation results are given. The estimates obtained from the kSTAPEN+ had been compared to those obtained from the program written on Matlab. Furthermore, the program had been tested with a heater, a stirred-tank reactor and a microfeeder. In kSTAPEN-C, the component had been developed by using Component Object Model (COM) technology. The estimates obtained from kSTAPEN-C had been compared to those obtained from kSTAPEN+. Results had shown that both kSTAPEN-C and kSTAPEN+ were equivalent.

CHAPTER 3

THEORY

The aim of this work is to apply mathematical models of nanofiltration to flux control. The economics and energy consumption of membrane separation processes can be directly related to the permeate flux deterioration. Therefore, a clear understanding of nanofiltration process is necessary. To solve this problem, the model of nanofiltration is developed to predict, design, and optimise the nanofiltration process. To start model development, the first step is to establish the basic characteristics of membrane processes and the mechanisms that are responsible for the separation.

The purpose of this chapter is to provide the practical introduction to some theoretical groundwork and background information. This introduction includes a description some discussion of membrane separation process, optimization, Kalman filter, and Generic Model Control (GMC) configuration.

3.1 Membrane Separation Process

The details on a general introduction to membrane separation technology and transfer mechanism in membrane separation are provided in the following sections.

3.1.1 Introduction

Starting in the late sixties, membrane processes gradually have found their way into industrial applications and serve as viable alternatives for more traditional processes like distillation, evaporation, or extraction. Based on the main driving force, which is applied to accomplish the separation, many membrane

processes can be distinguished. An overview of the driving forces and the related membrane separation processes is given in Table 3.1 (Timmer, 2001).

Table 3.1. Driving forces and their related membrane separation processes

Driving force	Membrane processes
• Pressure difference	microfiltration, ultrafiltration, nanofiltration, reverse osmosis or hyperfiltration
• Chemical potential difference	pervaporation, pertraction, dialysis, gas separation, vapor permeation, liquid membranes
• Electrical potential difference	electrodialysis, membrane electrophoresis, membrane electrolysis
• Temperature differential	membrane distillation

This thesis will focus on pressure driven membrane separations.

Pressure driven membrane processes

Four pressure driven membrane processes are distinguished in practice:

1. Microfiltration (MF) is characterised by a membrane pore size between 0.05 and 2 µm and operating pressures below 2 bar. MF is primarily used to separate particles and bacteria from other smaller solutes.
2. Ultrafiltration (UF) is characterised by a membrane pore size between 2 nm and 0.05 µm and operating pressures between 1 and 10 bar. UF is used to separate colloids like proteins from small molecules like sugars and salts.
3. Nanofiltration (NF) is characterised by a membrane pore size between 0.5 and 2 nm and operating pressures between 5 and 40 bar. Nanofiltration is used to achieve a separation between sugars, other organic molecules and multivalent salts on one hand and monovalent salts and water on the other.
4. Reverse osmosis (RO) or hyperfiltration. Reverse osmosis membranes are considered not to have pores. Transport of the solvent is accomplished through the

free volume between the segments of the polymer of which the membrane is constituted. The operating pressures in Reverse osmosis are generally between 10 and 100 bar and this membrane process is mainly used to remove water.

Nanofiltration is a form of pressure driven filtration that uses membranes to preferentially separate different fluids or ions. Nanofiltration is a membrane liquid separation technology that is positioned between reverse osmosis and ultrafiltration. The filtration process takes place on a selective separation layer formed by a semipermeable membrane. The driving force of the separation process is the pressure difference between the feed (retentate) and the filtrate (permeate) side at the separation layer of the membrane. However, because of its selectivity, one or several components of a dissolved mixture are retained by the membrane despite the driving force, while water and substances with a molecular weight < 200 D are able to permeate the semipermeable separation layer. Because nanofiltration membranes also have a selectivity for the charge of the dissolved components, monovalent ions can pass the membrane and divalent and multivalent ions are rejected.

The basic processes in membrane separation are dead–end and cross flow filtration. Comparison of dead-end and cross flow filtration are illustrated in figure 3.1.

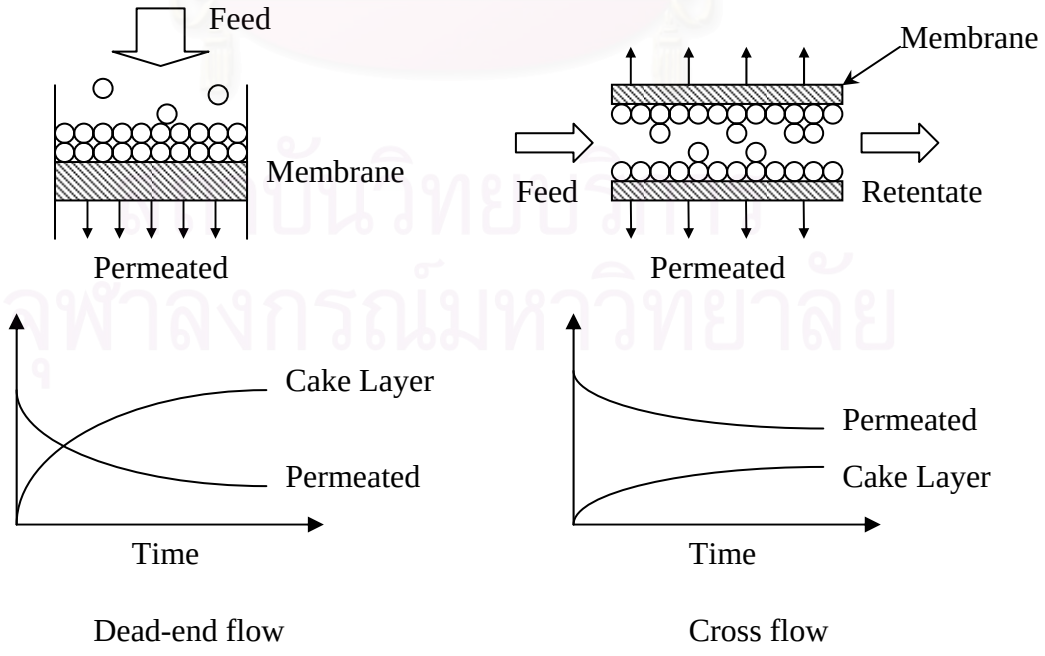

Figure 3.1. Comparison of dead-end and cross flow filtration

Membranes are manufactured as flat sheets, hollow fibers, capillaries, or tubes, for practical applications membranes are installed in a suitable device, which is referred to as membrane module. The most commonly used devices are pleated cartridges, tubular and capillary membrane modules, plate-and-frame and spiral-wound modules, and hollow-fiber modules. There are several other module types used in special applications, such as the rotation cylinder and the transversal flow capillary module. The key properties of efficient membrane modules are high packing density, good control of concentration polarization and membrane fouling, low operating and maintenance costs, and cost-efficient production. For the efficiency of a membrane process in a certain application, the choice of the proper membrane module is of great importance.

3.1.2 Mass Transfer in Nanofiltration

The membrane process is applied for separate or increase concentration of the species in mixture. The most important property of membranes is their ability to control the rate of permeate of different species. The two models used to describe the mechanism of permeation are illustrated in figure 3.2.

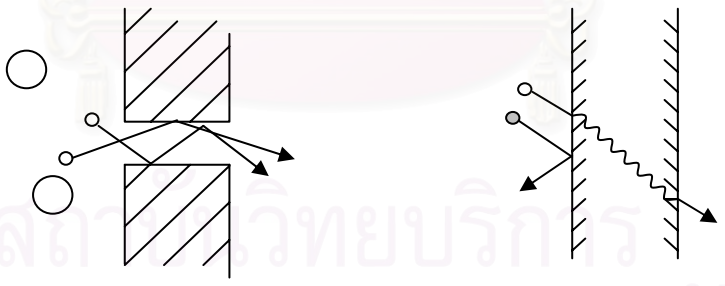

Microporous membranes separate by molecular filtration

Dense solution-diffusion membranes separate because of differences in the solubility and mobility of permeants in the membrane material

Figure 3.2. Molecular transport through membranes can be described by a flow through permanent pores or by the solution-diffusion mechanism.

One model is the solution-diffusion model, in which permeant dissolved in the membrane material and then diffuse through the membrane down a concentration gradient. The permeants are separated because of the differences in the solubilities of the materials in the membrane and the differences in the rates at which the materials diffuse through the membrane. The other model is the pore flow model that permeants are transported by pressure-driven convective flow through tiny pores. Separation occurs because one of the permeants is excluded from some of the pores in the membrane through which other permeants move.

Diffusion, the basis of the solution-diffusion model, is the process by which matter is transported from one part of a system to another by a concentration gradient. The individual molecules in the membrane medium are in constant random molecular motion, but in an isotropic medium, individual molecules have no preferred direction of motion. Although the average displacement of an individual molecule from its starting point can be calculated, after a period of time nothing can be said about the direction in which any individual molecule will move. However, if a concentration gradient of permeate molecules is formed in the medium, simple statistics show that a net transport of matter will occur from the high-concentration to the low-concentration region.

Mass transfer through nanofiltration membrane is usually described by the solution diffusion model (Strathmann et al., 1979). The driving force for solvent flow is the pressure gradient across the membrane. Solute transport in the membrane, according to the solution diffusion model, is driven by the concentration gradient of solute across the membrane (Timmer, 2001). In the solution diffusion model it is further assumed that no coupling between solute and solvent transport is present (Pusch, 1986). However, this assumption is not always valid. Drag by solvent flow may cause additional transfer of solute through the membrane. For the mass transfer in nanofiltration to be modeled, the following phenomena are then considered; concentration polarization in feed solution and advection-diffusion mechanisms. A representation of the mass transfer process occurring in nanofiltration is given in figure 3.3.

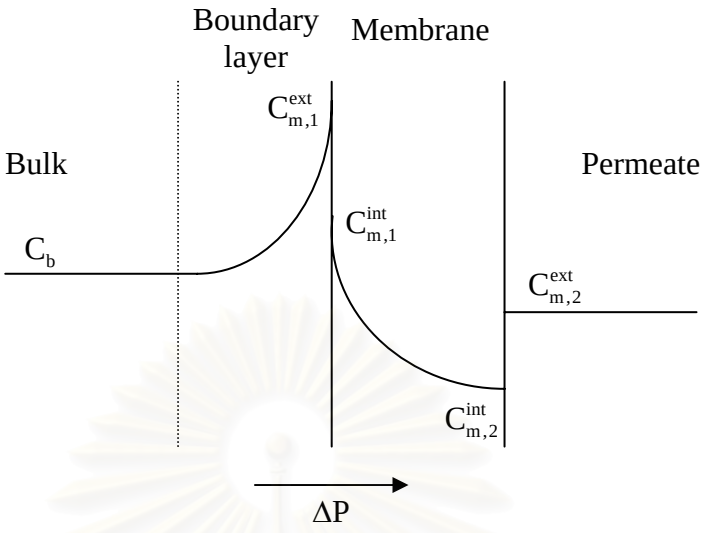

Figure 3.3. Mass transfer in nanofiltration

When an external pressure ΔP is imposed on a liquid which is adjacent to a semi-permeable membrane, solvent will flow through the membrane. A neutral solute dissolved in the solvent at a concentration level C_b will also flow towards the membrane. If the membrane exhibits rejections for the solute, partial permeation will occur and non-permeated solute accumulates in the boundary layer, and hence a concentration profile develops. This phenomenon is called concentration polarization (Mulder, 1991; Cheryan, 1998). Thesolute distributes at the membrane/solution interface and will be transported through the membrane by convection and diffusion. At the permeate side, a second distribution process will occur and a final concentration of solute in the permeate, $C_{m,2}^{ext}$, will be reached.

The fundamental equation of membrane transport model is the classic is advection-diffusion equation. The general form of the advection-diffusion equation for a binary system (solute/solvent system) can be written as show below:

$$\frac{\partial C}{\partial t} + v \cdot \nabla C = D\nabla^2 C \qquad (3.1.1)$$

Where C is the concentration of the solute and D is the diffusivity of the solute in the solvent phase.

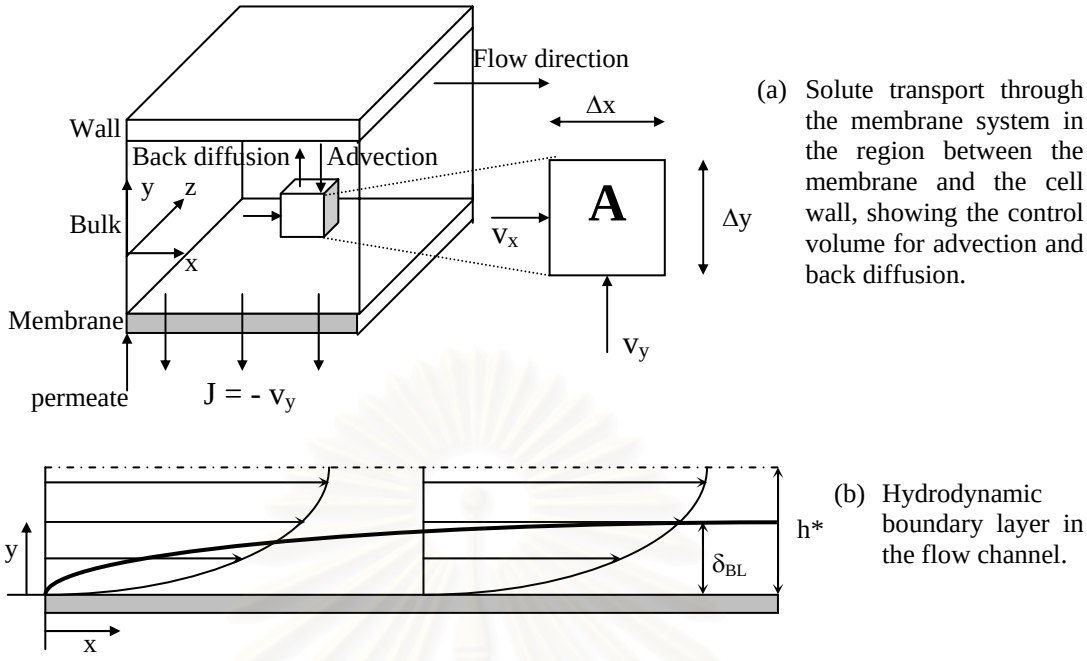

Figure 3.4. Mathematical representation of mass transport in the membrane module.

The proposed membrane transport model considers only the solute mass transfer in the region between the membrane surface and membrane cell wall. And internal pore fouling is neglected. The mathematical model that represent solute transport through the membrane system in the region between the membrane and the membrane cell wall is illustrated in figure 3.4. Marked A in the figure 3.4 is the control volume for advection and back diffusion. According to the rectangular Cartesian coordinate system, the bulk solution flow between the membrane and the membrane cell wall in the x-direction. The solute transport occurs in the y-direction that is controlled by advection from bulk solution to the membrane and diffusion from membrane surface back to the bulk solution. It must be noted that the advective and diffusive transport mechanisms are not exactly balanced before steady state, and consequently the concentration polarlization and gel layers exhibit variable thickness with time. The advection-diffusion equation, shown in equation (3.1.1), developed for the control volume that is illustrated in figure 3.4 can be simplified using the following assumptions:

1. No concentration gradient exists in the z-direction; that is$\partial C/\partial z$ and $\partial C^2/\partial z^2$ are equal to zero.

2. The concentration gradient in the direction of product flow ($\partial C/\partial x$) can be considered negligible in comparison with $\partial C/\partial y$.

According to the preceding assumptions and considering the relation $v_y = -J_v$, equation (3.1.1) can be transformed as

$$\frac{\partial C}{\partial t} - J_v \frac{\partial C}{\partial y} = D \frac{\partial^2 C}{\partial y^2} \qquad (3.1.2)$$

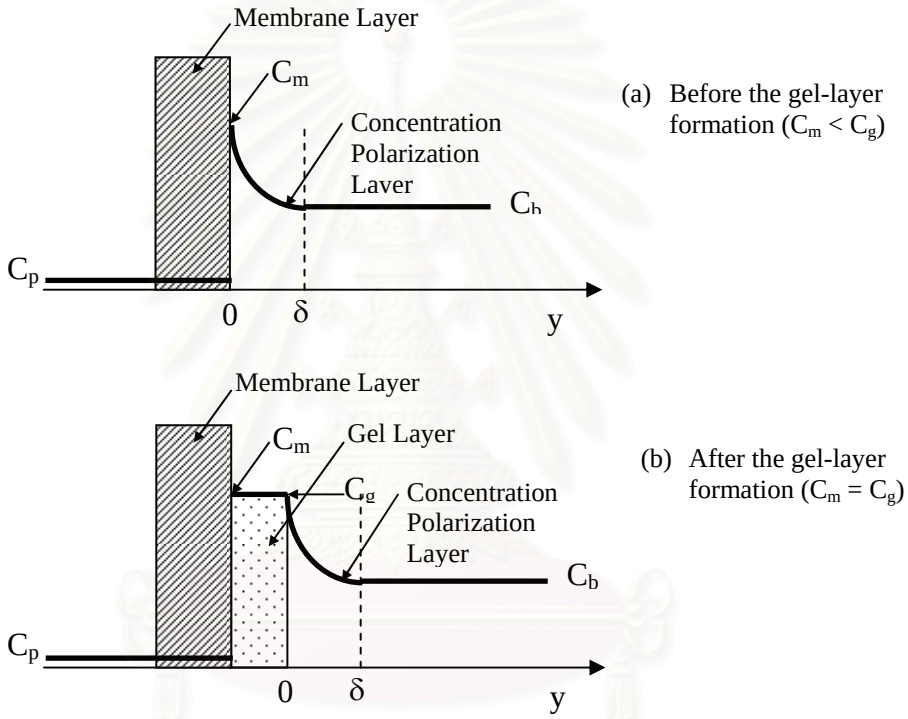

Figure 3.5. Concentration profiles of the proposed model without internal fouling.

As illustrates in figure 3.5, The boundary conditions for equation (3.1.2) can be written as follows.

For the temporal and spatial stages before the gel-layer formation ($C_m < C_g$), figure 3.5(a).

at $t = 0$, $C = C_{m,0} = C_{b,0}$

at $y = \delta$, $C = C_b$

at $y = 0$, $J_v C_m = -D \left(\frac{\partial C}{\partial t}\right)_{y=0}$

For the temporal and spatial stages after the gel-layer formation ($C_m = C_g$), figure 3.5(b).

at $y = L + \delta$, $C = C_b$

at $y \leq L$, $C = C_b$.

Under steady-state conditions ($dC/dt = 0$), the solution to equation (3.1.2) with the boundary conditions becomes

$$J_v = \frac{D}{\delta} \ln \frac{C_m}{C_b} = k \ln \frac{C_m}{C_b}, \qquad (3.1.3)$$

where k represents the mass-transfer coefficient for solute transport through the membrane cell. After the gel-layer formation, the solute concentration on the membrane surface will equal the gel-layer concentration ($C_m = C_g$), and equation (3.1.3) can therefore be written as

$$J_v = k \ln \frac{C_m}{C_b} = k \ln \frac{C_g}{C_b}. \qquad (3.1.4)$$

Driving forces such as concentration gradient and/or pressure gradient that drive the mixture transport through the membrane separates the permeants. According to Darcy's law, permeate flux decline is caused by decreased driving forces and increased resistances (van den Berg and Smolders, 1988; Ho and Sirkar, 1992). Membrane permeate flux (J_v) can be described by the relation following:

$$\text{Flux, } J_v = \frac{\text{Driving force (such as } \Delta P, \Delta C, \text{ or } \Delta T)}{\text{Viscosity x Total resistance}} \qquad (3.1.5)$$

Concentration polarization, reversible and directly occurring phenomena, and Fouling, irreversible and long term phenomena, are two major phenomena that affect to flux decline. The resistance occurring in membrane processes could be caused by the membrane, concentration polarization, internal pore

fouling, and gel-layer formation. The resistance of virgin membrane (R_m) is a constant factor during filtration. Concentration polarization resistance increases due to solute retention by the membrane when solvent transport is facilitated. Solute accumulates on the membrane and forms a layer at the membrane interface with a relatively high concentration. The resistance due to the concentration profile layer (R_{cp}) increases during membrane filter operation until the system reach steady state. For some cases, the solution concentration at the membrane interface can reach certain high values and will progressively evolve into a gel layer accumulation on the membrane surface (R_g). Internal pore fouling occurring inside the membrane can also lead to permeate flux decline (R_{in}).

The advantage of membrane processes are summarized below:

1. In the membrane processes, each species are separated by difference of molecular size so the processes can be operated at normal temperature. Then the membrane processes are suitable to separate species that decline by heat.
2. Most of the membrane processes consume lower energy than other separation processes because they are not necessary to change phase.
3. Because both of permeate and retentate are products of the membrane processes, it dose not generate waste.
4. Most of membrane units are designed for high separation area per volume of module so they are compact.
5. The membrane processes can operate as batch or continuous processes. And they are not complicated to install automatic process control.

The disadvantage of membrane processes are summarized below:

1. Accumulation of solute particles on retentate side, known as “concentration polarization”, is cause of high concentration at membrane surface and flux decline.
2. Flux decline due to fouling in the membrane pores and surface affects to performance of membrane processes.
3. Membranes stability is limited by their material such as; cellulous membranes are appropriate to operate at pH 4-8.

3.2 Optimization

Optimization is the use of specific methods to determine the most effective and efficient solution to a problem or design for a process. This technique is one of the major quantitative tools in industrial decision making. A wide variety of problem in the design, construction, operation, and analysis of chemical plants (as will as many other industrial processes) can be resolved by optimization (Edgar et al., 2001).

3.2.1 The Essential Features of Optimization Problems

The essential elements of the optimization problems are:

1. Objective function,
2. Decision variable,
3. Constraint.

The objective function is a mathematical function that, for the best values of the decision variables, reaches a minimum (or maximum). Thus, the objective function is the measure of value or goodness for the optimization problem. There may be more than one objective function for a given optimization problem. There are different types of objective function depending on the needs and uses.

The decision variables are those independent variables over which the engineer has some control. These can be continuous variables such as temperature or discrete (integer) variables such as number of stages in a column.

Constraints are values that indicate the ability and limit of the feasible path of the process. Constraints can be classified into two types as follow:

1. Equality constraints are constraints that indicate the limits of the process or its product such as the purity of the products, mass and energy balance.
2. Inequality constraints are constraints that indicate the limit due to design and other limits

Constraints in optimization arise because a process must describe the physical bounds on the variables, empirical relations, and physical laws that apply to a specific problem. Examples of equality and inequality constraints follow:

- Production limitations,
- Raw material limitations (e.g., limitation of feedstock supplies),
- Safety or operability restrictions (e.g., temperature, pressure),
- Environmental limitations (e.g., production of toxic material),
- Physical property specifications on products.

The optimization models represent problem choices as decision variables and seek values that maximize or minimize objective functions of the decision variables subject to constraints on variable values expressing the limits on possible decision choices. The optimization model description is stated as:

$$\begin{array}{lll} & f(\mathbf{x}) & \text{objective function} \\ \text{Subject to:} & \boldsymbol{h(x)} = \mathbf{0} & \text{equality constraints} \\ & \boldsymbol{g(x)} \geq \mathbf{0} & \text{inequality constraints} \end{array} \qquad (3.2.1)$$

where $\boldsymbol{x}$ is a vector of n decision variables ($x_1, x_2, \ldots, x_n$),

$\boldsymbol{h(x)}$ is a vector of equations of dimension m_1,

$\boldsymbol{g(x)}$ is a vector of inequalities of dimension m_2.

An efficient and accurate solution to this problem is not only dependent on the size of the problem in terms of the number of constraints and decision variables but also on characteristics of the objective function and constraints.

From equation (3.2.1), it is unconstrained problem if there are no constraint functions and no bounds on the x_i. Linear Programming (LP) refer to problems in which both the objective function and the constraints are linear. More difficult to solve is the Nonlinear Programming (NLP) problem in which the objective functions and constraints may be nonlinear functions of the decision variables.

3.3 Kalman Filter

To develop advanced control system for filtration process performance, uncertainty parameters and unmeasurable variables must be estimated. Therefore, estimation is a necessary procedure in control strategy to estimate measured and unmeasured process data and reduce errors from mathematical model in order to force the process to satisfied state. The Kalman filter is an efficiently estimated technique. It is a tool that can estimate the variables of a wide range of processes. The Kalman filter not only works well in practice, but it is theoretically attractive because it can be shown that of all possible filters, it is the one that minimizes the variance of the estimation error. Kalman filter is often implemented in embedded control systems because in order to control a process, process control engineers first need an accurate estimate of the process variables.

The Kalman filter is a set of mathematical equations that provides an efficient computational (recursive) solution of the least-squares method. The filter is very powerful in several aspects: it supports estimations of past, present, and even future states, and it can do so even when the precise nature of the modeled system is unknown. A linear system is simply a process that can be described by the following two equations:

State equation: $$x_{k+1} = \mathrm{A}\,x_k + \mathrm{B}\,u_k + w_k \qquad (3.3.1)$$

Output equation: $$y_k = \mathrm{C}\,x_k + v_k \qquad (3.3.2)$$

In the above equations A,B, and C are matrices; k is the time index; x is called the state of the system; u is a known input to the system; y is the measured output; and the random variables w and v are the process and measurement noise, respectively. Each of these quantities are vectors and therefore contain more than one element. The vector x contains all of the information about the present state of the system, but x is not measured directly. Instead y , which is a function of x that is corrupted by the noise v , is measured.

From equation (3.3.1) and (3.3.2), the random variables w and v are assumed to be independent of each other and with normal probability distributions

$$P(w) \approx N(0,Q), \tag{3.3.3}$$

$$P(v) \approx N(0,R). \tag{3.3.4}$$

In practice, the process noise covariance Q and measurement noise covariance R matrices might change with each time step or measurement, however here they are assumed to be constant.

The $n \times n$ matrix A in the difference equation equation (3.3.1) relates the state at the previous time step k to the state at the current step k+1, in the absence of either a driving function or process noise. Note that in practice A might change with each time step, but here we assume it is constant. The $n \times l$ matrix B relates the optional control input $u \in R^l$ to the state x. The $m \times n$ matrix C in the measurement equation equation (3.3.2) relates the state to the measurement y_k. In practice C might change with each time step or measurement, but here it is assumed as constant.

3.3.1 The Computational Origins of the Filter

Define $\hat{x}_{k+1|k}$ to be a priori state estimate at step k+1 given knowledge of the process prior to step k+1, and $\hat{x}_{k+1|k+1} \in R^n$ to be a posteriori state estimate at step k+1 given measurement y_{k+1}.Thus, a priori and a posteriori estimate errors can be definded as

$$e_{k+1|k} = x_{k+1} - \hat{x}_{k+1|k}\ , \tag{3.3.5}$$

and

$$e_{k+1|k+1} = x_{k+1} - \hat{x}_{k+1|k+1}\ . \tag{3.3.6}$$

The a priori estimate error covariance is then

$$P_{k+1|k} = E[e_{k+1|k} \cdot e_{k+1|k}^T]\ , \tag{3.3.7}$$

And the a posteriori estimate error covariance is

$$P_{k+1|k+1} = E[e_{k+1|k+1} \cdot e_{k+1|k+1}^T] \ . \qquad (3.3.8)$$

In deriving the equations for the Kalman filter, calculation begin with the goal of finding an equation that computes an a posteriori state estimate $\hat{x}_{k+1|k+1}$ as a linear combination of an a priori estimate $\hat{x}_{k+1|k}$ and a weighted difference between an actual measurement y_k and a measurement prediction $C\hat{x}_{k+1|k}$ as shown below in equation (3.3.9).

$$\hat{x}_{k+1|k+1} = \hat{x}_{k+1|k} + K_{k+1}(y_{k+1} - C_{k+1}\hat{x}_{k+1|k}) \qquad (3.3.9)$$

The difference $(y_{k+1} - C_{k+1}\hat{x}_{k+1|k})$ in equation (3.3.9) is called the measurement innovation, or the residual. The residual reflects the discrepancy between the predicted measurement $C\hat{x}_{k+1|k}$ and the actual measurement y_k. A residual of zero means that the two are in complete agreement.

The $n \times m$ matrix K in equation (3.3.9) is chosen to be the gain or blending factor that minimizes the a posteriori error covariance equation (3.3.8). This minimization can be accomplished by first substituting equation (3.3.9) into the above definition for $e_{k+1|k+1}$, substituting that into equation (3.3.8), performing the indicated expectations, taking the derivative of the trace of the result with respect to K, setting that result equal to zero, and then solving for K. For more details see (Maybeck 1979; Jacobs 1993; Brown and Hwang 1996). One form of the resulting K that minimizes equation (3.3.8) is given by

$$K_{k+1} = P_{k+1|k}C_{k+1}^T(C_{k+1}P_{k+1|k}C_{k+1}^T + R_{k+1})^{-1} \qquad (3.3.10)$$

From equation (3.3.10) show that as the measurement error covariance R approaches zero, the gain K weights the residual more heavily. Specially,

$$\lim_{R_{k+1}\to 0} K_{k+1} = C_{k+1}^{-1}.$$

On the other hand, as the a priori estimate error covariance $P_{k_{+1}|k}$ approaches zero, the gain K weights the residual less heavily. Specially,

$$\lim_{P_{k+1|k}\to 0} K_{k+1} = 0.$$

Another way of thinking about the weighting by K is that as the measurement error covariance R_{k+1} approaches zero, the actual measurement $y_{k_{+1}}$ is trusted more and more, while the predicted measurement $C\hat{x}_{k+1|k}$ is trusted less and less. On the other hand, as the a priori estimate error covariance $P_{k+1|k}$ approaches zero the actual measurement y_{k+_1} is trusted less and less, while the predicted measurement $C\hat{x}_{k+1|k}$ is trusted more and more.

3.3.2 The Kalman Filter Algorithm

The Kalman filter estimates a process by using a form of feedback control: the filter estimates the process state at some time and then obtains feedback in the form of (noisy) measurements. As such, the equations for the Kalman filter fall into two groups: time update equations and measurement update equations. The time update equations are responsible for projecting forward in time the current state and error covariance estimates to obtain the a priori estimates for the next time step. The measurement update equations are responsible for the feedback—i.e. for incorporating a new measurement into the a priori estimate to obtain an improved a posteriori estimate.

The time update equations can also be thought of as predictor equations, while the measurement update equations can be thought of as corrector equations. Indeed the final estimation algorithm resembles that of a predictor-corrector algorithm for solving numerical problems as shown below in figure 3.6.

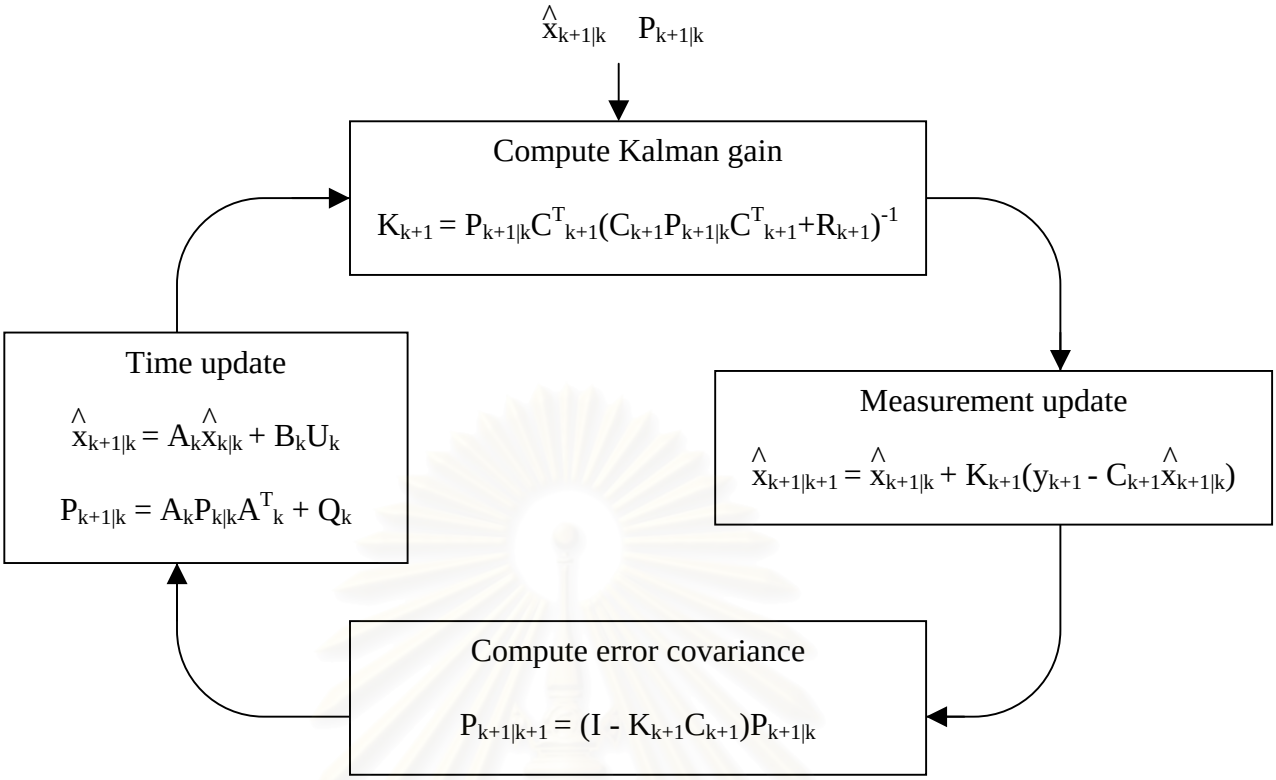

Figure 3.6. The ongoing Kalman filter cycle.

Figure 3.6 shows schematically the steps involved in the execution of the Kalman filter. The time update projects the current state estimate ahead in time. The measurement update adjusts the projected estimate by an actual measurement at that time.

The specific equations for the time and measurement updates are presented below. The predictor equations can be described by the following two equations:

(1) Project the state ahead:

$$\hat{x}_{k+1|k} = A_k\hat{x}_{k|k} + B_ku_k \ , \qquad (3.3.11)$$

(2) Project the error covariance ahead:

$$P_{k+1|k} = A_kP_{k|k}A_k^T + Q_k \ . \qquad (3.3.12)$$

Again notice how the time update equations in equation (3.3.11) and (3.3.12) project the state and covariance estimates forward from time step k to step k+1. A and B are from equation (3.3.1), while *Q* is from equation (3.3.3). Initial conditions for the filter are discussed in the earlier references.

The corrector equations can be presented by the following three equations:

(1) Compute the Kalman gain:

$$K_{k+1} = P_{k+1|k} C_{k+1}^T (C_{k+1} P_{k+1|k} C_{k+1}^T + R_{k+1})^{-1} \qquad (3.3.13)$$

(2) Update estimate with measurement y_{k+1}

$$\hat{x}_{k+1|k+1} = \hat{x}_{k+1|k} + K_{k+1}(y_{k+1} - C_{k+1}\hat{x}_{k+1|k}) \qquad (3.3.14)$$

(3) Update the error covariance

$$P_{k+1|k+1} = (I - K_{k+1} C_{k+1}) P_{k+1|k} \qquad (3.3.15)$$

The first task during the measurement update is to compute the Kalman gain, K_k. Notice that the equation given here as equation (3.3.13) is the same as equation(3.3.10). The next step is to actually measure the process to obtain y_k, and then to generate an a posteriori state estimate by incorporating the measurement as in equation (3.3.14). Again equation (3.3.14) is simply equation (3.3.9) repeated here for completeness. The final step is to obtain an a posteriori error covariance estimate via equation (3.3.15)

After each time and measurement update pair, the process is repeated with the previous a posteriori estimates used to project or predict the new a priori estimates. This recursive nature is one of the very appealing features of the Kalman filter—it makes practical implementations much more feasible than (for example) an implementation of a Wiener filter (Brown and Hwang 1996) which is designed to operate on all of the data directly for each estimate. The Kalman filter instead recursively conditions the current estimates on all of the past measurements.

3.3.3 Parameter Estimation and Tuning

In the actual implementation of the filter, the measurement noise covariance R_k is usually measured prior to operation of the filter. Measuring the measurement error covariance R_k is generally practical because process control engineers need to be able to measure the process anyway while operating the filter so they should generally be able to take some off-line sample measurements in order to determine the variance of the measurement noise.

The determination of the process noise covariance Q_k is generally more difficult because it does not have the ability to directly observe the process. Sometimes a relatively simple process model can produce acceptable results if one injects enough uncertainty into the process via the selection of Q_k. Certainly in this case one would hope that the process measurements are reliable.

The tuning of the filter parameters Q_k and R_k is usually performed off-line, frequently with the help of another (distinct) Kalman filter in a process generally referred to as system identification. Under conditions where Q_k and R_k are in fact constant, both the estimation error covariance $P_{k+1|k}$ and the Kalman gain K_k will stabilize quickly and then remain constant. If this is the case, these parameters can be pre-computed by either running the filter off-line, or for example by determining the steady-state value of $P_{k+1|k}$.

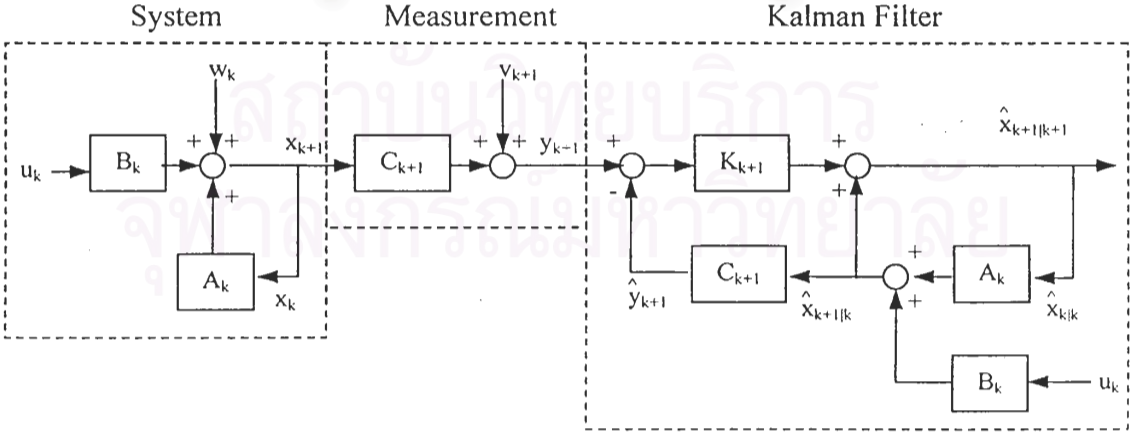

Figure 3.7 The process to by analysed by the Kalman filter

Figure 3.7 is a flowchart of the process to by analysed by the Kalman filter. Data from time step k are conducted to calculate the state from time k+1. The value of x_{k+1} is turned to calculate a new value of the state at next step and transmitted to the measurement unit. The measurement value (y_{k+1}) is sent to Kalman Filter to estimate $\hat{x}_{k+1|k+1}$. The estimated value, $\hat{x}_{k+1|k+1}$ is recurred to estimate the value of $\hat{x}_{k+1|k+1}$. These processes are repeated continuously.

3.4 Generic Model Control (GMC) Algorithm

In many chemical industries, the development of new control technology is quite motivated by practical need. This is certainly true of classical automatic process control where the emergence of the chemical process industries, with its large production volume and complex of the processes, created automatic process control technology. In process control technology with in the field of control itself, the model-based control techniques have been already developed such as State Feedback Control (SFC), Dynamic Matrix Control (DMC), Generic Model Control (GMC), and etc.

Most of membrane processes are nonlinear processes because there are nonlinear terms such as multiple terms and/or square terms of variables in the equations. Because of nonlinear of the processes, the linear control algorithm is rarely applied to control some nonlinear process. According to preceding, Using linear control algorithm is not appropriate to control nonlinear processes so nonlinear control technique application should be better than. A simple nonlinear control technique, developed by Lee and Sullivan in 1988, is Generic Model Control (GMC) that can be applied to control many SISO (Single Input Single Output) processes. The GMC, a model-based control technique, requires mathematical model of process and measured data of controlled variables in its algorithm. GMC uses a model of the process in formulating the control law. The design framework is similar to other model based approaches such as Dahlin's algorithm and IMC. However, rather than adopting a classical approach of comparing the trajectory of the process output against a desired trajectory, GMC defines the performance objective in terms of the time

derivatives of the process output, i.e. minimizing the difference between the desired derivative of the process output and the actual derivative.

A general mathematical model of process can be developed in relationship of state variables (x), manipulated variables (u), and time (t) as

$$\frac{dx}{dt} = F(x,u,t) \tag{3.4.1}$$

$$y = H(x) \tag{3.4.2}$$

where x is the vector of state variables,

u is the vector of manipulated variables,

y is the process output.

Good control performance will be given by combination of the proportional and derivative term of error. The rule of manipulated variable selection is

$$\dot{y} = K_1 e(t) + \int_0^{t_f} K_2 e(t)dt \tag{3.4.3}$$

where $e(t) = (y^* - y)$,

K_1 ,K_2 are tuning parameters of the GMC,

and y^* is the set point of out put.

From equation (3.4.3), the first term is used to control the process output to the desired target, y^* and the second term provides zero offset response.

By differentiate equation (3.4.2) becomes

$$\dot{y} = \frac{\partial H(x)}{\partial x} \cdot \frac{\partial x}{\partial t}. \tag{3.4.4}$$

Substituting equation (3.4.1) in equation (3.4.4) to obtain,

$$\dot{y} = \frac{\partial H(x)}{\partial x} \cdot F(x,u,t). \qquad (3.4.5)$$

From equation (3.4.3) and (3.4.5) the control algorithm can be written as following:

$$K_1 e(t) + \int_0^{t_f} K_2 e(t)dt = \frac{\partial H(x)}{\partial x} \cdot F(x,u,t). \qquad (3.4.6)$$

For nonlinear system with relative degree one, we can handle in linear form as following equation

$$F(x,u,t) = F'(x) + G(x) \cdot u. \qquad (3.4.7)$$

Combinating equation (3.4.6) and equation (3.4.7), gives

$$K_1 e(t) + \int_0^{t_f} K_2 e(t)dt = \frac{\partial H(x)}{\partial x} \cdot [F'(x) + G(x) \cdot u]. \qquad (3.4.8)$$

Mostly $$\frac{\partial H(x)}{\partial x} = 1$$

In general, the exact process model is rarely known, and an approximate model is introduced such that:

$$K_1 e(t) + \int_0^{t_f} K_2 e(t)dt = [F'(x) + G(x) \cdot u]. \qquad (3.4.9)$$

Considering equation (3.4.9), Ability of the GMC algorithm to handle the process depends on the accuracy of process model. Because the integral term in the algorithm ensures that the controller is robust despite modeling error, inaccuracies introduced by this approximation will be compensated by the integral term.

The process control performance is specified by choosing the values of K_1 and K_2, with the appropriate values of these parameters the process response provides the reasonable desired trajectory. These values are related to the natural

dynamic response of the process. How well the system matches this performance index is governed by how closely the chosen model matches the plant behavior. By taking Laplace transform of the equation (3.4.3), transfer function becomes,

$$\frac{y}{y^*} = \frac{2\tau\xi s + 1}{\tau^2 s^2 + 2\tau\xi s + 1} \tag{3.4.10}$$

where $\tau = \frac{1}{\sqrt{K_2}}$ and $\xi = \frac{K_1}{2\sqrt{K_2}}$ (3.4.11)

This system does not yield the same response as a classical second-order system (Stephanopoulos, 1984). However, similar plots to the classical second-order response showing the normalized response of the system y/y^* versus normalized time t/τ with ξ as a parameter can be produced and is shown in figure 3.8.

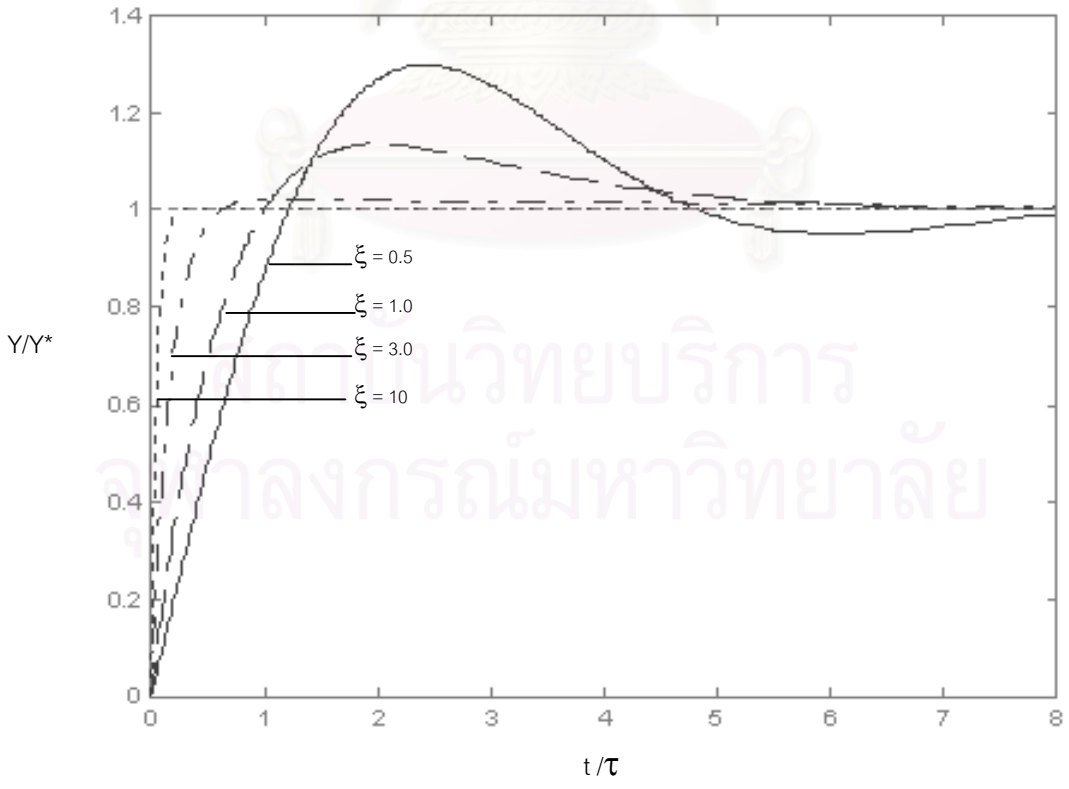

Figure 3.8. Generalized GMC profile specification

The design procedure can be specified as follows:

1. Choose ξ from figure 3.8 to obtain desired trajectory,
2. Choose τ from figure 3.8 to obtain appropriate time of response in relation to known or estimated plant speed of response,
3. Calculate K_1 and K_2 using these following equations:

$$K_1 = \frac{2\xi}{\tau}, \tag{3.4.12}$$

$$K_2 = \frac{1}{\tau^2}. \tag{3.4.13}$$

The pattern of the Generic model control shows in the following figure.

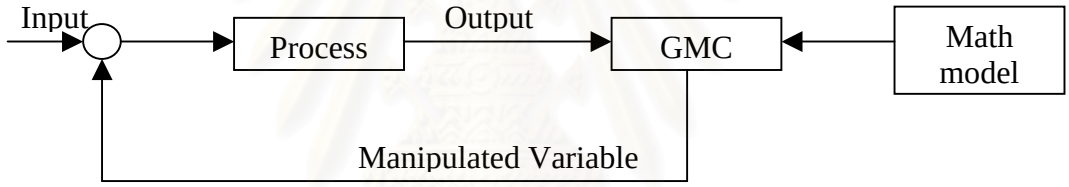

Figure 3.9. The pattern of the Generic model control

Figure 3.9 represents the GMC algorithm. The value of manipulated variable, calculated by GMC, is obtained by the model of process and measured output data. Therefore, the most important of control, using GMC, is accurate model or at least reliable model is required.

GMC has several advantages that make it a good framework for developing the process controllers:

1. The process model derived from mass and energy balances appears directly in the control algorithm.
2. The process model does not need to be linearized before use, allowing for the inherent nonlinearity of exothermic batch reactor operation to be taken into account.

3. The relationship between feedforward and feedback control is explicitly stated in the GMC algorithm.
4. Controller tuning is straightforward and easy to understand.
5. Finally and importantly, the GMC framework permits for developing a control algorithm that can be used for membrane separation process and therefore eliminates the need for a switching criterion between different algorithms; this should result in a much more robust control strategy.

Since GMC is the advanced controller based on mathematical modeling of the process so that the uncertainty of the process parameter or variable causes the poor control performance. Thus, with these conditions the estimator is imperative procedure in control strategy to evaluate these values.

3.5 GMC Coupled with Kalman filter

Since the uncertainty of the state variables and process parameters obtained with measurement or supposition, it affects to low process control performance. Hence, the estimation of these data is an important feature to efficient control operation of plants. The Kalman filter is then incorporated with GMC controller to estimate unknown parameter and variable.

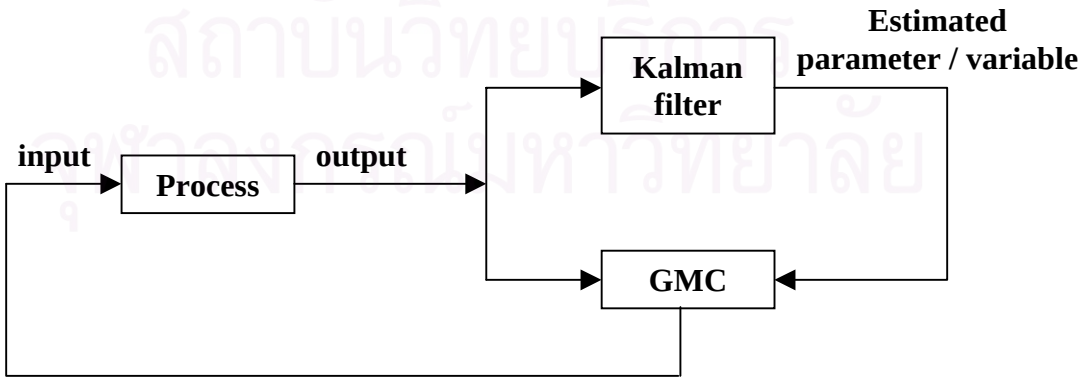

Figure 3.10. GMC integrated with Kalman filter

As seen figure 3.10, the unknown parameter and variable are estimated based on the reconciled estimates of measurements by Kalman filter algorithm. The GMC controller further calculates the control action relied upon these estimates. Thus Kalman filter is an imperative adjunct in control strategy. If the estimated quantities and the reconciled estimates are close to the actual values, the controller will give good control performance with less offset or none.

CHAPTER 4

NANOFILTRATION FOR ORGANIC COMPONENT IN AQUEOUS SOLUTION

Separation of molecules present in organic solvents by nanofiltration has a great potential in a wide range of industries from refining to fine chemical and pharmaceutical synthesis. Recently suitable organic solvent stable nanofiltration membranes have become available, and during the 1990s the first large-scale application of solvent NF was realised for lube oil solvent recovery. This research field is in its infancy, and is becoming an area of intensive study. However, there is still little information available on the processes controlling solvent fluxes and solute rejections during solvent nanofiltration. A series of papers in the last 2-3 years have presented measurements of solvent fluxes and solute rejections carried out using dead end filtration cells with pure solvents, and with dilute solutions (<1wt% solute). In actual applications however, solutes will typically be more concentrated (>5wt%) and phenomena such as concentration polarisation and osmotic pressure may contribute significantly to solvent flux, as they do in aqueous systems, which have been thoroughly studied.

In order to improve our understanding of organic solvent nanofiltration phenomena, experiments were performed in a continuous cross flow rig (plate-and frame module). In the membrane separation systems, permeate fluxes and separation properties of the membranes were determined along with their dependence on process parameters such as concentration of solution , applied pressure, and fluid flow rate.

This chapter is divided into three sections: mathematical model of a nanofiltration process, optimization study, and control study. Simulation results obtained

by simulating the optimization formulation and the formulation of a GMC controller are detailed in each section.

4.1 Process and Mathematical Model

This section describes the characteristics of membrane using in this study, the filtration process for tannic acid in aqueous solution and mathematical modeling. In this work, the membrane transport model is developed to predict the permeate flux decline in nanofiltration processes under unsteady-state conditions.

4.1.1 Membrane and Process Description

Model studies were performed with the aim of improving organic component separation from aqueous solution by nanofiltration process. In this work, a plate-and-and frame membrane system developed by Tu et al. (2001) is considered. The membranes tested in these studies were chosen from commercially available industrial products. The nanofiltration membranes used in the membrane separation tests were FilmTec NF-45 thin-film composite membranes (FilmTec Corporation, Dow Chemical Co., Midland MI). The important characteristics of the NF-45 membrane are summarized in table 4.1.

Table 4.1. Characteristics of membrane using in this study

Membrane Types	**NF-45**
Membrane material	Polypiperazine amide
Molecule weight cutoff (MWCO)	~ 200-300 Da
PH Operating range	2-11

Table 4.1. Characteristics of membrane using in this study (continued)

Membrane Types	NF-45
Contact angle	
Clean membrane	45^{o}
Exposed to 30 mg/L tannic acid	50.2^{o}
Maximum temperature, ^{o}c	45
Maximum pressure, MPa	4.1
Surface charge or surface potential (at pH of 6-9)	
Deionized distilled water	-22 mV to –33 mV
Tannic acid, 10 mg/L	-17 mV to –20 mV
Water flux (at 1.0 Mpa, clean membrane), L/m^2·h	56

Source: Redondo and Lanari, 1997; Van der Bruggen et al., 1998; Sadr Ghayeni et al., 1998

A plate-and-frame membrane system was employed in the membrane filtration experiments, which is illustrated in figure 4.1. The feed solution is pump from the feed tank to the stainless-steel plate-and-frame membranes cell, as shown in the figure. The system was maintained under high transmembrane pressures of 750-1,500 kPa (110-220 psi). The feed solutions consisted of tannic acid at concentrations in the range of 0-10 mg/L. The feed is allowed to flow into the plate-and-frame cell, and the flow rate into the cell is controlled by the recirculation flow rate into the feed tank. Permeate and reject flow rates are continuously measured. The transmembrane pressure is carefully monitored and maintained at the desired levels. The temperature of the feed is maintained at 20 ^{o}c, and the feed flow velocity is varied from 0.4 cm/s to 1 cm/s. The permeate and the concentrates are collected at their corresponding outlets as shown in the figure. Samples are obtained from the permeates and the concentrates, and are analyzed for tannic acid concentrations to evaluate the solute rejection characteristics of the membrane.

Membrane fouling is generally explained by the phenomena of boundary-layer development and gel-layer formation, as previously discussed. However, the fouling potential of a membrane is greatly influenced by its surface characteristics. Three major factors are generally believed to contribute to the flux-decline phenomenon: (1) sorption of organic molecules on membrane surface, (2) chemical interaction between membrane surface and the organic molecules, and (3) electrostatistic interactions between membrane surface and the organic molecules. Physical adsorption organic molecules on the hydrophobic sites of the membrane surface is an important factor with refference to organic rejection, but its effect on permeate flux is highly dependent on whether polymer-organic molecule interactions occur.

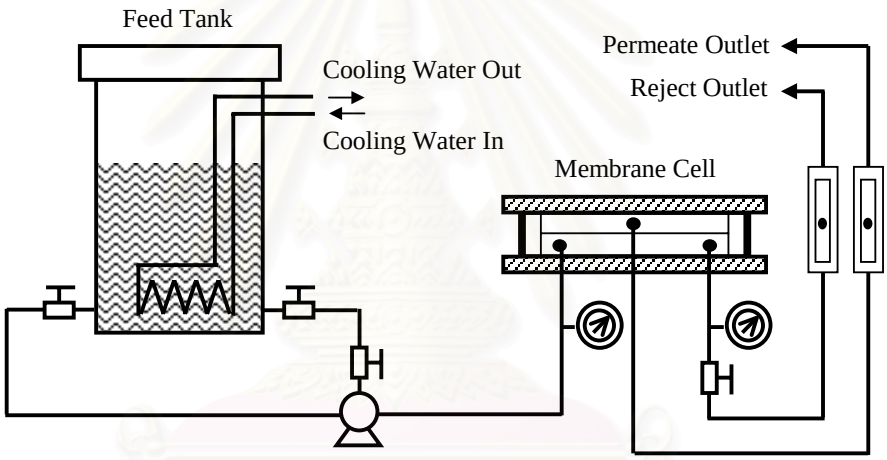

Figure 4.1. Cross flow membrane experimental setup.

Tannic acid is chosen for these tests to represent natural organic compounds present in surface and ground waters. It is a hydrophilic organic compound that contain both saccharide and aromatic acid components of significance in surface waters (Mallevialle et al., 1989). Tannic acid ($C_{76}H_{52}O_{46}$, molecular weight = 1701.22) is a derivative of glucose in which five hydroxyl groups are substituted for digalic acids, and thus contains a large number of phenolic hydroxyl groups. The molecule structure of tannic acid is presented in figure 4.2. The charge phenolic groups in tannic acid and the carbonyl groups in the membrane polymer dictate the overall surface charge that showed

in figure 4.3. Under low pH conditions, the membrane surfaces charges, mainly contributed by the charged phenolic groups generated by hydrolysis of tannic acid.

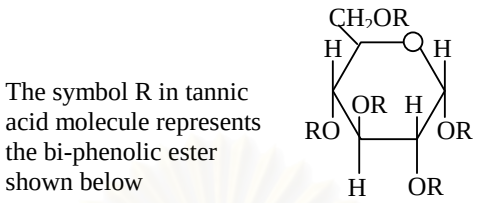

Figure 4.2. Approximate molecule structure of tannic acid.

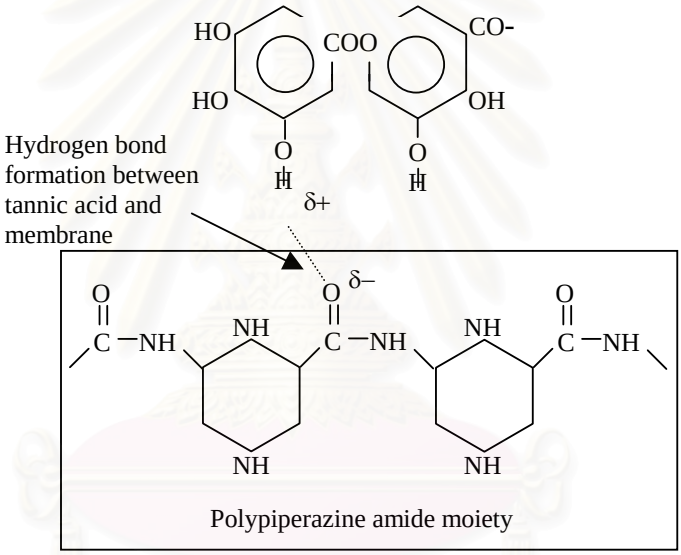

Figure 4.3. Interactions between NF-45 polypeperazine amide membrane and tannic acid.

4.1.2 Model Framework

Several key assumptions are made for the purposes of this study:

1. The filtration process is batch membrane system.
2. No solute adsorption in the membrane.
3. No internal pore fouling.
4. No effect of charge during mass transfer.

5. Thickness of the concentration polarization layer is assumed as a constant.
6. Transmembrane pressure and temperature is supposed to be constant.
7. The physical properties of solution are assumed to be constant.

Mathematical modeling of a plate-and-frame membrane system as presented in figure 4.1 can be derived under the assumptions above as follows:

$$\frac{dC_b}{dt} = \frac{A_m J_v C_b}{V_0(1-r)} \tag{4.1.1}$$

$$\frac{dr}{dt} = \frac{A_m}{V_0} J_v \tag{4.1.2}$$

where C_b is the concentration in the bulk solution,

C_p is the concentration in the permeate solution,

J_v is the permeation flux,

r *is the product recovery* $= \dfrac{\text{permeate volume}}{\text{initial feed volume}} \times 100$,

A_m is the membrane surface area,

V_0 is the initial feed volume.

From equation (3.1.5) in chapter 3, The membrane permeate flux can be described by the fundamental relation

$$\text{Flux, } J_v = \frac{\Delta P - \Delta\pi}{\mu(R_m + R_g + R_{cp})} , \tag{4.1.3}$$

where is ΔP the applied pressure, $\Delta\pi$ is total osmotic pressure between the bulk solution and permeate solution, (R_m + R_g + R_{cp}) denotes the total resistance, R_{total} of the system, and μ is the feed solution dynamic viscosity.

Differentiating equation (4.1.1) with respect to time, and regarding ΔP, μ, and, R_m as constants, the equation becomes

$$(\Delta P - \Delta\pi)\times\frac{dJ_v}{dt} + \mu J_v^2 \times (\frac{dR_g}{dt} + \frac{dR_{cp}}{dt}) + J_v \frac{d\Delta\pi}{dt} = 0 \qquad (4.1.4)$$

where the osmotic pressure variation with time is given by the following equation base on virial coefficients (Haynes et al., 1992)

$$\Delta\pi = \frac{RT}{M}(C_b + B_2 C_b^2 + B_3 C_b^3 + ...) . \qquad (4.1.5)$$

The concentration polarization resistance R_{cp} referred to in equation (4.1.3) and (4.1.4) can be estimated by a modification of the power law suggested by several investigators (van Boxtel et al., 1991; Pradanos et al., 1992; Akay and Wakeman, 1993; Timmer etal., 1994) as shown below

$$R_{cp} = \frac{a}{\delta} v^b k^c C_b^d C_f^e . \qquad (4.1.6)$$

In the preceding equation, the concentration polarization resistance R_{cp} is considered as a time-dependent variable. Hence, differentiating the preceding relation with respect to time results in

$$\frac{dR_{cp}}{dt} = \frac{a}{\delta} d v^b k^c C_b^{d-1} C_f^e \frac{dC_b}{dt} . \qquad (4.1.7)$$

The progressive accumulation of solute on the membrane (gel-layer formation) is due to the difference between the net solute transport from the bulk solution to the membrane and solute back-diffusion from the membrane to the bulk solution (van

Boxtel et al., 1991; Timmer et al., 1994). The gel-layer resistance R_g variation with time can be written as:

$$\frac{dR_g}{dt} = \frac{\in}{\rho_g} C_b J_v - \frac{\in k}{\rho_g} C_b \ln \frac{C_g}{C_b} \qquad (4.1.8)$$

where $\in$ is the resistance per unit of the gel-layer thickness.

4.1.3 Model parameters estimation

As the compositions of the membrane are proprietary, and their material properties are not available, results from membrane filtration tests are employed for parameter estimation. These parameters included the following: the intrinsic membrane resistance, R_m, the osmotic pressure, $\Delta\pi$, the mass transfer coefficient, k, and the specific gel layer resistance, ε. The parameter estimation is outlined in this section.

The membrane resistance, R_m, was measured by conducting membrane filtration tests employing deionized distilled water as the feed solution. The membrane resistance, R_m determined from equation (4.1.3), for NF-45 membrane were 6.412×10^{13}. Several investigators, including Nabetani and coworkers (1990), and Haynes et al. (1992), had observed that the osmotic pressure ($\Delta\pi$) could be expressed by the empirical relationship of equation (4.1.5). These works demonstrated the fact that osmotic pressure for tannic acid solutions were negligible in comparison with the applied transmembrane pressures. Therefore, the total driving force for the tannic acid with nanofiltration in the propose model was only represented by the transmembrane pressure. Equation (4.1.4) can be written as:

$$\frac{dJ_v}{dt} = -\frac{\mu J_v^2}{\Delta P} \times \left(\frac{dR_g}{dt} + \frac{dR_{cp}}{dt}\right). \qquad (4.1.9)$$

The constants a, b, c, d, and e can be estimated by multiple regression, where it is assumed that gel-layer resistance does not exist ($R_g = 0$) at the commencement of membrane operations ($t = 0$). From the membrane performance test results, the

constants *a*, *b*, *c*, *d*, and *e* for the NF-45 membrane were estimated as 3.80×10^{-16}, - 3.02, 3.65, 3.18, -3.18, respectively. The parameters, namely *k*, ε/ρ_g ,and C_g were determine from the preceding relationship using experimental data. The estimated values of ε/ρ_g and C_g were 1.54×10^{16} m/kg and 0.10 kg/m^3, respectively. Determination of mass transfer coefficients was demonstrated in Appendix B. It must be noted that the membrane performance tests were conducted under laminar flow conditions, and so estimates of mass-transfer coefficients varied between 1.28×10^{-6} and 1.68×10^{-5} m/s, depending on fluid dynamic regimes and operation conditions. The input parameters for the proposed membrane transport model are listed in table 4.2.

It must be noted that the parameters associated with concentration polarization and gel-layer formation cannot be estimated with reliability for complex solute-solvent and membrane systems from equations without using experimental data. Additionally, due to the complex structure of tannic acid, and the proprietary nature of commercial membrane materials, regression techniques represented the only well-established, reliable, and accurate for estimating the resistances R_g and R_{cp} from experimental data.

Table 4.2. Entry values for model parameters and operating condition

Parameter	Symbol	Unit	Value
Feed solution concentration	C_f	kg/m^3	2.50×10^{-3}
Gel-layer concentration	C_g	kg/m^3	1.00×10^{-1}
Applied pressure	ΔP	Pa	1.50×10^{6}
Diffusion coefficient	D	m^2/s	2.64×10^{-10}
Mass-transfer coefficient	k	m/s	2.28×10^{-6}
Cross-flow rate	v	m/s	4.81×10^{-3}
Solution dynamic viscosity	μ	Pa•s	1.002×10^{-3}
Resistance of membrane	R_m	1/m	6.41×10^{13}

Table 4.2. Entry values for model parameters and operating condition (continued)

Parameter	Symbol	Unit	Value
Resistance per unit of L_g / gel-layer density	ε / ρ_g	m/kg	1.54×10^{16}
Thickness of the conc. polarization layer	δ	m	2.0586×10^{-4}
Initial solution volume	V_0	m^3	1.50×10^{-3}
Membrane surface area	A_m	m^2	1.55×10^{-2}
Membrane cell cross-section area	A_c	m^2	1.25×10^{-4}
Coefficient for resistance of concentration polarization layer	a	-	3.80×10^{-16}
	b	-	-3.02
	c	-	3.65
	d	-	3.18
	e	-	-3.18

The initial values for the proposed membrane transport model are listed in table 4.3.

Table 4.3. Initial values in the nanofiltration process

Parameter	Symbol	Unit	Value
Bulk concentration	C_b	kg/m^3	2.50×10^{-3}
Permeate flux	J_v	$m^3/m^2/min$	1.78×10^{-5}
Rate of recovery	r	-	0
Resistance of gel-layer	R_g	m^{-1}	0
Resistance of concentration polarization	R_{cp}	m^{-1}	9.23×10^{12}

4.1.4 Open-loop behavior

The simulation results presented in figure 4.4 illustrate the open-loop response for the nanofiltration process.

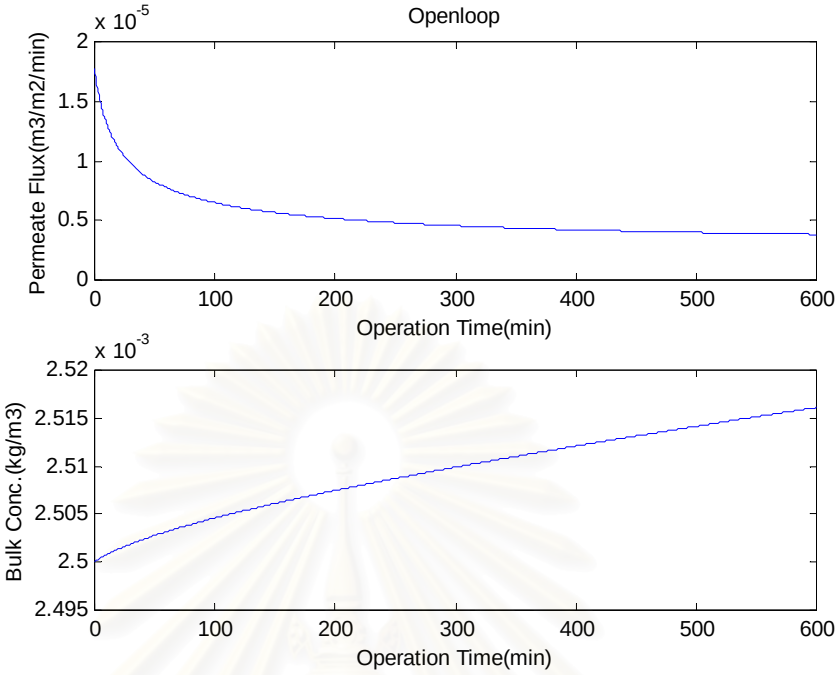

(a) Permeate flux and Bulk concentration of the tannic solution

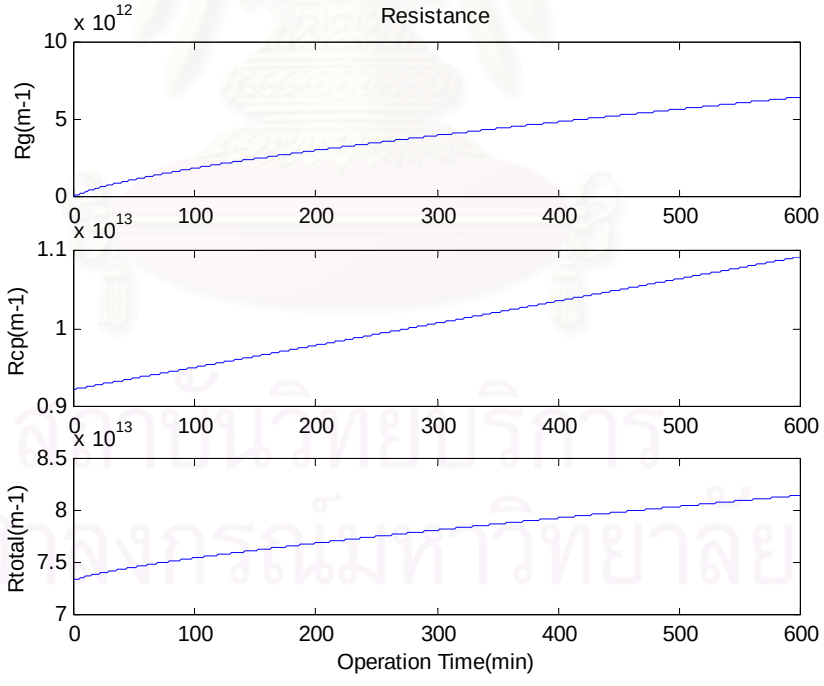

(b) Resistance of gel-layer, Resistance of conc. polarization, and Total resistance

Figure 4.4. Open-loop behavior of the nanofiltration process

The open-loop behavior shows the progressive permeate flux deterioration due to the resistance of the membrane, gel-layer, and concentration polarization. In these simulations, the operating conditions were identical; the transmembrane pressure was 1,500 kPa, the cross flow rate was maintained at 4.81×10^{-3} m/s, and the duration of simulation was 10 hours. The parameters and the initial values are shown in table 4.2 and 4.3, respectively.

4.2 Optimization Study

The mathematical models of a nanofiltration process indicate that an operating permeate flux is one of key factors of the membrane filtration process. In order to operate the nanofiltration process efficiently, optimaization framework is formulated to determine an optimal permeate flux of water in tannic acid solution studied by Shih-Chieh Tu et al. (2001). An optimization goal is to determine an optimal permeate flux for the filtration process to maximize volume of permeate (water) with a semi-batch time.

In this work, a Matlab program is written to solve the optimization problem by using a successive quadratic programming (SQP) algorithm in Matlab Optimization Toolbox as detailed in Appendix E.

4.2.1 Optimization Formulation

An off-line optimal control is solved with fixed batch time to calculate the maximum permeate flux of water for the nanofiltration process of tannic solution. The maximum permeate flux is applied as a trajectory set point of control strategies. The objective function is to maximize the water-permeate flux of tannic solution over the batch time intervals. The next step in formulating the optimization problem is to determine the constrains by considering the fundamental chemical and physical phenomena and physical limitations that influence the nanofiltration process behavior. For the case of nanofiltration process, the construction of the process mathematical model

and operating pressure of the nanofiltration membrane are constrains that limit the membrane separation. The objective function and the constraints can be written as following problem.

$$\max \quad f \quad = \quad J_v(t_f) \tag{4.2.1}$$

Subject to $5\times10^5 \le \Delta P_k \le 4\times10^6$ (inequality constrain)

and $G\,x_k + H\,u_k - x_{k+1} = 0$ (equality constrains)

where $G = \begin{bmatrix} \frac{df_1}{dx_1} & \frac{df_1}{dx_2} & \frac{df_1}{dx_3} \\ \frac{df_2}{dx_1} & \frac{df_2}{dx_2} & \frac{df_2}{dx_3} \\ \frac{df_3}{dx_1} & \frac{df_3}{dx_2} & \frac{df_3}{dx_3} \end{bmatrix}$ and $H = \begin{bmatrix} \frac{df_1}{du} \\ \frac{df_2}{du} \\ \frac{df_3}{du} \end{bmatrix}$.

Matrices *G* and *H* are obtained by substitution the members of the matrices with the equation (4.1.1), (4.1.2), and (4.1.9). Determination of matrices *G* and *H* are detailed in Appendix C.

Table 4.4. The optimal results

Case	Off-line optimal permeate flux ($m^3/m^2/min$)			Summation of permeant volume (m^3)	%increasing of permeant volume
	Time intervals (min)				
	0-200	201-400	401-600		
1	6.5770×10^{-6}	6.5770×10^{-6}	6.5770×10^{-6}	6.12170×10^{-5}	22.57%
2	8.6813×10^{-6}	8.4212×10^{-6}	8.3963×10^{-6}	7.9114×10^{-5}	58.40%

In this research, two cases of the off-line optimal control are carried out. One is an optimal flux set point using one control time interval (case 1). The other is an optimal flux profile using three fixed control intervals (case 2). The optimization results are shown in table 4.4 and figure 4.5.

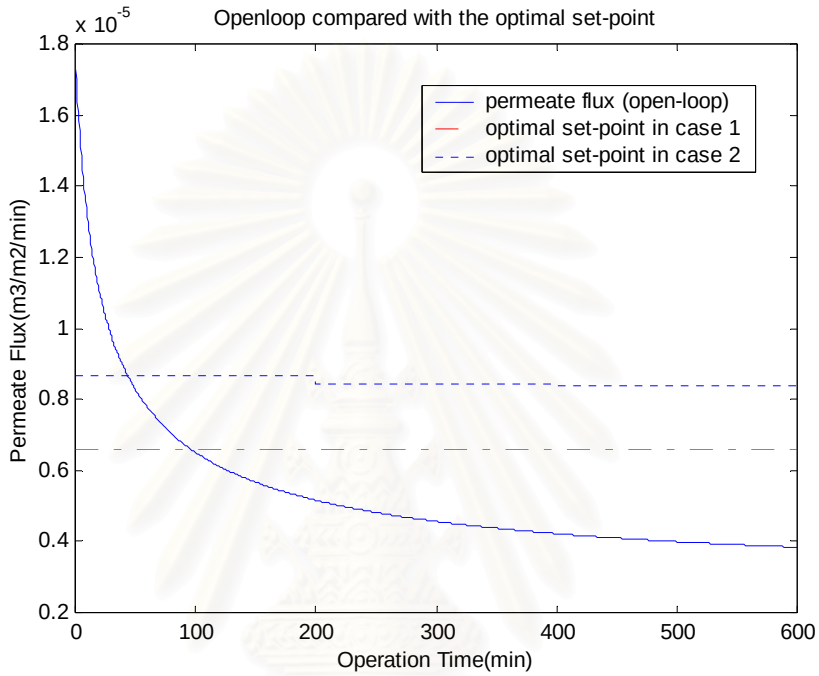

Figure 4.5. Permeate flux in open-loop compared with the optimal permeate fluxes of both cases.

4.2.2 Discussion

In this research, the volume of permeant (water) is measured to represent the water permeate flux. The optimization results given in table 4.4 indicate the comparison of permeant volume of open-loop with the optimal permeant volume of both cases that the water-permeate volume gives 22.57% improvement for an optimal permeate flux set point (case 1) and 58.40% improvement for an optimal permeate flux profile (case 2). It can be concluded that the operation of the nanofiltration process by the

trajectory optimal flux profile (case 2) gives an increase in the performance of filtration than using an optimal flux set point (case 1).

4.3 Design and Study of Controllers

The purpose of this section is to design a control configuration for a nanofiltration membrane to track an optimal operating flux. In this work, a PID controller, a GMC controller, and a generic model control (GMC) coupled with a Kalman filter is implemented to track an optimal operating flux. The controlled variable and manipulated variable are permeate flux of water, J_v and applied pressure, ΔP, respectively. The volume of permeant (water) is employed as a measurement variable to track the controlled variable.

4.3.1 PID Configuration

PID controller is a classical controller. The control strategy of PID does not need mathematical model of the process because it takes a control action to force the process response to the desired set point via the final control element based on the error (deviation of the process measurement from its desired set point value). The digital PID controller in the form of continuous equation is

$$p(t) = p_s + K_c\left[e(t) + \frac{1}{\tau_I}\int_0^t e(t)dt + \tau_D\frac{de(t)}{dt}\right]. \qquad (4.3.1)$$

Here the operating equation in the discrete form is

$$p(k) = p(k-1) + K_c\left\{[e(k)-e(k-1)] + \frac{\Delta t}{\tau_I}e(k) + \frac{\tau_D}{\Delta t}[e(k)-2e(k-1)+e(k-2)]\right\}. \qquad (4.3.2)$$

where p is controller output,

p_s is controller output when $e(t)$ is zero,

Δt is the sampling period,

K_c is controller gain, 5.0×10^{11},

τ_I is integral time constant, 21 minutes,

τ_D is derivative time constant, 0.009 minutes.

In this work, controlled variable is permeate flux and manipulated variable is applied pressure. The error in this studied process is a different between the optimal flux set point, $J_{v,sp}$ and the permeate flux of the process, J_v. The manipulated equation of PID controller in this research is

$$\Delta P(k) = \Delta P(k-1) + K_c \left\{ [e(k) - e(k-1)] + \frac{\Delta t}{\tau_I} e(k) + \frac{\tau_D}{\Delta t} [e(k) - 2e(k-1) + e(k-2)] \right\} \quad (4.3.3)$$

where $e(k) = J_{v,sp} - J_v(k)$.

4.3.2 Generic Model Control (GMC) Configuration

GMC controller is an automatic process controller. It is a good control strategy model-based controller because it can handle the nonlinear process to the trajectory set point and the nonlinear process model does not need to be linearized for this control scheme. Furthermore, in the situation where the controlled nonlinear processes are required to operate in a wide range condition, the linear controllers may give a poor control response because approximate linear models cannot be represented the effect of nonlinearities. According to the above reasons, GMC is chosen as a controller for the permeate flux control studied in this research. Two tunning parameters, K_1 and K_2 are used to obtain the desired shape of the trajectory response. The general form of the GMC algorithm can be written as:

$$\frac{dy}{dt} = K_1(y_{sp} - y) + K_2\int(y_{sp} - y)dt \qquad (4.3.4)$$

This may be further rearranged to give:

$$u(k) = \frac{K_1[y_{sp} - y(k)] + K_2\sum_{k=0}^{k}[y_{sp} - y(k)]\Delta t - F'(k)}{G(k)} \qquad (4.3.5)$$

where y is the current value of controlled variable,
y_{sp} is a desired value of controlled variable,
u is a manipulated variable,
and K_1 and K_2 are tuning parameters.

For permeate flux control of the nanofiltration process, the manipulated input of this tracking system is the inverse of applied pressure, ΔP^{-1} and the controlled variable is the permeate flux, J_v.

To implement the GMC, a model of membrane permeatte flux relation is required; it gives the relation between the permeate flux (controlled variable) and the inverse of applied pressure (manipulated variable). Equation (4.1.9) is rearranged in form as:

$$\frac{dJ_v}{dt} = \left[-\mu J_v^2\left(\frac{dR_g}{dt} + \frac{dR_{cp}}{dt}\right)\right] \times \frac{1}{\Delta P} \qquad (4.3.6)$$

Rearranging the equation (4.3.6) as in the form of GMC algorithm, the following functions, *F'(k)* and *G(k)* can be defined

$$F'(k) = 0 \qquad (4.3.7)$$

$$G(k) = -\mu J_v^2(k)\left(\frac{\Delta R_g(k)}{\Delta t} + \frac{\Delta R_{cp}(k)}{\Delta t}\right) \quad (4.3.8)$$

Replacing these equations in equation (4.3.5) and substituting water permeate flux, optimal permeate flux set point, and inverse of applied pressure for y, y_{sp}, and u, respectively, the manipulated variable of the GMC in the discrete form can be written as:

$$\Delta P^{-1}(k) = \frac{K_1[J_{v,sp} - J_v(k)] + K_2\sum_{k=0}^{k}[J_{v,sp} - J_v(k)]\Delta t}{-\mu J_v^2(k) \times [\frac{\Delta R_g(k)}{\Delta t} + \frac{\Delta R_{cp}(k)}{\Delta t}]} \quad (4.3.9)$$

where Δt is the sampling time of the controller.

In this work, the appropriate values of the tunning parameters of the GMC controller are K_1 = 0.04 min^{-1} and K_2 = 0.0025 min^{-2}.

4.3.3 GMC with Kalman Filter

For membrane filtration performance, an estimator is applied with the model-based controller to estimate uncertainty parameters or unmeasurable variables. In the studied system, the filtration performance is depended on two physical parameters: mass-transfer coefficient, k and dynamic viscosity, μ. The Kalman filter is employed to estimate these parameters. To use the Kalman filter as a parameter estimator, it is important to check observability of the system. The detail of observability checking is detailed in Appendix C.

To estimate the deviated parameters, two equations of the process in state space form are applied to explain the relationship between the measurement variable and the estimated parameters. The mathematical model of the process can be written as following:

$$\dot{x} = Ax + Bu \tag{4.3.10}$$

and the measurement equation is described as

$$y = Cx\,. \tag{4.3.11}$$

In this research, the volume of permeate water, V_{out} is measured and used to estimate the entire state, $\hat{x}$ = [J_v r C_b k μ] ^{T} and manipulated variable, u is ΔP^{-1}. Volume of permeated water, V_{out} that is selected as the measurement variable, y can be written the relationship with the permeate flux as following equation

$$V_{out} = A_m J_v\,. \tag{4.3.12}$$

The mathematical model of the nanofiltration process that is inserted into the Kalman filter algorithm is shown below

$$f_1 = \frac{dJ_v}{dt} = \frac{J_v^2}{\Delta P}\left[z_1 C_b^{d-1}\frac{dC_b}{dt} + z_2 C_b J_v - z_3 C_b \ln\frac{C_g}{C_b}\right], \tag{4.3.13}$$

$$f_2 = \frac{dr}{dt} = \frac{A_m}{V_0} J_v\,, \tag{4.3.14}$$

$$f_3 = \frac{dC_b}{dt} = \frac{A_m J_v C_b}{V_0(1-r)}\,, \tag{4.3.15}$$

$$f_4 = \frac{dk}{dt} = 0\,, \tag{4.3.16}$$

$$f_5 = \frac{d\mu}{dt} = 0\,, \tag{4.3.17}$$

$$z_1 = -ad\frac{\mu}{\delta}v^b k^c C_f^e$$

where $$z_2 = -\mu\frac{\varepsilon}{\rho_g}$$

$$z_3 = -\mu\frac{\varepsilon}{\rho_g}k.$$

From equation (4.3.13), (4.3.14), (4.3.15), (4.3.16), and (4.3.17), state space form of the system can be determined matrix *A*, *B*, and *C* as

$$A = \begin{bmatrix} \frac{df_1}{dx_1} & \frac{df_1}{dx_2} & \frac{df_1}{dx_3} & \frac{df_1}{dx_4} & \frac{df_1}{dx_5} \\ \frac{df_2}{dx_1} & \frac{df_2}{dx_2} & \frac{df_2}{dx_3} & \frac{df_2}{dx_4} & \frac{df_2}{dx_5} \\ \frac{df_3}{dx_1} & \frac{df_3}{dx_2} & \frac{df_3}{dx_3} & \frac{df_3}{dx_4} & \frac{df_3}{dx_5} \\ \frac{df_4}{dx_1} & \frac{df_4}{dx_2} & \frac{df_4}{dx_3} & \frac{df_4}{dx_4} & \frac{df_4}{dx_5} \\ \frac{df_5}{dx_1} & \frac{df_5}{dx_2} & \frac{df_5}{dx_3} & \frac{df_5}{dx_4} & \frac{df_5}{dx_5} \end{bmatrix}, \qquad B = \begin{bmatrix} \frac{df_1}{du} \\ \frac{df_2}{du} \\ \frac{df_3}{du} \\ \frac{df_4}{du} \\ \frac{df_5}{du} \end{bmatrix},$$

and $C = \begin{bmatrix} A_m & 0 & 0 & 0 & 0 \end{bmatrix}$

where $$\frac{df_1}{dx_1} = \frac{C_b J_v}{\Delta P}\left[2z_1 C_b^{d-2}\frac{dC_b}{dt} + 3z_2 J_v - 2z_3 \ln\frac{C_g}{C_b}\right],$$

$$\frac{df_1}{dx_2} = 0,$$

$$\frac{df_1}{dx_3} = \frac{J_v^2}{\Delta P}\left[z_1 C_b^{d-1}\left(\frac{d^2 C_b}{dt^2} + \frac{(d-1)}{C_b}\frac{dC_b}{dt}\right) + z_2 J_v + z_3\left(1 + \ln\frac{C_b}{C_g}\right)\right],$$

$$\frac{df_1}{dx_4} = \frac{J_v^2}{\Delta P}\left[z_1\frac{c}{k}C_b^{d-1}\frac{dC_b}{dt} - \frac{z_3}{k}C_b \ln\frac{C_g}{C_b}\right],$$

$$\frac{df_1}{dx_5} = \frac{J_v^2}{\Delta P}\left[\frac{z_1}{\mu} C_b^{d-1} \frac{dC_b}{dt}\right],$$

$$\frac{df_2}{dx_1} = \frac{A_m}{V_0}, \qquad \frac{df_2}{dx_2} = 0,$$

$$\frac{df_2}{dx_3} = 0, \qquad \frac{df_2}{dx_4} = 0,$$

$$\frac{df_2}{dx_5} = 0,$$

$$\frac{df_3}{dx_1} = \frac{A_m C_b}{V_0(1-r)}, \qquad \frac{df_3}{dx_2} = \frac{A_m J_v C_b}{V_0(1-r)^2},$$

$$\frac{df_3}{dx_3} = \frac{A_m J_v}{V_0(1-r)}, \qquad \frac{df_3}{dx_4} = 0,$$

$$\frac{df_3}{dx_5} = 0,$$

$$\frac{df_4}{dx_1} = 0, \qquad \frac{df_4}{dx_2} = 0,$$

$$\frac{df_4}{dx_3} = 0, \qquad \frac{df_4}{dx_4} = 0,$$

$$\frac{df_4}{dx_5} = 0,$$

$$\frac{df_5}{dx_1} = 0, \qquad \frac{df_5}{dx_2} = 0,$$

$$\frac{df_5}{dx_3} = 0, \qquad \frac{df_5}{dx_4} = 0,$$

$$\frac{df_5}{dx_5} = 0,$$

The flow chart diagram of the GMC controller coupled with Kalman filter is illustrated in figure 4.6.

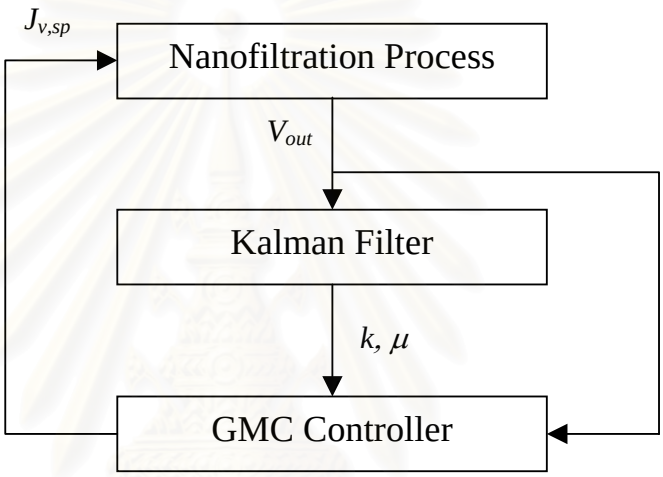

Figure 4.6. The estimation diagram of μ , k in the nanofiltration process

To determine mismatch parameters, μ and k via Kalman filter, the set of matrices, P, Q, and R is used to determine covariance of estimated values, process model values, and measurement value, respectively. The matrices can be written as following:

$$P = \begin{bmatrix} p_{1,1} & 0 & 0 & 0 & 0 \\ 0 & p_{2,2} & 0 & 0 & 0 \\ 0 & 0 & p_{3,3} & 0 & 0 \\ 0 & 0 & 0 & p_{4,4} & 0 \\ 0 & 0 & 0 & 0 & p_{5,5} \end{bmatrix}, \quad Q = \begin{bmatrix} q_{1,1} & 0 & 0 & 0 & 0 \\ 0 & q_{2,2} & 0 & 0 & 0 \\ 0 & 0 & q_{3,3} & 0 & 0 \\ 0 & 0 & 0 & q_{4,4} & 0 \\ 0 & 0 & 0 & 0 & q_{5,5} \end{bmatrix},$$

and $\quad R = \begin{bmatrix} r_{1,1} \end{bmatrix}$

where $p_{1,1} = 7.00\times10^{2}$, $p_{2,2} = 4.00\times10^{2}$, $p_{3,3} = 4.00\times10^{2}$,
$p_{4,4} = 2.32\times10^{9}$, $p_{5,5} = 3.14\times10^{10}$,
$q_{1,1} = 3.10\times10^{3}$, $q_{2,2} = 1.20\times10^{2}$, $q_{3,3} = 1.20\times10^{2}$,
$q_{4,4} = 2.20\times10^{3}$, $q_{5,5} = 1.90\times10^{3}$,
and $r_{1,1} = 5.00\times10^{3}$.

4.3.4 Control Results

In this section, the simulation of closed-loop behaviors is studied in two parts: nominal case and robustness tests. Nominal case is studied to compare the performance of PID and GMC controllers. Robustness cases are studied the control result of controllers when some process parameters have deviated from their nominal values. The GMC controller couple with the Kalman filter is developed to estimate parameter mismatch and handle the permeate flux to the trajectory set point. In this study, IAE (Integral absolute error) and ISE (Integral square error) are used as the control performance index to compare each controller.

Nominal Case

In this section, two cases of permeate flux control are carried out in table 4.5. The simulation results are shown in figure 4.7- 4.10.

Table 4.5. The comparison of IAE and ISE for nominal case

Case	Controller	IAE	ISE
1	PID	0.4966	1.3542×10^{-6}
	GMC	0.2416	1.2052×10^{-6}
2	PID	0.5614	1.3384×10^{-6}
	GMC	0.1900	6.7457×10^{-7}

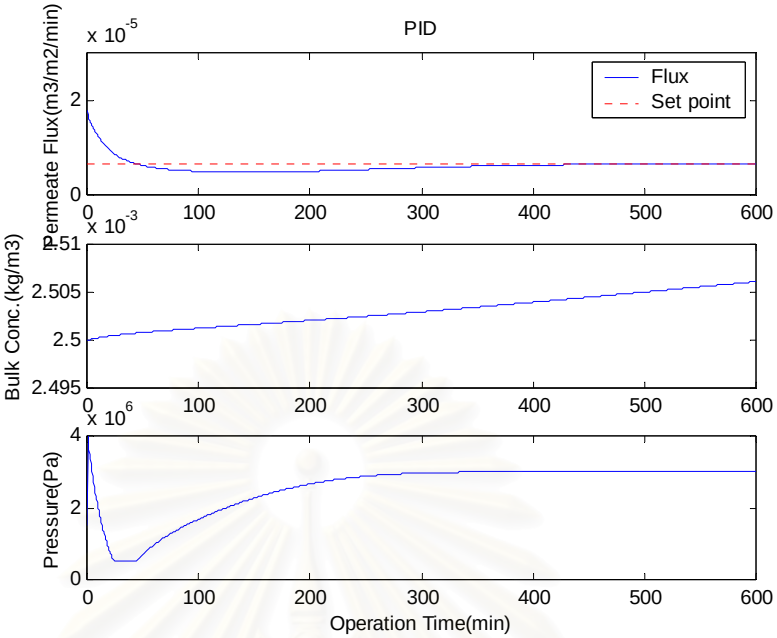

(a) Permeate flux, Bulk conc. of the tannic solution and applied pressure

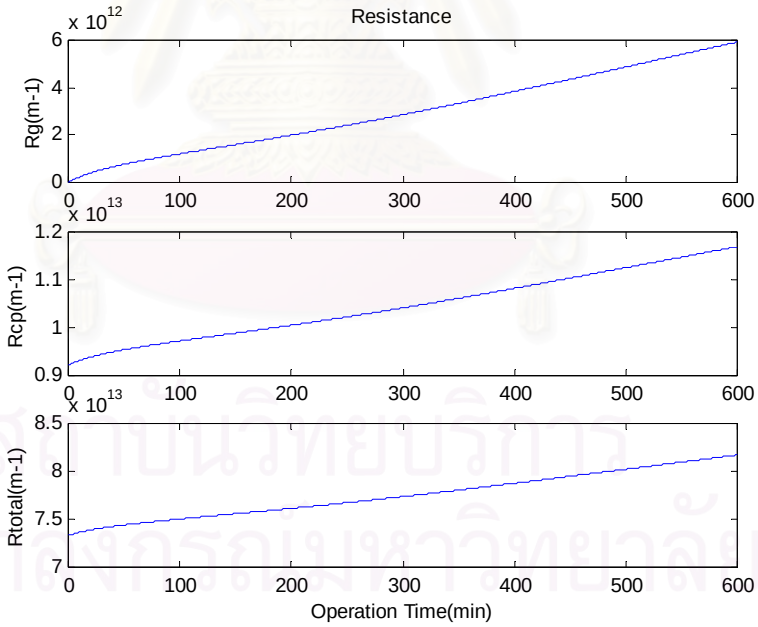

(b) Resistance of gel-layer, Resistance of conc. polarization, and Total resistance

Figure 4.7. The controlled response for nominal case of the nanofiltration process using PID (case 1)

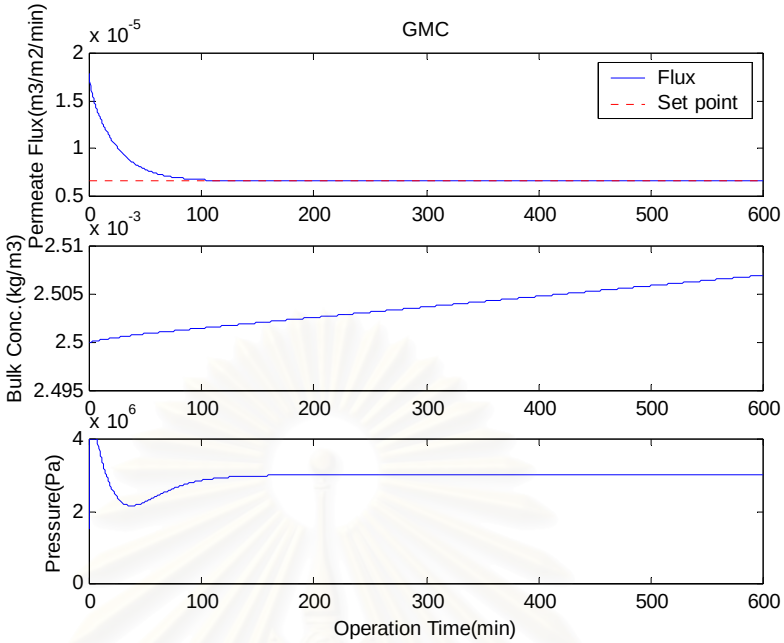

(a) Permeate flux, Bulk conc. of the tannic solution and applied pressure

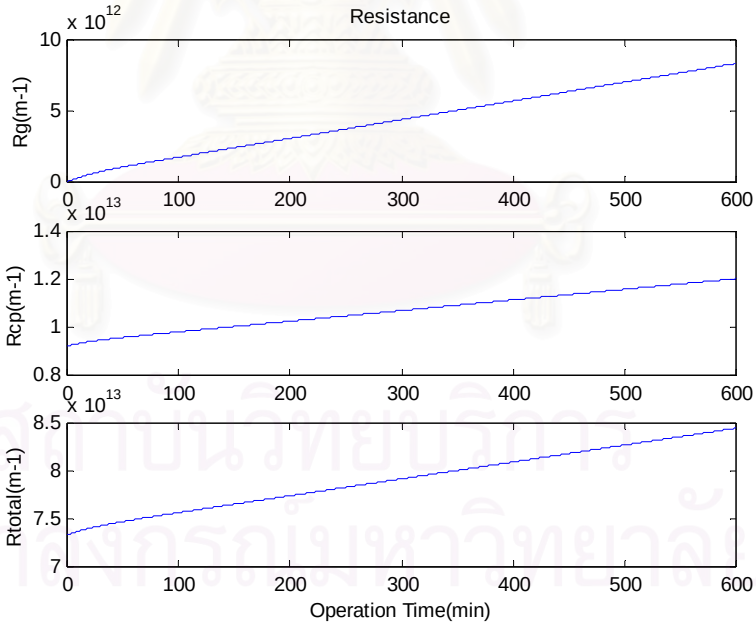

(b) Resistance of gel-layer, Resistance of conc. polarization, and Total resistance

Figure 4.8. The controlled response for nominal case of the nanofiltration process using GMC (case 1)

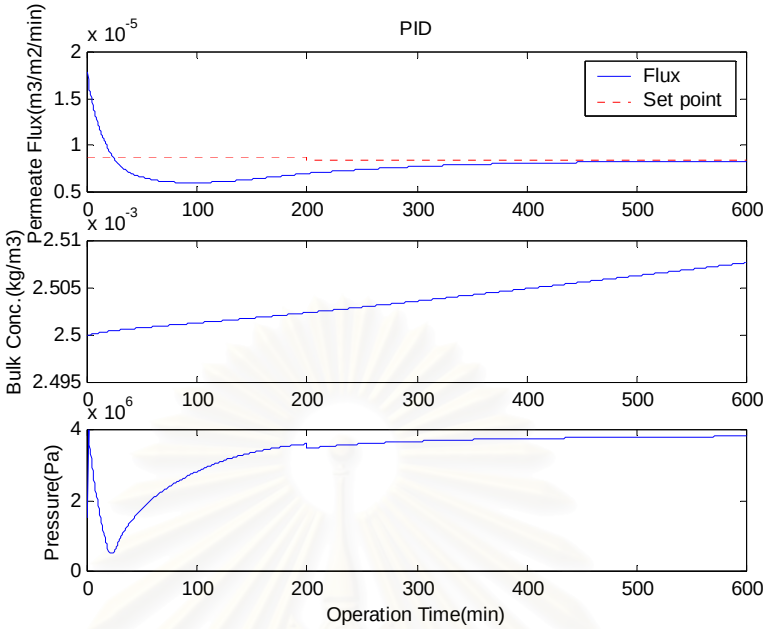

(a) Permeate flux, Bulk conc. of the tannic solution and applied pressure

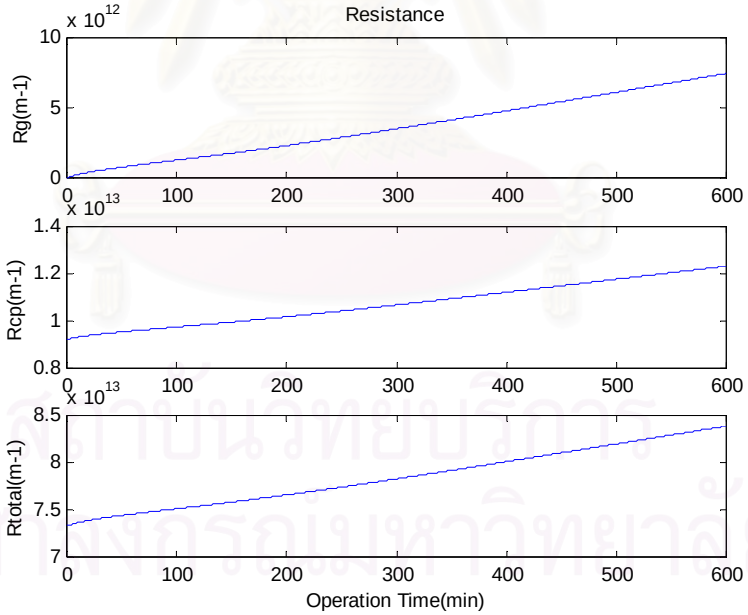

(b) Resistance of gel-layer, Resistance of conc. polarization, and Total resistance

Figure 4.9. The controlled response for nominal case of the nanofiltration process using PID (case 2)

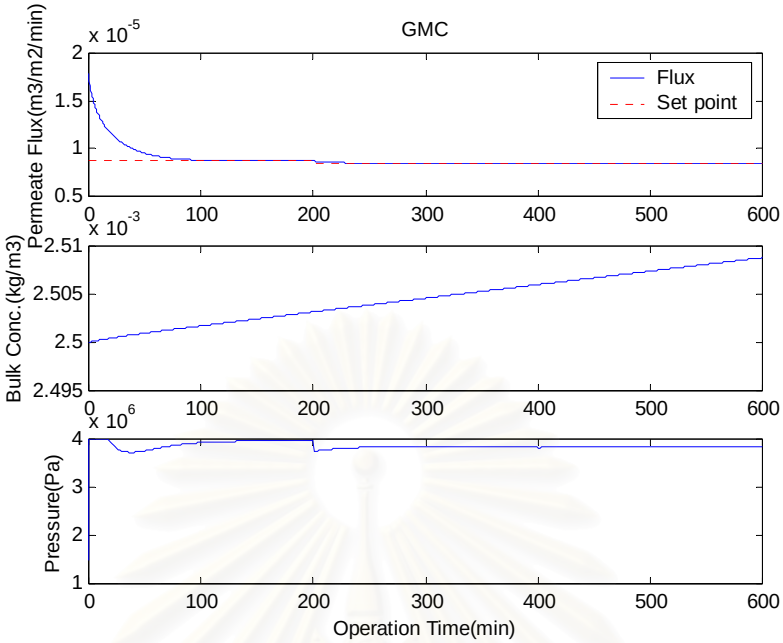

(a) Permeate flux, Bulk conc. of the tannic solution and applied pressure

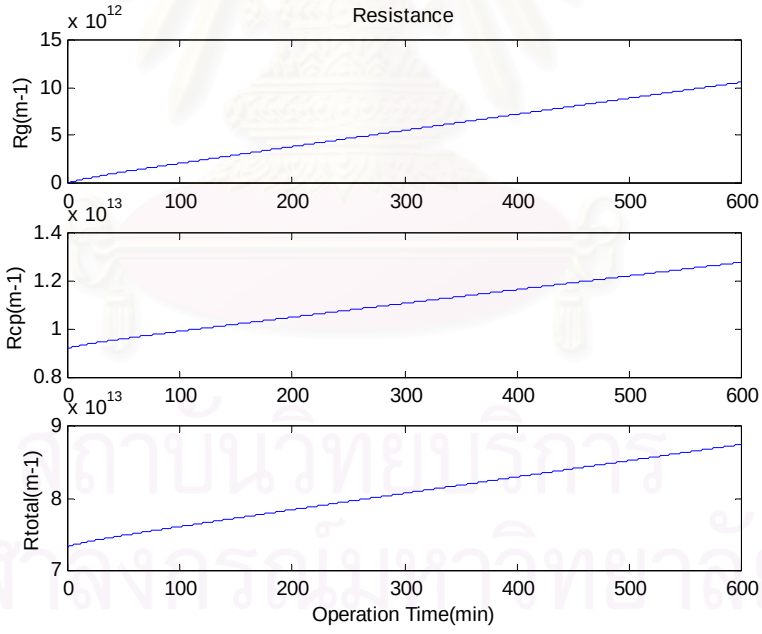

(b) Resistance of gel-layer, Resistance of conc. polarization, and Total resistance

Figure 4.10. The controlled response for nominal case of the nanofiltration process using GMC (case 2)

Robustness Tests

As seen the control results for the nominal case, The GMC controller is effective to handle the permeate flux to the trajectory set point. The GMC controller is a model-based controller so the mathematical model that represents the real process is required. However the developed model cannot represent all of the real process because of complexity of the real process or changing of some process physical properties. These are the main cause that determined parameters deviate from their real values. Changing of process parameters may be effected to the stability of the controlled process so it is important to examine the robustness of controllers with respect to changes in process parameters. The GMC controller coupled with Kalman filter, tuned for nominal case, is used to control the nanofiltration process where some of the conditions have changed from their nominal value. In this work, two process parameters: mass-transfer coefficient, k and solution dynamic viscosity, μ are set to deviate 20% from their nominal values. The robustness tests are divided into five cases as listed below:

- Mass-transfer coefficient, k, increase 20%
- Mass-transfer coefficient, k, decrease 20%
- Solution dynamic viscosity, μ, increase 20%
- Solution dynamic viscosity, μ, decrease 20%
- Mass-transfer coefficient, k and Solution dynamic viscosity, μ, increase 20%

In this section, two cases of the optimal permeate flux set point are considered as following:

Case 1: Tracking an optimal flux set point using one control time interval

In this case, parameter mismatches are studied by tracking an optimal flux set point using one control time interval. Table 4.6 shows the comparison of the control performance index in robustness tests for case 1. The simulation results are illustrated in figure 4.11 – 4.20.

Table 4.6. The comparison of IAE and ISE for robustness tests (case 1)

Condition	GMC		GMC coupled with Kalman filter	
	IAE	**ISE**	**IAE**	**ISE**
+20% k	0.25087	1.1844×10^{-6}	0.2250	9.6251×10^{-7}
-20% k	0.2817	1.4702×10^{-6}	0.2414	1.1012×10^{-6}
+20% μ	0.2498	1.1840×10^{-6}	0.2208	9.3885×10^{-7}
-20% μ	0.2822	1.4732×10^{-6}	0.2456	1.1306×10^{-6}
+20% k and +20% μ	0.2893	1.5476×10^{-6}	0.2177	9.0658×10^{-7}

Case 2: Tracking an optimal flux profile using three fixed control intervals

In this case, the control objective is to track an optimal flux profile when the mass-transfer coefficient and/or solution viscosity changes. Table 4.6 shows the comparison of the control performance index in robustness tests for case 2. The simulation results are illustrated in figure 4.21 – 4.30.

Table 4.7. The comparison of IAE and ISE for robustness tests (case 2)

Condition	GMC		GMC coupled with Kalman filter	
	IAE	**ISE**	**IAE**	**ISE**
+20% k	0.1928	5.7681×10^{-7}	0.1888	6.7088×10^{-7}
-20% k	0.2140	8.2054×10^{-7}	0.2025	7.7243×10^{-7}
+20% μ	0.4151	7.7884×10^{-7}	0.1833	6.4627×10^{-7}
-20% μ	0.2208	8.6686×10^{-7}	0.2074	7.9991×10^{-7}
+20% k and +20% μ	0.4225	7.4961×10^{-7}	0.2094	6.4606×10^{-7}

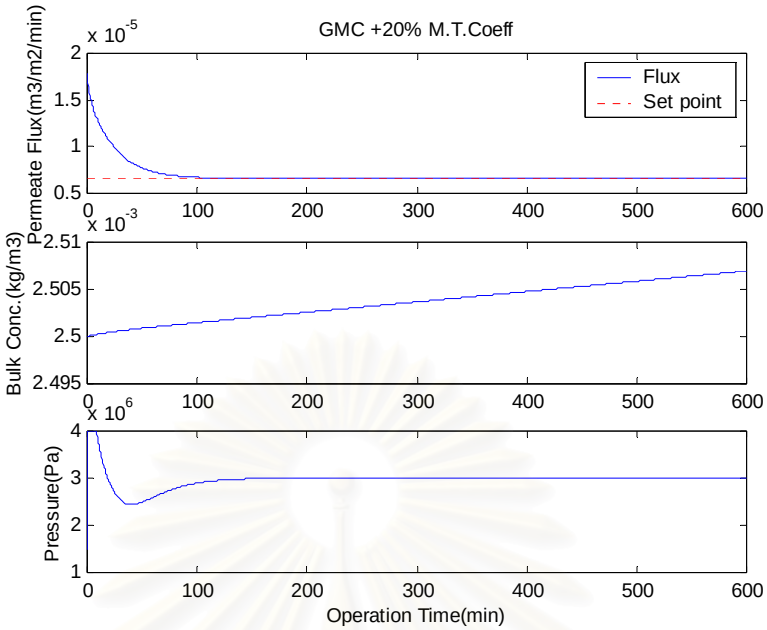

(a) Permeate flux, bulk conc. of the tannic solution and applied pressure

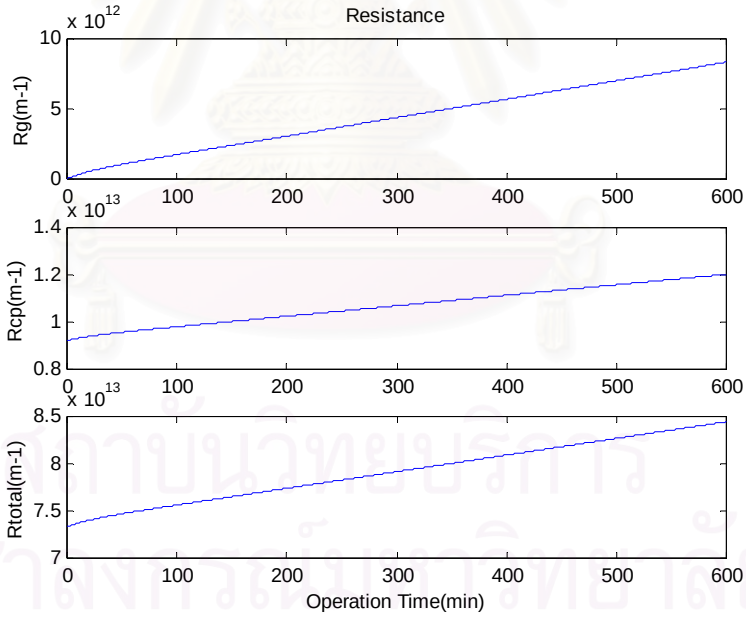

(b) Resistance of gel-layer, resistance of conc. polarization, and total resistance

Figure 4.11. The controlled response for +20% *k* change of the nanofiltration process using GMC (case 1)

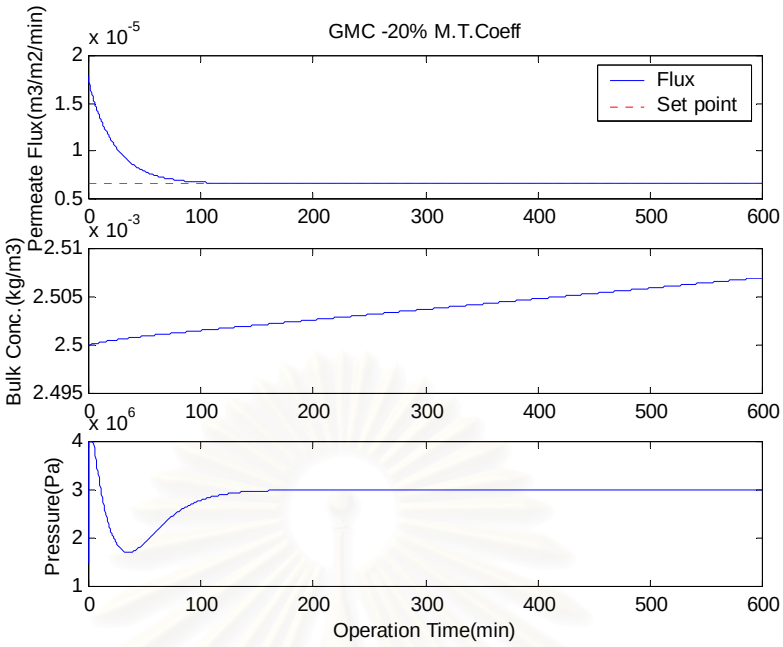

(a) Permeate flux, bulk conc. of the tannic solution and applied pressure

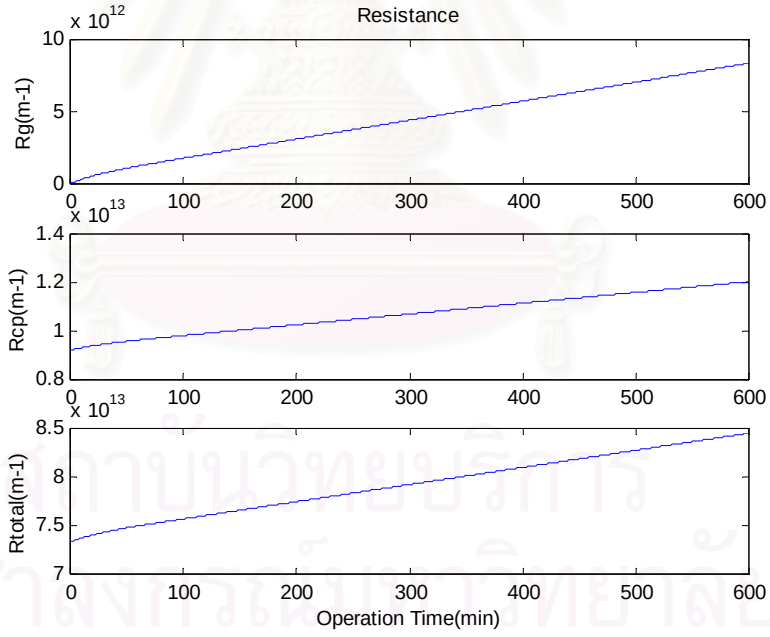

(b) Resistance of gel-layer, resistance of conc. polarization, and total resistance

Figure 4.12. The controlled response for -20% *k* change of the nanofiltration process using GMC (case 1)

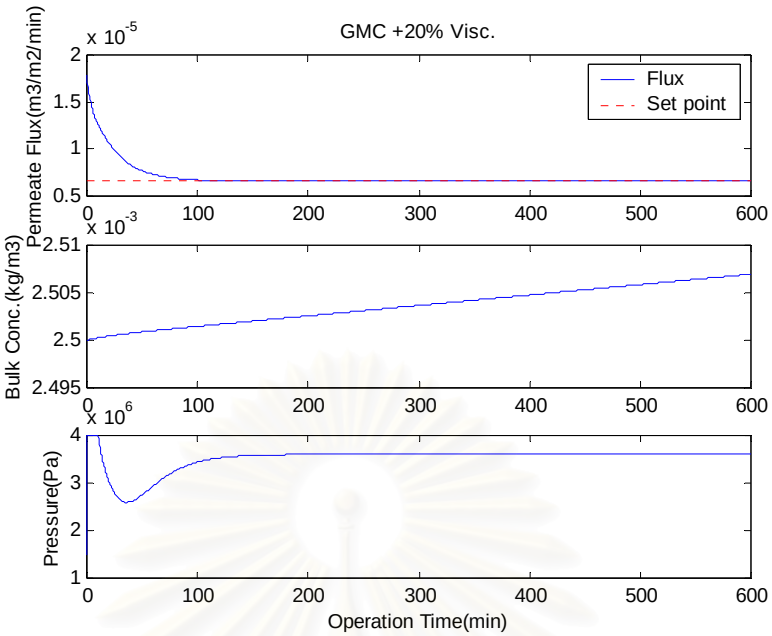

(a) Permeate flux, bulk conc. of the tannic solution and applied pressure

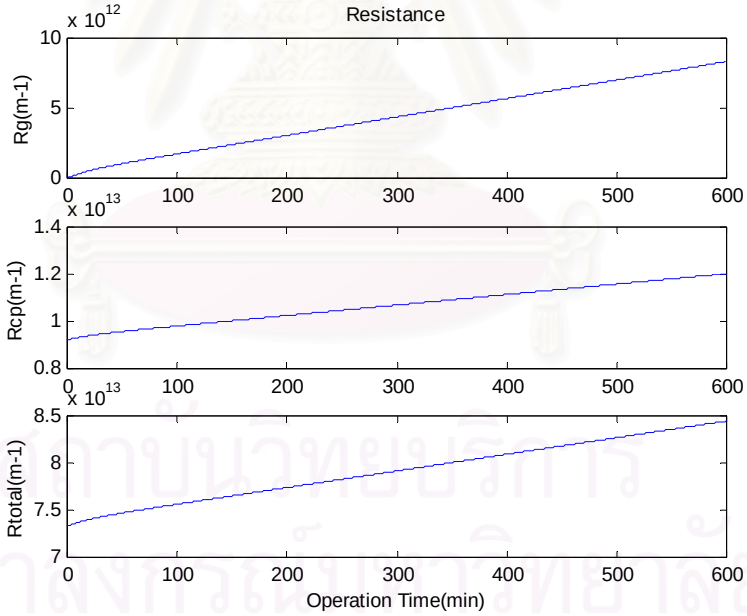

(b) Resistance of gel-layer, resistance of conc. polarization, and total resistance

Figure 4.13. The controlled response for +20% μ change of the nanofiltration process using GMC (case 1)

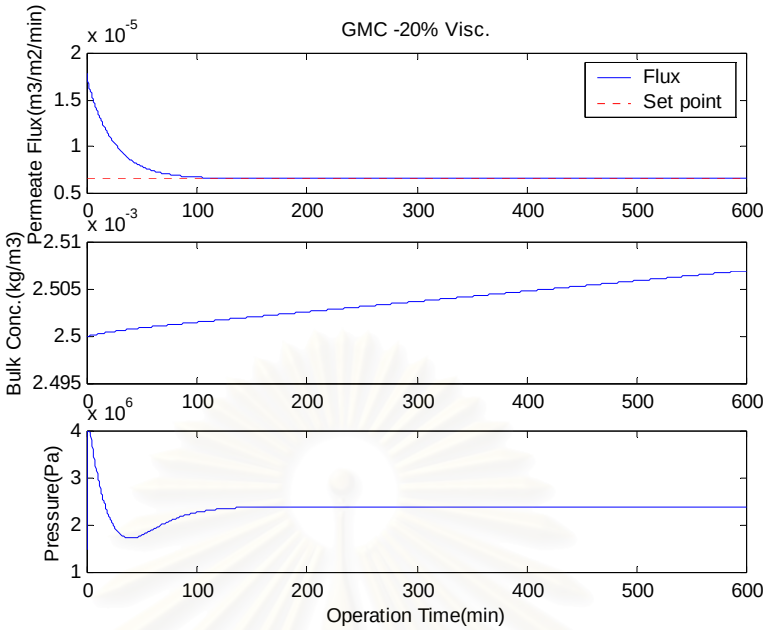

(a) Permeate flux, bulk conc. of the tannic solution and applied pressure

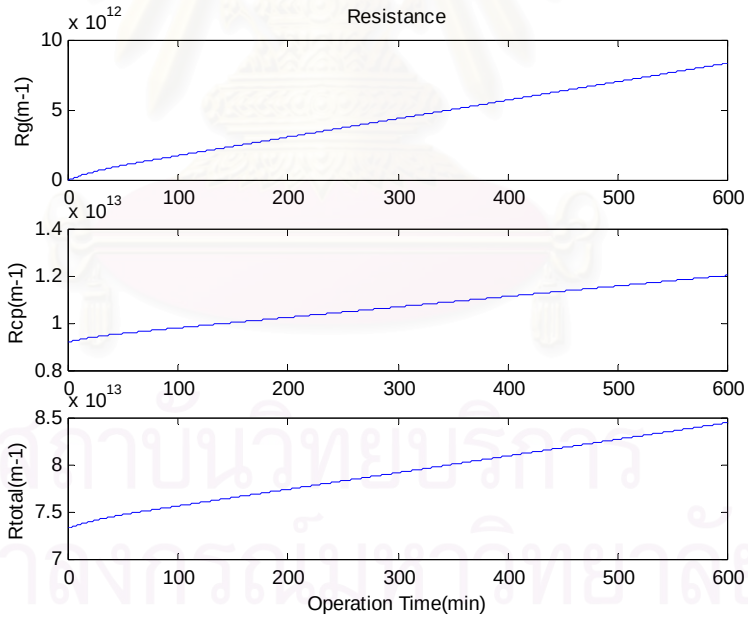

(b) Resistance of gel-layer, resistance of conc. polarization, and total resistance

Figure 4.14. The controlled response for -20% μ change of the nanofiltration process using GMC (case 1)

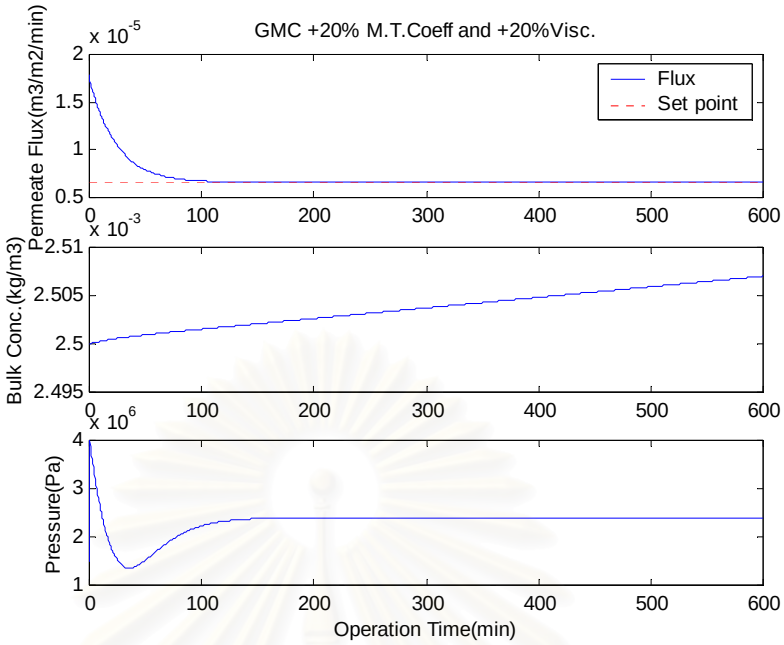

(a) Permeate flux, bulk conc. of the tannic solution and applied pressure

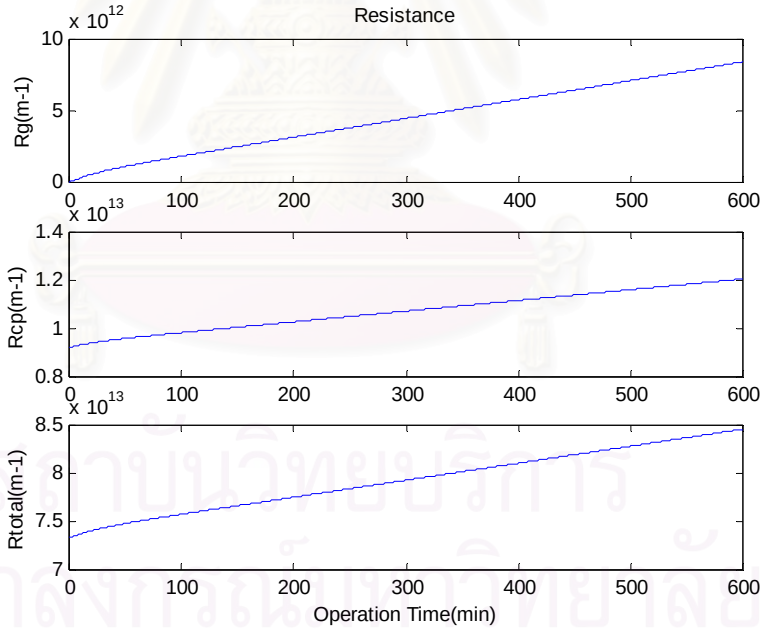

(b) Resistance of gel-layer, resistance of conc. polarization, and total resistance

Figure 4.15. The controlled response for +20% k and +20% μ change of the nanofiltration process using GMC (case 1)

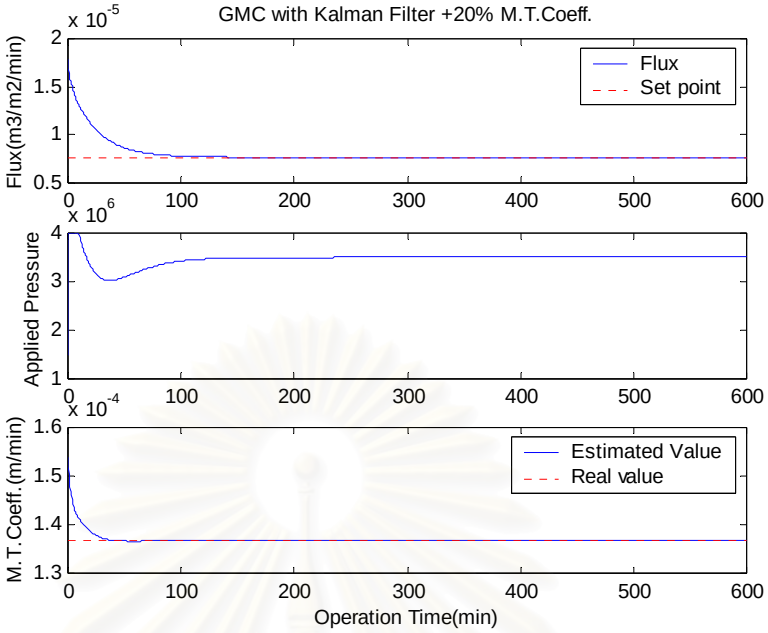

Figure 4.16. The controlled response and estimate of mass-transfer coefficient for +20% *k* change of the nanofiltration process using GMC coupled with Kalman filter (case 1)

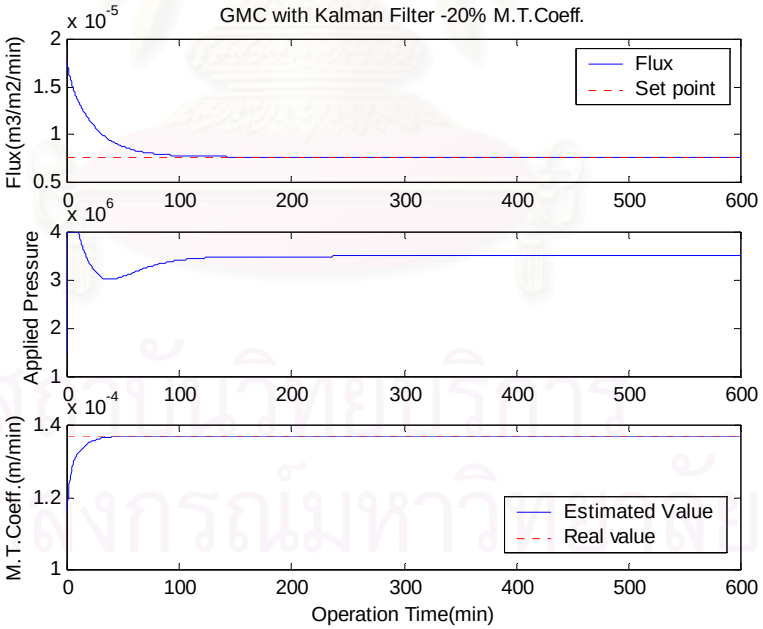

Figure 4.17. The controlled response and estimate of mass-transfer coefficient for -20% *k* change of the nanofiltration process using GMC coupled with Kalman filter (case 1)

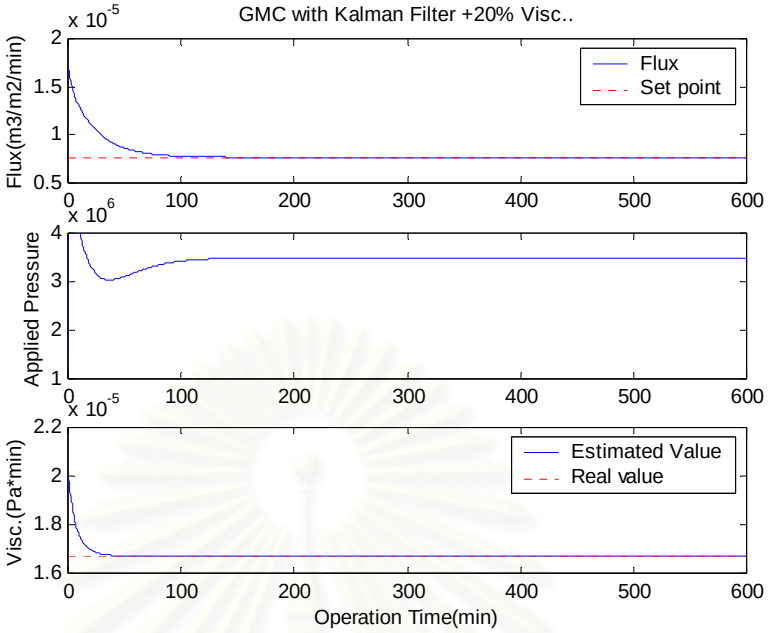

Figure 4.18. The controlled response and estimate of solution viscosity for +20% μ change of the nanofiltration process using GMC coupled with Kalman filter (case 1)

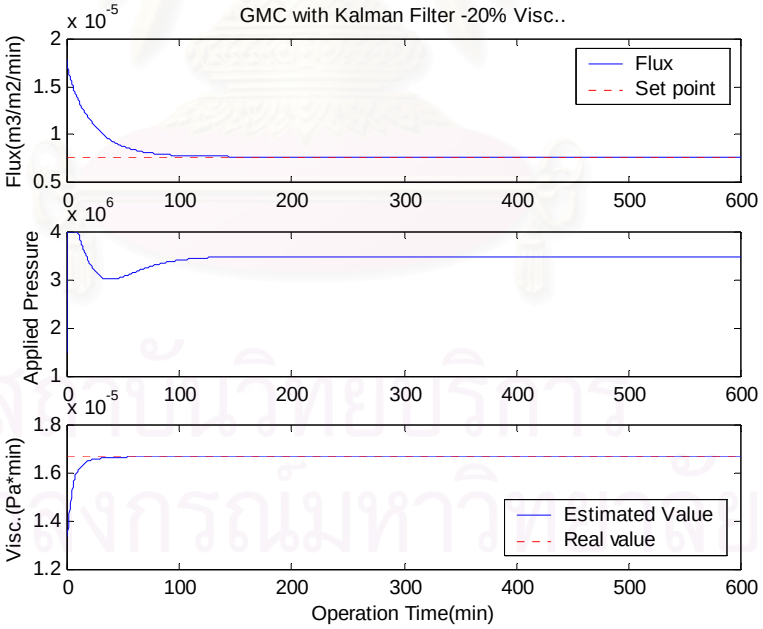

Figure 4.19. The controlled response and estimate of solution viscosity for -20% μ change of the nanofiltration process using GMC coupled with Kalman filter (case 1)

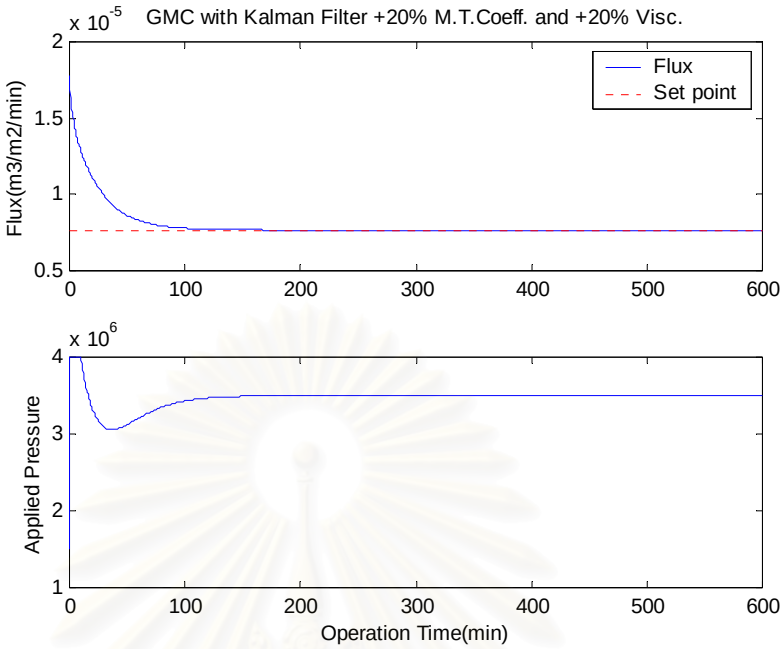

(a) Permeate flux and applied pressure

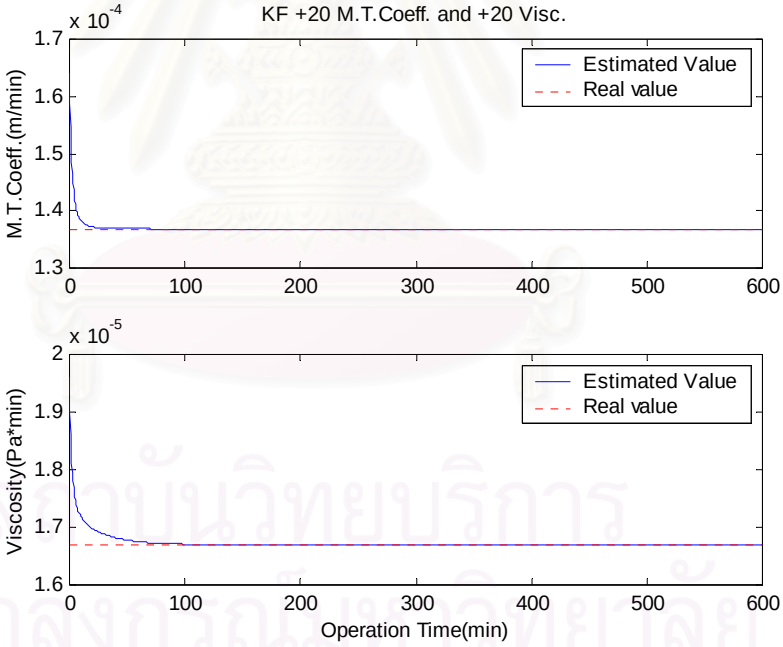

(b) Estimates of mass-transfer coefficient and solution viscosity

Figure 4.20. The controlled response and estimates of parameters for +20% k and +20% μ change of the nanofiltration process using GMC coupled with Kalman filter (case 1)

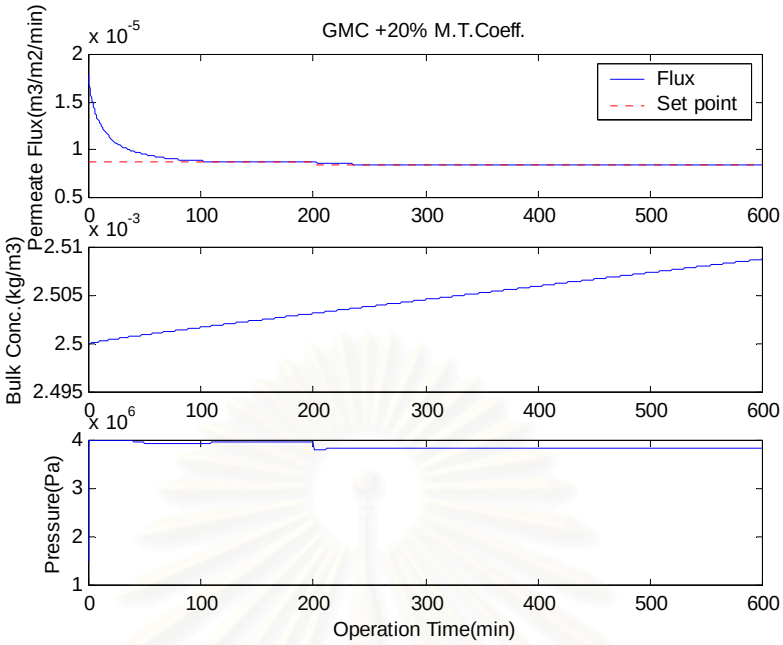

(a) Permeate flux, bulk conc. of the tannic solution and applied pressure

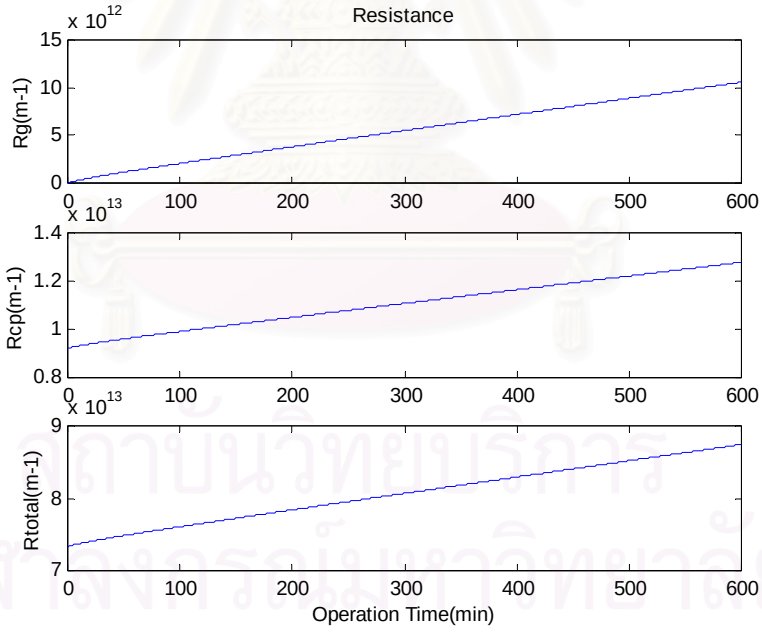

(b) Resistance of gel-layer, resistance of conc. polarization, and total resistance

Figure 4.21. The controlled response for +20% *k* change of the nanofiltration process using GMC (case 2)

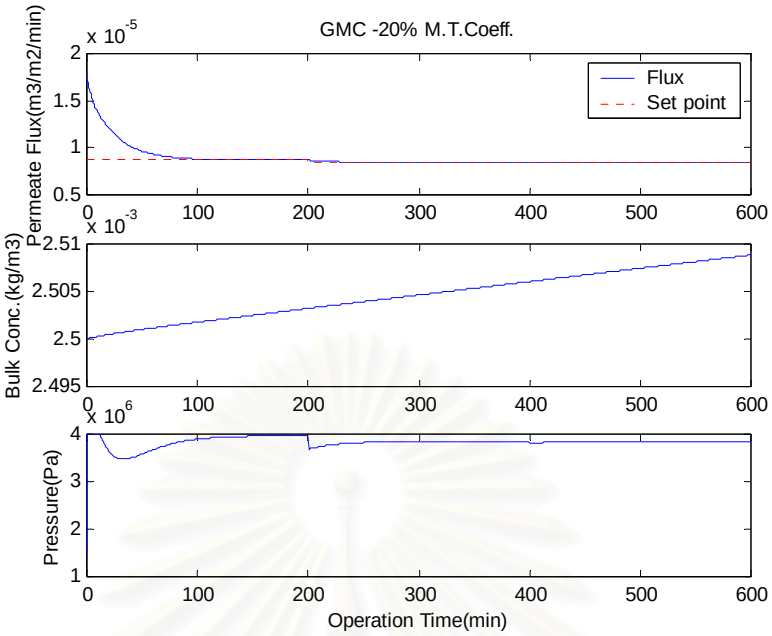

(a) Permeate flux, bulk conc. of the tannic solution and applied pressure

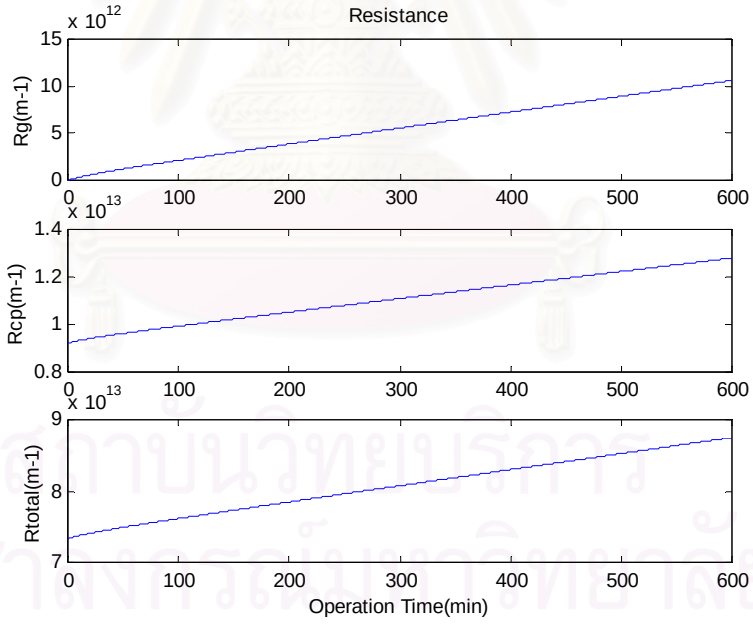

(b) Resistance of gel-layer, resistance of conc. polarization, and total resistance

Figure 4.22. The controlled response for -20% *k* change of the nanofiltration process using GMC (case 2)

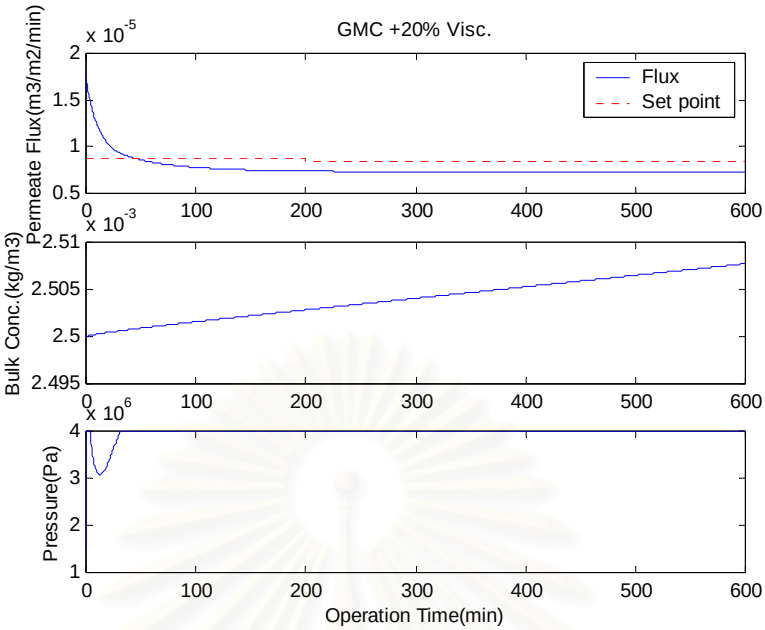

(a) Permeate flux, bulk conc. of the tannic solution and applied pressure

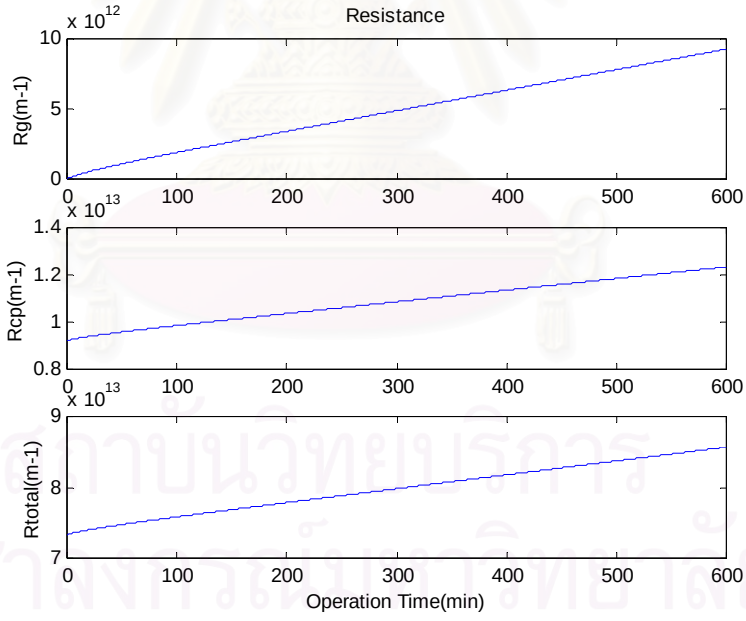

(b) Resistance of gel-layer, resistance of conc. polarization, and total resistance

Figure 4.23. The controlled response for +20% μ change of the nanofiltration process using GMC (case 2)

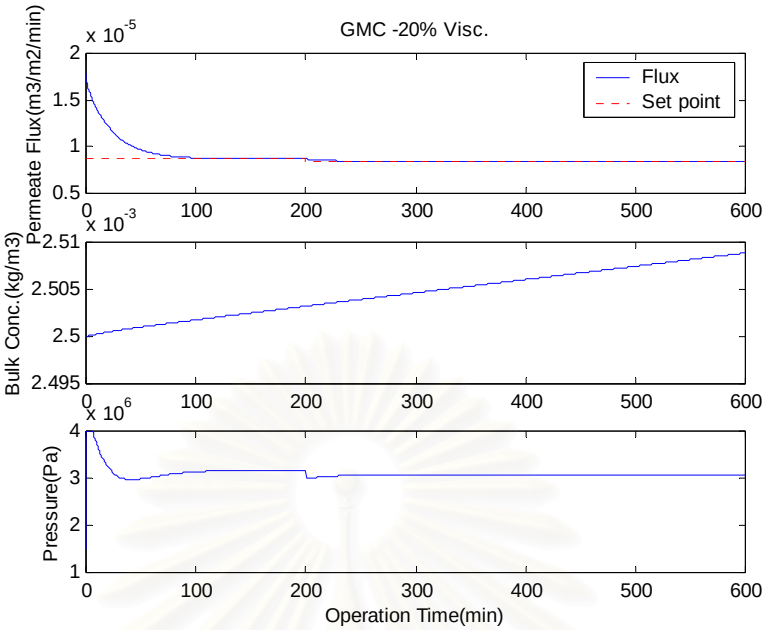

(a) Permeate flux, bulk conc. of the tannic solution and applied pressure

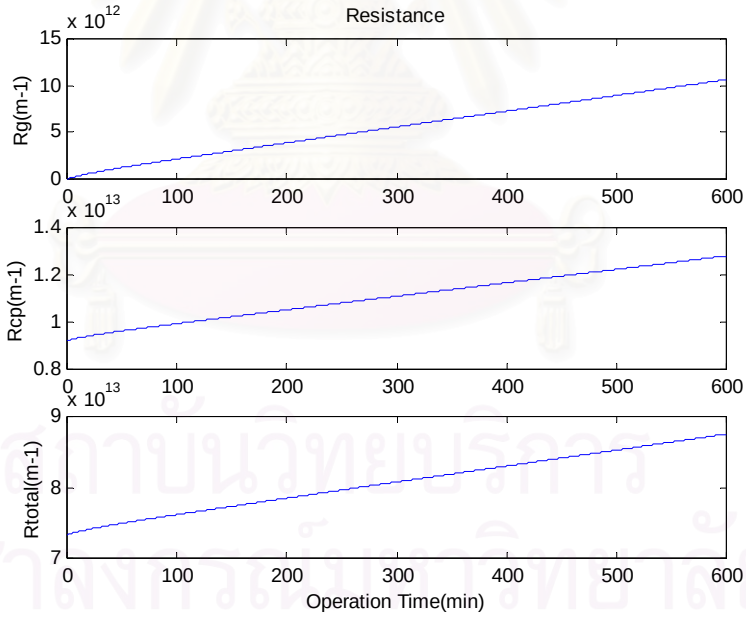

(b) Resistance of gel-layer, resistance of conc. polarization, and total resistance

Figure 4.24. The controlled response for -20% μ change of the nanofiltration process using GMC (case 2)

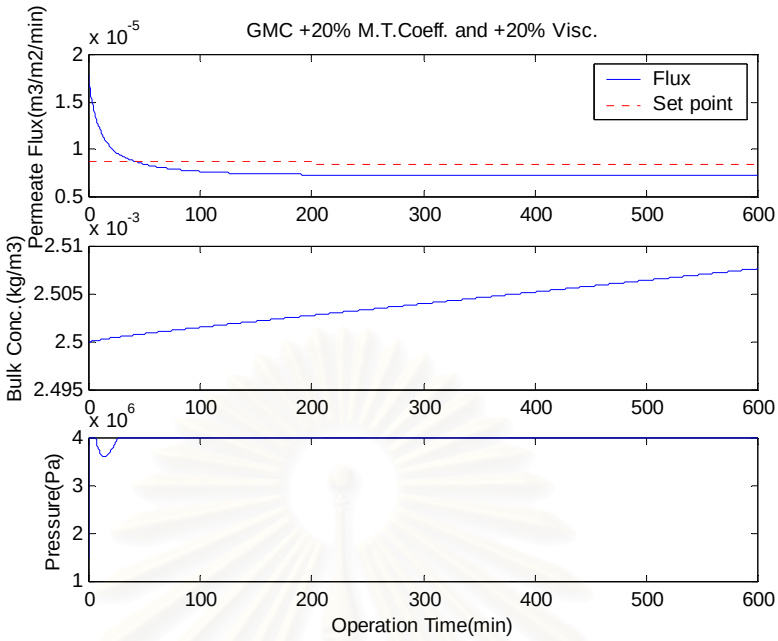

(a) Permeate flux, bulk conc. of the tannic solution and applied pressure

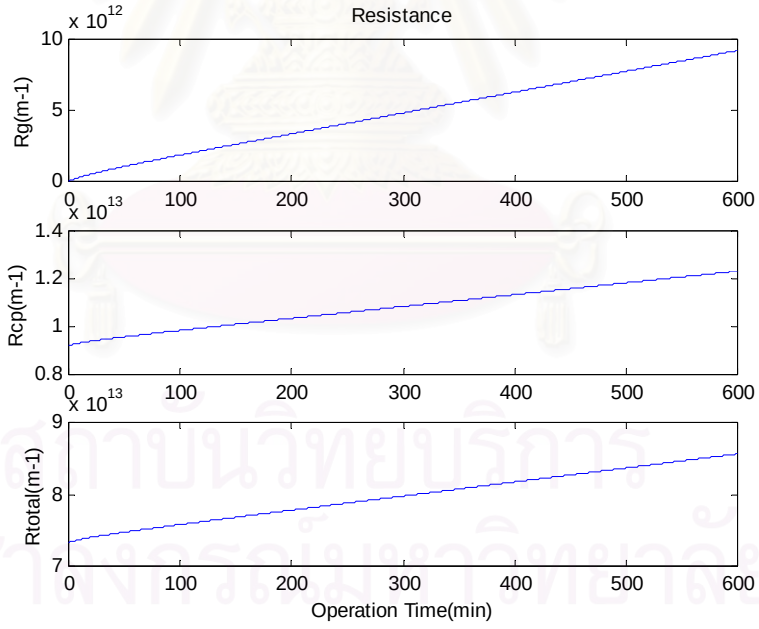

(b) Resistance of gel-layer, resistance of conc. polarization, and total resistance

Figure 4.25. The controlled response for +20% k and +20% μ change of the nanofiltration process using GMC (case 2)

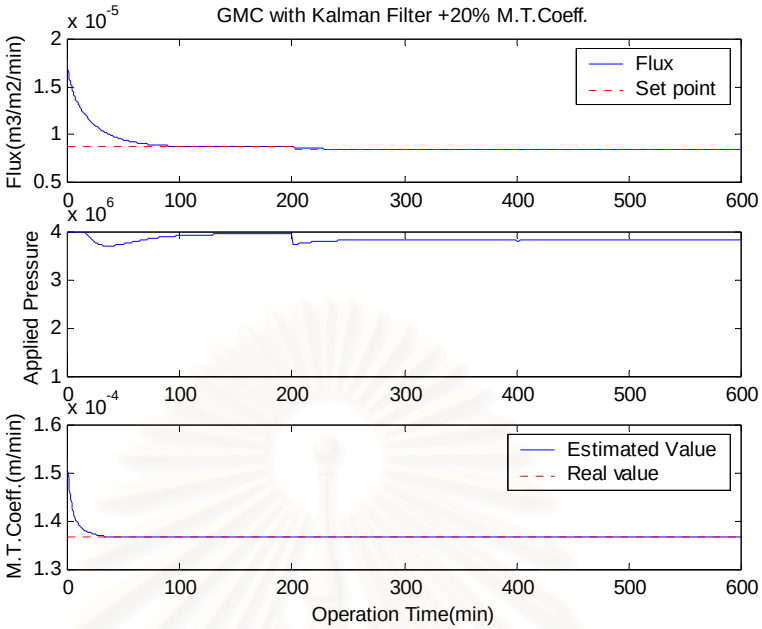

Figure 4.26. The controlled response and estimate of mass-transfer coefficient for +20% *k* change of the nanofiltration process using GMC coupled with Kalman filter (case 2)

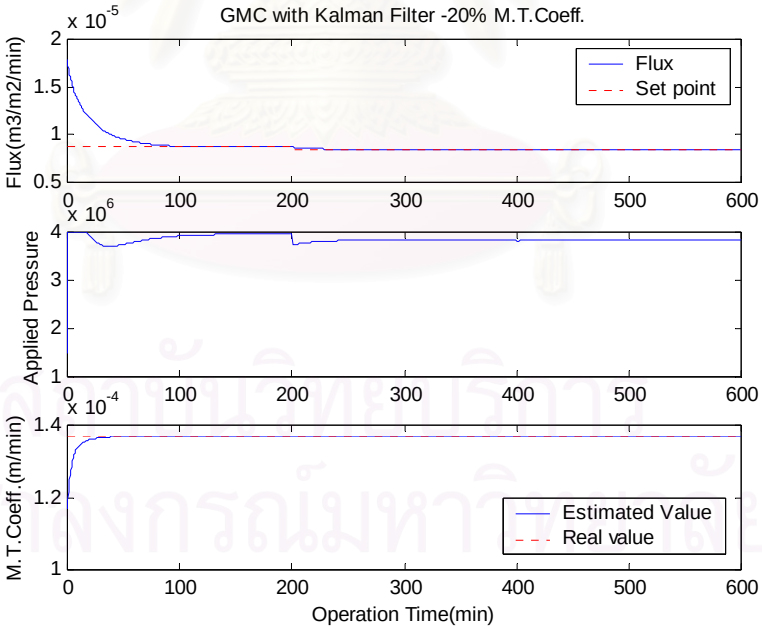

Figure 4.27. The controlled response and estimate of mass-transfer coefficient for -20% *k* change of the nanofiltration process using GMC coupled with Kalman filter (case 2)

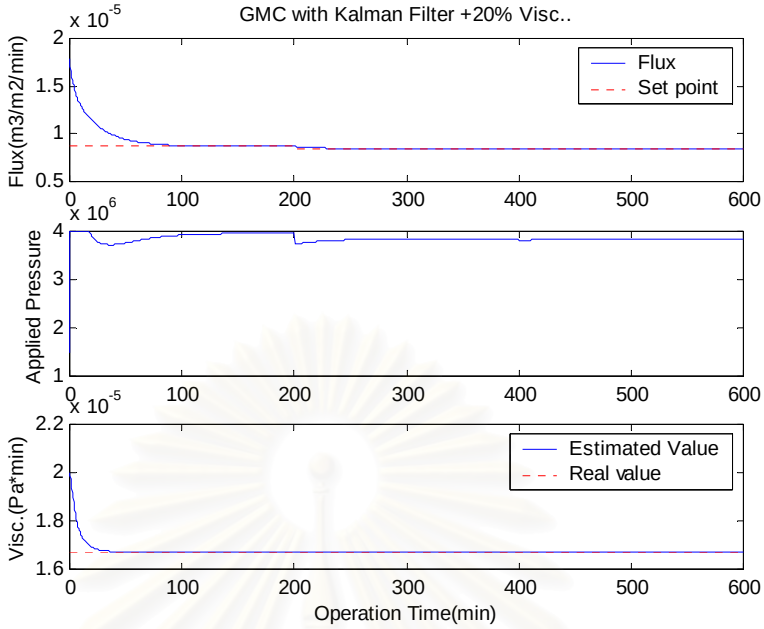

Figure 4.28. The controlled response and estimate of solution viscosity for +20% μ change of the nanofiltration process using GMC coupled with Kalman filter (case 2)

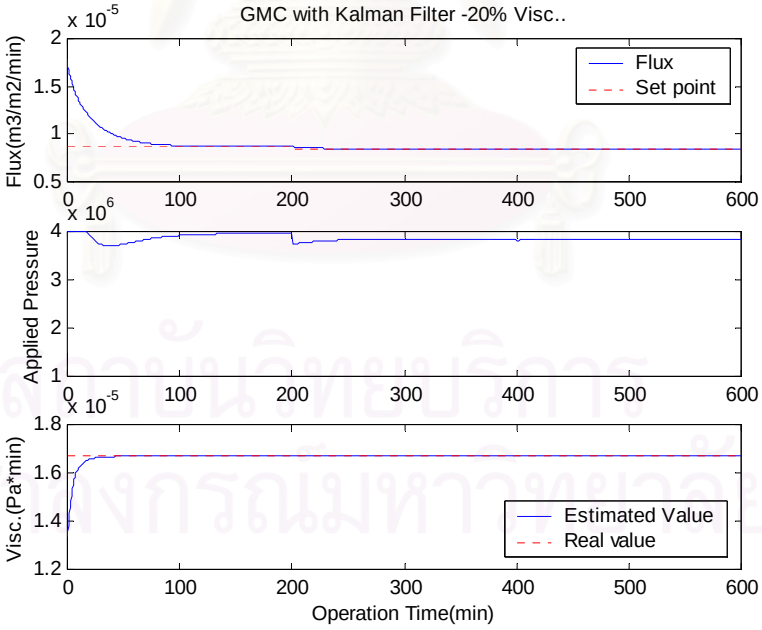

Figure 4.29. The controlled response and estimate of solution viscosity for -20% μ change of the nanofiltration process using GMC coupled with Kalman filter (case 2)

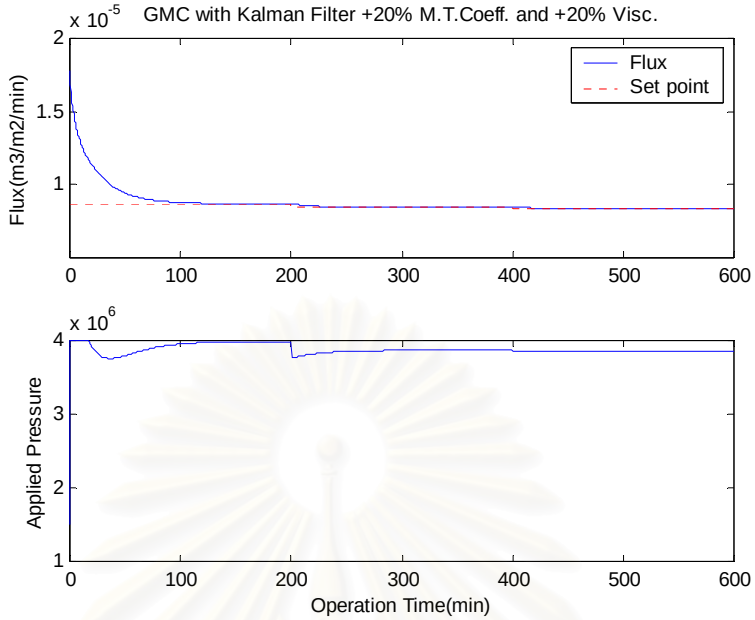

(a) Permeate flux and applied pressure

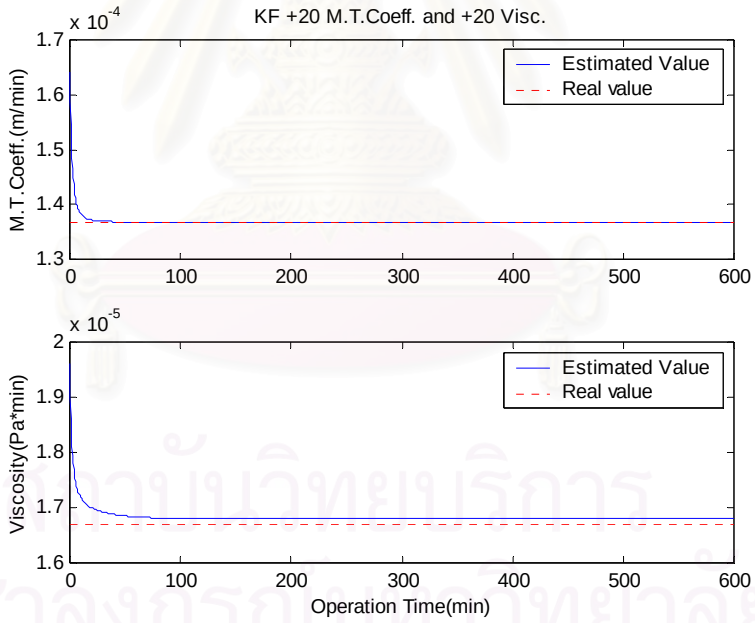

(b) Estimates of mass-transfer coefficient and solution viscosity

Figure 4.30. The controlled response and estimates of parameters for +20% k and +20% μ change of the nanofiltration process using GMC coupled with Kalman filter (case 2)

4.3.5 Discussion

Nominal Case

Performances of PID and GMC controller are compared in this part. The studied process is nanofiltration which has highly nonlinear behavior as seen in its mathematical model. From the performance index in table 4.5 and the closed-loop responses in figure 4.7 – 4.10, the control results in nominal case show that the performance of the GMC controller is better than PID for both cases. The GMC controller can force the permeate flux to the desires set point but the PID controller cannot handle the studied process because the water permeate fluxes take long time to reach their set points in both cases. These can conclude that the GMC controller is more suitable than PID to use as a controller for track the nanofiltration process because the GMC calculates the control action based on the mathematical model and it directly inserts nonlinear process model into its controller output. PID controller uses the error to calculate the control action and equation of its manipulated variable is linear equation.

Robustness Tests

In this part, the closed-loop responses of the nanofiltration process when the mass-transfer coefficient and/or solution viscosity have changed are studied. The GMC controller and GMC coupled with Kalman filter are developed to control the process. The comparisons of IAE and ISE for each robustness tests are shown in table 4.6 for case1 and table 4.7 for case 2.

Case 1: Tracking an optimal flux set point using one control time interval

- **Mass-transfer coefficient change**

The results given in figure 4.11-4.12 for the GMC and figure 4.16-4.17 for the GMC coupled with Kalman filter. The simulations show that the GMC controller has still provided control action similar to the nominal case. The GMC is robust to the mass-

transfer coefficient changes. However, the Kalman filter improves the control performance of the controller when compared IAE of GMC with GMC coupled with Kalman filter because a reasonable estimation token from the filter decreases the deviation of the model and real process.

- **Solution viscosity change**

In the cases of solution viscosity changes, the results are given in figure 4.13-4.14 for the GMC and figure 4.18-4.19 for the GMC coupled with Kalman filter. It can be seen that the estimations of the viscosity are approached to the nominal value. The GMC controller is still robust to the solution viscosity changes.

- **Mass-transfer coefficient and solution viscosity change**

Figure 4.15 and 4.20 show the control results for the case that combines the increment in the mass-transfer and the solution viscosity for the GMC and GMC coupled with Kalman filter, respectively. It can be seen from the figure 4.20 (b) that the Kalman filter gives reasonable estimations, As shown in figure 4.15 (a) and 4.20 (a), the controllers perform satisfactorily; the permeate flux is delivered to the desired set point.

Case 2: Tracking an optimal flux profile using three fixed control intervals

- **Mass-transfer coefficient change**

The simulation results of mass-transfer coefficient change are illustrated in figure 4.21-4.22 for GMC and figure 4.26-4.27 for GMC coupled with Kalman filter. It can be seen that the Kalman filter gives the reasonable estimations of the mass-transfer coefficient. The GMC controller is still robust to the mass-transfer coefficient changes.

- **Solution viscosity change**

Figure 4.23-4.24 show the closed-loop responses of the process controlled with the GMC controller for the case that solution viscosity changes. Figure 4.23 illustrates that the GMC controller can not handle the process when the solution viscosity has increased. While in the case of solution viscosity declination, the GMC controller is

still robustness. These can be explained by solution-diffusion model. The permeant dissolved in the membrane material and diffuse through the membrane down the concentration gradient. The permeant is separated because of the differences in the solubilities of the materials in the membrane and the differences in the rates at which the materials diffuse through the membrane. The solution viscosity increment is a cause of the permeant solubility declination and deterioration of permeant diffusion rate through the membrane. Figure 4.28-4.29 show the control response of the process controlled with the GMC coupled with Kalman filter. The Kalman filter gives the reasonable estimations of the solubility viscosity and the controller gives the satisfied response for these cases.

- **Mass-transfer coefficient and solution viscosity change**

In the case of combines the increment in the mass-transfer and the solution viscosity, the results are given in figure 4.25 for the GMC and figure 4.30 for the GMC coupled with Kalman filter. Figure 4.25 illustrates that the GMC controller can not handle the process to the set point. The GMC controller is not robust for this case because of affect of solution viscosity increment. Figure 4.30 (b) shows the estimated values of the parameter mismatch. The Kalman filter gives the reasonable estimation for mass-transfer coefficient but for the solution viscosity estimation, the filter gives the estimation value that deviate 0.62% from the nominal value. However, the GMC coupled with Kalman filter is still robust for this case.

The GMC controller and GMC coupled with the Kalman filter are implementted to track either optimal permeate flux set point or optimal permeate flux profile of the nanofiltration process for tannic acid solution. From the simulation results, it can be summarized that the GMC controller coupled with the Kalman filter is robust for all the changes. The control response of the GMC controller is sensitive to the case that solution viscosity increases and mass-transfer coefficient and viscosity increase when it is applied to track the optimal permeate flux profile (case 2). For these robustness tests, The GMC controller coupled with the Kalman filter has been found to be effective and robust in tracking the nanofiltration process.

CHAPTER 5

CONCLUSIONS AND RECOMMENDATIONS

In this work, the nanofiltration process for tannic acid solution has been studied. In summary, to achieve the desired successful control of the process, the system depends on the integration of three important ingredients: a reliable mathematical model, an optimal operating trajectory, and a suitable design of the control configuration. The GMC controller is a model-based control, which is a simple nonlinear control technique. For this reason, the GMC controller is chosen to track the studied process that has highly nonlinear behavior. Although the GMC can handle the studied process in nominal case, the developed controller has to have a good performance and robustness. In this research, the Kalman filter is applied to improve the performance and robustness of the GMC controller when the operating condition has changed.

5.1 Conclusions

From studying of the nanofiltration process, the filtration performance index is permeate flux. A serious limitation in such membrane filtration process is flux declination. The factors that have impact on the progressive permeate flux deterioration are membrane resistance, gel-layer resistance, and concentration polarization resistance. To improve the performance of the nanofiltration process, the GMC is develop to track the permeate flux to the optimal trajectory set point. Due to the significant of the operating condition, the optimization framework is formulated to determine the optimal permeate flux. The obtained optimal permeate flux is used as the set point for the nanofiltration membrane in the control study. In this work, the determination of off-line optimal flux control is studied in two cases. One is an optimal flux set point using one time interval (case 1). The other is an optimal flux set point using three fixed control

intervals (case 2). From the optimization study it can be concluded that the use of an optimal permeate flux profile give an increase in the performance of filtration rather than an optimal permeate flux set point.

In the control study, A GMC controller and a GMC coupled with Kalman filter are implemented to track the permeate flux. Both optimal flux in case 1 and case 2 are used as the trajectory set point. From the study it can be conclude that:

- For nominal case, the GMC controller performs satisfactorily in tracking both optimal flux set point and optimal flux profile of the nanofiltration process.
- The robustness of the controllers is evaluated by changing the process parameters such as mass-transfer coefficient and solution viscosity. It has been found that the GMC controller can handle the process for all cases of parameter mismatch except tracking the optimal flux profile in the case of solution viscosity increase and case of combines the increment in mass-transfer and solution viscosity. While the GMC coupled with Kalman filter is robust for all cases of parameter change because the filter gives the reasonable estimations of the parameter mismatch.

5.2 Recommendations

To explain the behavior of nanofiltration process, model in partial differential equation (PDE) is more accurate and reliable than ordinary differential equation (ODE) although developed mathematical model of the nanofiltration process which is in the term of ODE gives the satisfactorily results. In this research, researcher keeps off PDE to study the behavior of the process because the limitation of computer and software, solving of PDE spend long time in calculation.

REFERENCES

Thai

ไพศาล กิตติศุภกร. เอกสารประกอบการสอน 2105-619 การควบคุมกระบวนการอัตโนมัติขั้นสูง. ภาควิชาวิศวกรรมเคมี จุฬาลงกรณ์มหาวิทยาลัย, 2543.

รัตนา จิระรัตนานนท์. กระบวนการแยกด้วยเยื่อแผ่นสังเคราะห์. พิมพ์ครั้งที่ 2. กรุงเทพมหานคร: สำนักพิมพ์ไทยเส็ง, 2000.

English

Alag, G. S., and Gilyard, G.B. A Proposed Kalman Filter Algorithm for Estimation of Unmeasured Output Variables for an F100 Turbofan Engine, NASA Technical Memorandum (1990): 4234.

Alvarez, S., et al. Prediction of flux and Aroma Compounds Rejection in a Reverse Osmosis Concentration of Apple Juice Model Solutions, Ind. Eng. Chem. Res., 40 (2001): 4925-4934.

Avery, P. Applied Fitting Theory V: Track Fitting Using the Kalman Filter, CBX 92-39, 1992

Baker, W. R. Membrane Technology and Applications. New York: McGraw-Hill, 2000.

Baker, R., and Blume, I. Handbook of Industrial Membrane Technology. New Jersey: Noyes Pubications, (n.d.).

Bhattacharyya, D., Back S.L., and Kermode, R.I. Prediction of Concentration Polarization and Flux Behavior in Reverse Osmosis by Numerical Analysis, J. Memb. Sci. 48 (1990): 231.

Bowen, W.R., and Mohammad, A.W. Diafiltration by Nanofiltration: Prediction and Optimization, AIChE Journal 44 (1998): 1799-1812.

Brown, R.G., & Hwang, P. Y. C. Introduction to Random Signals and Applied Kalman Filtering: with MATLAB Exercises and Solutions. Third ed. (n.p.) Wiley & Sons, 1996.

Cheryan, M. Ultrafiltration and microfiltration handbook. Technomic Pulishing Company, Lancaster.,1998.

Cho, Jaeweon. Natural Organic Matter Rejection by, and Flux Decline of, Nanofiltrafion and Ultrafiltration Membranes, doctoral dissertation, Department of Civil, Environmental, and Architectural Engineering, University of Colorado at Boulder., 1998

Cornel, P., R. S. Summers, and P. V. Roberts. Diffusion of Humic Acid in Dilute Aqueous Solution, *J. Colloid Interface Sci*. (1986): 110, 149.

DeCarlo, R., and Meirina, C. Parameter Identification and Adaptive Control of an Ultrafiltration Process in Hemodialysis, Proceedings of the American Control Conference (2000): 2967-2971.

Driels, M. Linear Control Systems Engineering., Singapore: McGraw-Hill (1996): 515-523.

Edgar, T. F.; Himmelblau, D. M.; and Lasdon, L. S. Optimization of Chemical Processes. 2nd ed. New York: McGraw-Hill, 2001.

Jacobs, O. L. R. Introduction to Control Theory. Second ed. Oxford University Press., 1993.

Jounela, S., and Oja, M. Modeling Module of the Intelligent Control System for the Variable Volume Pressure Filter, Filtration+Separation (2000): 39-49.

Kershenbaum, L. S., and Kittisupakorn, P. The use of a partially simulated exothermic (PARSEX) reactor for experimental testing of control algorithms. Trans IChemE. 72, Part A (1994): 55-63.

Ko, M.K., and Pellegrino, J.J. Determination of Osmotic Pressure and Fouling Resistances and their Effects on Performance of Ultrafiltration Membranes, J. Memb. Sci., 74 (1992): 141.

Lee, P. L., and Sullivan, G. R. Generic model control (GMC). Comp. Chem. Eng. 12 (1988): 573-580.

Lee, P. L; Nowell, R. B.; and Sullivan, G. R. Generic model control- a case study. Can. J. Chem. Eng. 67 (1989): 478-484.

Lee, P. L.; Zhou, W.; Cameron, I. T.; Newell, R. B.; and Sullivan, G. R. Constrained generic model control of a surge tank. Comp. Chem. Eng. 15 (1991): 191-195.

Li, Z., et al. Comparison of Numerical Modeling of water Uptake in Poly(vinyl chloride)-Based Ion-Selective Membranes with Experiment, Analytical Chemistry, 68 (1996): 1726-1734.

Mallevialle, J., et al. Water Treatment Membrane Process, New York: McGraw-Hill, 1996.

Maskan, F., et al. Optimal Design of Reverse Osmosis Module Networks, AIChE Journal, 46 (2000): 946-954.

Maybeck, P. S. Stochastic models, estimation, and control. Vol. 141 (1979).

Maybeck, P. S. The Kalman Filter—An Introduction for Potential Users, TM-72-3, Air Force Flight Dynamics Laboratory, Ohio: Wright-Patterson AFB, June 1972.

Mulder, M. Basic principles of membrane technology, Kluwer Academic Publishers, Dordrecht, 1991.

Nussara Boonprasert. Generic model controller application for polyvinyl chloride polymerization reactor. Master's Thesis, Department of Chemical Engineering, Faculty of Engineering, Chulalongkorn University, 1999.

Ogunnagaike B.A., and Ray W.H. Process Dynamic, Modeling, and Control., New York: Oxford University Press, 1994.

Orladda Moolasartsatorn. Optimization and control of pervaporative membrane reactor. Master's Thesis, Department of Chemical Engineering, Faculty of Engineering, Chulalongkorn University, 2002.

Perry, R.H, and D.W. Green. Perry's Chemical Engineers' Handbook. 7th edition. (n.p.): McGraw-Hill, 1997.

Pijak Meethong. GMC for relative degree higher than one processes a case study: A concentration control of continuous stirred tank reactor with first-order

exothermic reaction. Master's Thesis, Department of Chemical Engineering, Faculty of Engineering, Chulalongkorn University, 2002.

Porter, Mark C. Concentration Polarization with Membrane Ultrafiltration, Ind. Eng. Chem. Prod. Res. Develop. 11, 3 (1972): 234-248.

Pusch, W. Measurements techniques of transport through membranes, Desalination 59, 105-198, 1986.

Riggs, J. B., and Rhinehart, R. R. Comparison between two nonlinear process-model based controllers. Comp. Chem. Eng. 14, 1075-1081, 1990.

Skogestad S., and Postlethwaite I. Multivariable Feedback Control. (n.p.): John Wiley & Sons, England (1996): 122-131.

Timmer, J.M.K., Kromkamp, J., and Robbertsen, T. Lactic Acid Separation from Fermentation Broths by Reverse Osmosis and Nanofiltration, J. Membr. Sci. (1994): 92, 185.

Timmer, J.M.K. Properties of Nanofiltration Membranes; Model Development and Industrial Application. Technische University Eindhoven, 2001.

Tu, S.C., et al. Predictive Membrane Transport Model for Nanofiltration Processes in water Treatment, AICHE Journal, 47 (2001): 1346-1362.

van Boxtel, A.J.B., Otten, Z.E.H., and van der Linden, H.J.L.J. Evaluation of Process Model for Fouling Control of Reverse Osmosis of Cheese Whey, J. Memb. Sci., 58 (1991): 89.

van Der Bruggen, B., and Vandecasteele, C. Flux Decline during Nanofiltration of Organic Components in Aqueous Solution, Environ. Sci. Technol, 35 (2001): 3535-3540.

Veerayut Lersbamrungsuk. Kalman filter algorithm software design and development for chemical engineering. Master's Thesis, Department of Chemical Engineering, Faculty of Engineering, Chulalongkorn University, 2000.

Weerawun Weerachaipichasgul. Model predictive control for liquid-solid cross flow ultrafiltration membrane separation. Master's Thesis, Department of Chemical Engineering, Faculty of Engineering, Chulalongkorn University, 2002.

Williams, M.E., et al. Separation of Organic Pollutants by Reverse Osmosis and Nanofiltration Membranes: Mathematical models and Experimental Verification, Ind. Eng. Chem. Res., 38 (1999): 3683-3695.

Zhou K., and Doyle J.C. Essentials of Robust Control. U.S.A.: Prentice-Hall, (1998): 27-40, 129-156.

APPENDICES

APPENDIX A

MATHEMATICAL MODEL DEVELOPMENT

For the incorporation of the transport model equation in a batch membrane system, the volume and concentration changes as a function of time must be included. The model is based on the general material balance equation, given as;

Accumulation = Input – Output +Generation – Consumption. (A.1)

For a batch system, a solute material balance results in

$$\frac{d(C_b V)}{dt} = 0 - A_m J_v C_p + 0 - 0 \tag{A.2}$$

$$V\frac{dC_b}{dt} + C_b\frac{dV}{dt} = -A_m J_v C_p \tag{A.3}$$

$$\frac{dC_b}{dt} = \frac{-A_m J_v C_p - C_b\dfrac{dV}{dt}}{V}. \tag{A.4}$$

The solution volume in the membrane unit at any time is given as:

$$V = V_0(1-r), \tag{A.5}$$

where V_0 is the initial feed volume. The rate of water recovery from the cell can be presented as:

$$\frac{dr}{dt} = \frac{A_m}{V_0} J_v \ . \tag{A.6}$$

Substituting into equation (A.4), it follows that:

$$\frac{dC_b}{dt} = \frac{A_m J_v (C_b - C_p)}{V_0 (1-r)}. \qquad \text{(A.7)}$$

For the membrane filtration process, bulk concentration, C_b is very greater than concentration of species in the permeate side of membrane, C_p. Equation (A.7) can be written as following:

$$\frac{dC_b}{dt} = \frac{A_m J_v C_b}{V_0 (1-r)}. \qquad \text{(A.8)}$$

APPENDIX B

MASS-TRANSFER COEFFICIENT DETERMINATION

The mass-transfer coefficient, k can be calculated from Sherwood correlations of the form used by several researchers (Bird et al., 1960; van den Berg et al., 1989; Pradanos et al., 1992, 1995; von Meien and Nobrega, 1994):

$$Sh = kd_h / D = pRe^q Sc^r, \qquad \text{(B.1)}$$

where d_h is the hydraulic diameter of the system,

D is the diffusion coefficient,

Re is the Reynold number ($Re = \rho v d_h / \mu$),

Sc is the Schmidt number ($Sc = \mu / \rho D$),

and p, q, and r are constants depending on the hydraulic regimes.

Aqueous diffusion coefficients of the natural organic mater in dilute solution can be estimated by the Stokes-Einstein equation (Cornel et al., 1986). The diffusion coefficient evaluated for tannic acid is 2.635×10^{-10} m^2/s.

Wiley et al. (1985) and van den Berg et al. (1989) used the following correlations for membrane filtration systems operating under laminar flow conditions ($Re \leq 2{,}000$).

$$L < L^* : Sh = 0.664 Re^{0.5} Sc^{0.33} (d_h / L)^{0.33} \qquad \text{(B.2)}$$

$$L > L^* : Sh = 1.86 Re^{0.33} Sc^{0.33} (d_h / L)^{0.33}, \qquad \text{(B.3)}$$

where L and L^* are length of a membrane module and length of the entry region in the module, respectively. The entry length L^* is given by the relation

$$L^* = 0.029 d_h Re. \qquad \text{(B.4)}$$

These correlations establish the dependence of the mass-transfer coefficient on fluid dynamics of the system and the solute/solvent characteristics for positions represented by L less than or greater than the characteristics entry length L^* required for fully developed flow. While the Reynolds number characterizes the fluid flow and momentum transport along the membrane surface in relation to inertial forces, the Schmidt number describes the diffusion transport of solute (foulant) molecules to and from the membrane surface under these conditions.

APPENDIX C

SYSTEM CHECKING

System Stability

The determination of system stability is based on the same principle as that for SISO systems: by investigating the location of the open-loop poles on the complex plane. The open-loop poles, or eigenvalues are determined from

$$\det(\lambda I - A) = 0 \qquad \text{(C.1)}$$

where λ is pole of the system.

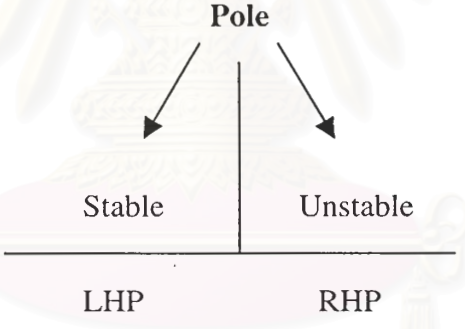

Note that this determinant has to be evaluated anyway in calculating the resolvent. As before, if any of the eigen values are positive or have a positive real part, the system is unstable.

Controllability

The dynamical system described by equation

$$\dot{x} = Ax + Bu\,, \qquad \text{(C.2)}$$

or equivalently the pair (A, B), is said to be state controllable if it is possible to bring a state variable to any arbitrary value in a finite period of time using the manipulated variables that are available. Otherwise the system is said to be state uncontrollability.

There are many ways to check whether a system is state controllable. In this work, controllability matrix is formed to determine controllability.

$$\text{Controllability Matrix} = [B \quad AB \quad A^2B \quad \ldots\ldots \quad A^{n-1}B] \qquad \text{(C.3)}$$

where n is number of state variables.

The system is controllability if the rank of the matrix is n (full row rank).

Observability

The dynamical system

$$\dot{x} = Ax + Bu\,, \qquad \text{(C.4)}$$

$$y = Cx + Du \qquad \text{(C.5)}$$

(or the pair (A, C)) is said to be state observable if measurement of output, y contains sufficient information to enable us to completely identify the state x. Otherwise the system, or (A, C), is said to be state unobservable.

The system (A, C) is state observable if and only if the observability matrix

$$\text{Observability Matrix} = [C^T \quad A^TC^T \quad \ldots\ldots \quad (A^T)^{n-1}C^T] \qquad \text{(C.6)}$$

has rank n (full column rank).

In this study, the state of equations is

$$f_1 = \frac{dJ_v}{dt} = \frac{J_v^2}{\Delta P}\left[c_1 C_b^{d-1} \frac{dC_b}{dt} + c_2 C_b J_v - c_3 C_b \ln \frac{C_g}{C_b} \right], \qquad \text{(C.7)}$$

$$f_2 = \frac{dr}{dt} = \frac{A_m}{V_0} J_v , \qquad \text{(C.8)}$$

$$f_3 = \frac{dC_b}{dt} = \frac{A_m J_v C_b}{V_0 (1-r)} \qquad \text{(C.9)}$$

where

$$c_1 = -ad \frac{\mu}{\delta} v^b k^c C_f^e$$

$$c_2 = -\mu \frac{\varepsilon}{\rho_g}$$

$$c_3 = -\mu \frac{\varepsilon}{\rho_g} k.$$

State variables, x_n are J_v, r, and C_b and manipulated variable, u is ΔP^{-1}. Volume of permeated water, V_{out} is selected as the measurement variable, y that can be written the relationship with the permeate flux as following equation

$$V_{out} = A_m J_v . \qquad \text{(C.10)}$$

From equation (C.4), (C.5), (C.7), (C.8), and (C.9), state space form of the system can be determined matrix A, B, and C as

$$A = \begin{bmatrix} \frac{df_1}{dx_1} & \frac{df_1}{dx_2} & \frac{df_1}{dx_3} \\ \frac{df_2}{dx_1} & \frac{df_2}{dx_2} & \frac{df_2}{dx_3} \\ \frac{df_3}{dx_1} & \frac{df_3}{dx_2} & \frac{df_3}{dx_3} \end{bmatrix}, \qquad B = \begin{bmatrix} \frac{df_1}{du} \\ \frac{df_2}{du} \\ \frac{df_3}{du} \end{bmatrix}, \qquad \text{and } C = \begin{bmatrix} A_m & 0 & 0 \end{bmatrix}$$

where $\frac{df_1}{dx_1} = \frac{C_b J_v}{\Delta P}\left[2c_1 C_b^{d-2}\frac{dC_b}{dt} + 3c_2 J_v - 2c_3 \ln\frac{C_g}{C_b}\right]$,

$\frac{df_1}{dx_2} = 0$,

$\frac{df_1}{dx_3} = \frac{J_v^2}{\Delta P}\left[c_1 C_b^{d-1}\left(\frac{d^2 C_b}{dt^2} + \frac{(d-1)}{C_b}\frac{dC_b}{dt}\right) + c_2 J_v + c_3\left(1 + \ln\frac{C_b}{C_g}\right)\right]$,

$\frac{df_2}{dx_1} = \frac{A_m}{V_0}$,

$\frac{df_2}{dx_2} = 0$,

$\frac{df_2}{dx_3} = 0$,

$\frac{df_3}{dx_1} = \frac{A_m C_b}{V_0(1-r)}$,

$\frac{df_3}{dx_2} = \frac{A_m J_v C_b}{V_0(1-r)^2}$,

$\frac{df_3}{dx_3} = \frac{A_m J_v}{V_0(1-r)}$,

$\frac{df_1}{du} = J_v^2\left[c_1 C_b^{d-1}\frac{dC_b}{dt} + c_2 C_b J_v - c_3 C_b \ln\frac{C_g}{C_b}\right]$,

$\frac{df_2}{du} = 0$,

and $\frac{df_3}{du} = 0$.

Substituting all variables in matrix *A*, *B*, and *C* with the steady state values, the determination of the system checking via MATLAB program can be summarized as following:

1. The poles of this system are on left hand side of complex plane. This can be concludes that the open-loop of system is stable.
2. Determinant of the controllability matrix is not equal to zero (The rank of the matrix is full rank.). This can be conclude that the control variable can be controlled by the selected manipulate variable.

3. Determinant of the observability matrix is not equal to zero (The rank of the matrix is full rank.). This can be concluded that the measurement variable contains sufficient information to completely identify the state variable.

APPENDIX D

INTEGRAL ERROR CRITERIA

Integral error measures indicate the cumulative deviation of the controlled variable from its set point during the transient response. The following formulations of the integral can be proposed.

Figure D1. Definition of error integrals

Integral absolute error (IAE)

$$IAE = \int_0^\infty |e(t)|\,dt \qquad \text{(D.1)}$$

Integral square error (ISE)

$$ISE = \int_0^\infty e^2(t)dt \qquad \text{(D.2)}$$

Integral of time-weighted absolute error (ITAE)

$$ITAE = \int_0^\infty |e(t)|tdt \qquad \text{(D.3)}$$

where e is the usual error (i.e., set point – control variable).

Each of the three figures of merit given by equation (D.1), (D.2), and (D.3) have different purposes. The ISE will penalize (i.e., increase the value of ISE) the response that has large errors, which usually occur at the beginning of a response, because the error is squared. The ITAE will penalize a response, which has errors that persist for a long time. The IAE will be less severe in penalizing a response for large errors and treat all errors (large and small) in a uniform manner. The ISE figure of merit is often used in optimal control theory because it can be used more easily in mathematical operations (for example differentiation) than the figures of merit, which use the absolute value of error. In applying the tuning rules to be discussed in the next section, these figures of merit can be used in comparing responses that are obtained with different tuning rules.

APPENDIX E

SUCCESSIVE QUADRATIC PROGRAMMING (SQP)

Successive quadratic programming (SQP) method solved a sequence of quadratic programming approximation to nonlinear programming problem. Quadratic programs (QPs) have a quadratic objective function and linear constraints, and there exist efficient procedures for solving them

Problem formulation with equality constraints

To derive SQP, we again consider a general NLP

$$\begin{aligned} &Minimize: f(x) \\ &Subjectto: g(x) = b \end{aligned} \tag{E.1}$$

The Lagrangian function for this problem is

$$L(x,\lambda) = f(x) + \lambda^T (g(x) - b) \tag{E.2}$$

and the KTC are

$$\nabla_x L = \nabla f(x) + \sum_{i=1}^{m} \lambda_i \nabla g_i(x) = 0 \tag{E.3}$$

and

$$g(x) = b \tag{E.4}$$

The equation (E.1)-(E.2) is a set of $(n+m)$ nonlinear equations in the n unknowns x and m unknown multipliers λ. Linearization of (E.2) and (E.3) with respect to x and λ

$$\nabla_x L - \nabla_x^2 L \Delta x + \nabla g^T \Delta\lambda = 0 \tag{E.5}$$

$$g + \nabla g \Delta x = 0 \tag{E.6}$$

For problem with only equality constraints, we could simply solve the linear equations (E.2)-(E.3). To accommodate both equalities and inequality, an alternative viewpoint is useful. Consider the quadratic programming problem

$$\begin{aligned} &\min imize : \nabla L^T \Delta x + \frac{1}{2} \Delta x^T \nabla_x^2 L \Delta x \\ &Subject\ to : g + \nabla g \Delta x = 0 \end{aligned} \tag{E.7}$$

If we call the Lagrange mutipliers for (E.7) $\Delta\lambda$, the Lagrangian for the QP is

$$L_1(\Delta x, \Delta\lambda) = \nabla L^T \Delta x + \frac{1}{2} \Delta x^T \nabla_x^2 L \Delta x + \Delta\lambda^T (g + \nabla g \Delta x) \tag{E.8}$$

Inclusion of the both equality and inequality constraints

When the original problem has a mixture of equalities and inequalities, it can be transformed into a problem with equalities and simple bounds by adding slacks, so the problem has an objective function f, equalities (E.1), and bounds

$$l \le x \le u \tag{E.9}$$

This system is the KTC for the QP in (E.6) with the additional bound constraints

$$l \le \bar{x} + \Delta x \le u \tag{E.10}$$

Here the QP sub problem now has both equality constraints and must be solved by some iterative QP algorithm.

The approximate Hessian

Solving a QP with a positive-definite Hessian is fairly easy. Several good presented in (E.6) and (E.10) is $\nabla_x^2 L(\overline{x}, \overline{\lambda})$, and this matrix need not be positive-definite, even if $(\overline{x}, \overline{\lambda})$ is an optimal point. In addition, to compute $\nabla_x^2 L$, one must compute second derivative of all problem functions. Both difficulties are eliminate by replacing $\nabla_x^2 L$ by positive-definite quasi-Newton approximate B, which is updated using only values of L and $\nabla_x L$. Most SQP algorithms use Powell's modification of BFGS update. Hence the QP subproblem becomes

$QP(\overline{x}, B)$

$$\begin{aligned} &\min imize: \nabla L^T \Delta x + \frac{1}{2} \Delta x^T B \Delta x \\ &Subject\ to: \nabla g \Delta x = -g, \quad I \le \overline{x} + \Delta x \le u \end{aligned} \tag{B.11}$$

The SQP line search

TO arrive at a reliable algorithm, one more difficulty must be over come. Newton and quasi-Newton method may not converge if a step of 1.0 is used at each step. Both trust region and time search versions of SQP have been developed that converge reliability. A widely used line search strategy is to use the L_1 exact penalty function $P(x, w)$. In a line search SQP algorithm, $P(x, w)$ is used only to determine the step size along the direction determined by the QP subproblem $QP(\overline{x}, B)$. The L_1 exact penalty function for the NLP problem is

$$P(x, w) = f(x) + \sum_{i=1}^{m} w_i \mid g_i(x) - b_i \mid \tag{E.12}$$

where a separate penalty weight w_i is used for each constraint. The SQP line search chooses a positive step size α to find an approximate minimum of

$$r(\alpha) = P(\overline{x} + \alpha\Delta x, w) \tag{E.13}$$

A typical line search algorithm, which uses the derivative of $r(\alpha)$ evaluated at $\alpha = 0$ denote by $r'(0)$, is

1. $\alpha \leftarrow 1$
2. if $r(\alpha) < r(0) - 0.1\alpha r'(0)$ (E.14)

   stop and return the current α value

3. Let α_1 be the unique minimum of the convex quadratic function that passes through $r(0), r'(0)$ and $r(\alpha)$. Take the new estimate of α as

$$\alpha \leftarrow \max(0.1\alpha, \alpha_1) \tag{E.15}$$

4. Go to step 2.

SQP algorithm

Base on this line search and the QP subproblem $QP(\overline{x}, B)$

1. Initialize: $B^0 \leftarrow I, x^0 \leftarrow x, k \leftarrow 0$
2. Solved the QP subproblem $QP(\overline{x}, B)$, yieldiging a solution Δx^k and Langrange multiplier estimates λ^k
3. Update the penalty weights in penalty function
4. Apply the line search algorithm, yielding a positive step size α^k

5. $x^{k+1} = x^k + \alpha^k \Delta x^k, \lambda^{k+1} = \lambda^k$

6. Evaluated all problem function and their gradients at new point. Update matrix B^k

7. Replace k by k+1, and go to step 2

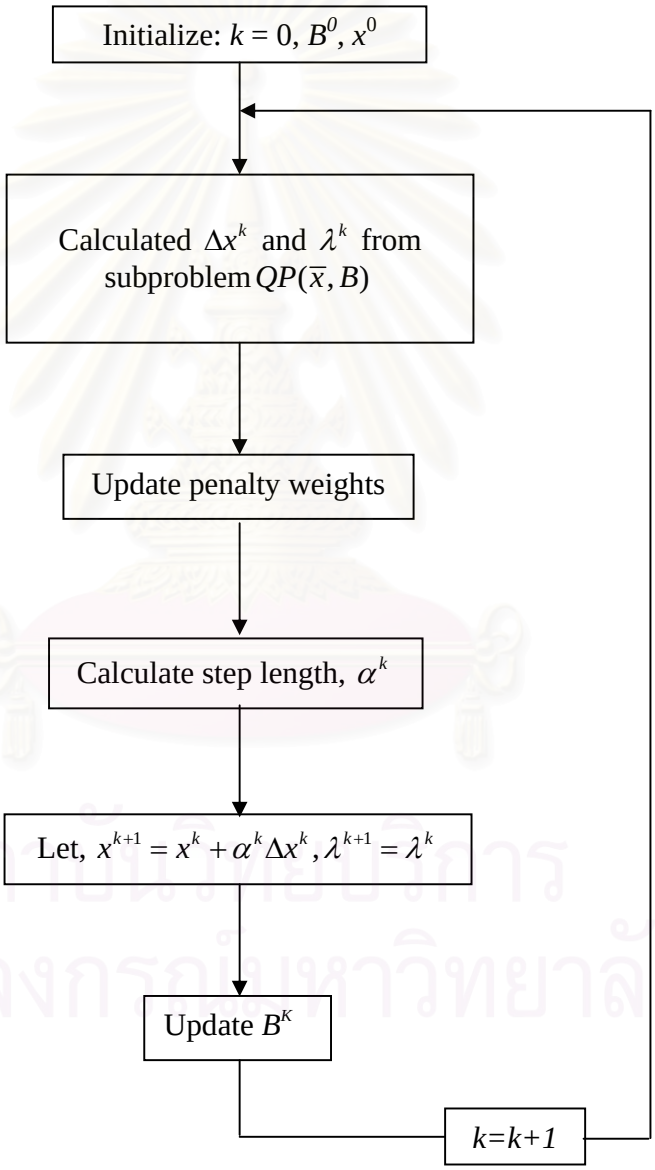

Figure E.1. Flowchart of SQP algorithm

VITA

Mr. Sampanpong Bhensirikul was born in Bangkok on August 28, 1978. He studied at Assumption College, Bangkok in 1985-1996. After completing his high school, he graduates his Bachelor Degree in Chemical Engineering from Chulalongkorn University, Bangkok in 2000. In 2003, he completed his Master Degree of Engineering in Chemical Engineering, Chulalongkorn University.